Theoretical and Computational Challenges with Rods

by Ajeet Kumar

THEORETICAL AND COMPUTATIONAL CHALLENGES WITH RODS

A Dissertation

Presented to the Faculty of the Graduate School

of Cornell University

in Partial Fulfillment of the Requirements for the Degree of

Doctor of Philosophy

by

Ajeet Kumar

August 2010

THEORETICAL AND COMPUTATIONAL CHALLENGES WITH RODS

Ajeet Kumar, Ph.D.

Cornell University 2010

A rod is a long and slender object whose lateral dimension is very small compared to its length. In solid mechanics, the theory of rods can be thought of as a generalized and geometrically exact version of the classical beam theory. There are two major variants of rod theory which are used commonly: Kirchoff rods and Cosserat rods. In Kirchoff rod theory, a rod is assumed to be unstretchable as well as unshearable characterized by linear elasticities, whereas in Cosserat rod theory, these restrictions are done away with. Due to its one-dimensional character, a rod serves as an excellent and efficient tool for theoretical as well as computational modeling of several biomolecules, arteries, cables, carbon nanotubes as well as several bacteria and viruses. The present dissertation deals with addressing the theoretical and computational challenges associated with rods so that its area of applicability can be further broadened.

Broadly speaking, this dissertation addresses three important issues: (1) development of a general and efficient computational framework to determine stability of equilibria of constrained elastic rods, (2) extension of the Cosserat rod theory in a mathematically consistent way to allow deformation of a rod's cross-section and (3) explanation of some peculiar atomistic simulation data of carbon nanotubes using an extended version of the special Cosserat rod theory.

It is found that the determination of stability of constrained elastic systems leads

to a generalized and singular eigenvalue problem. A new numerical algorithm is developed to remove the singularity present and at the same time maintain efficiency of the algorithm. The present state-of-the-art for determination of stability of rods was limited to Dirichlet problems and in the presence of integral constraints, while the algorithm developed here has the capacity to address any general boundary conditions, general loadings and equality constraints of all types. A new variational principle for extensible and unshearable rods is also proposed to facilitate application of the developed numerical algorithm for extensible rods. This is followed by development of a novel formulation of a rod model that allows in-plane deformation of its cross-section. The resulting theory has the potential to bridge the gap between 1-d rod theory and 2-d shell theory, efficiently. It also opens the door for modeling and analysis of hollow tubes such as arteries and nanotubes using a one-dimensional theory. The proposed model also explains a new coupling effect: extension, twist and cross-sectional shrinkage coupling of chiral carbon nanotubes. The peculiarity of a (9,6) carbon nanotube such as rotation of its neighboring cross-sections in alternate directions and fluctuation in twist and axial stretch along its axis at exactly two levels, when the ends of a nanotube are axially moved apart, are also explained using the proposed rod model.

BIOGRAPHICAL SKETCH

Ajeet Kumar was born on Nov 11, 1984 in Purnea (Bihar), India. He did his schooling from Sainik School Tilaiya, Koderma, India. After completing his schooling in 2002, Ajeet joined the Indian Institute of Technology Kharagpur, India (IIT Kharagpur) for his Bachelor's degree in Mechanical Engineering. Following his graduation from Kharagpur in 2006, Ajeet came to the USA to pursue his Ph.D. in the Department of Theoretical & Applied Mechanics (T&AM) at Cornell University, Ithaca, NY. Upon his graduation from T&AM, Ajeet will join the Department of Aerospace Engineering & Mechanics at University of Minnesota as a Postdoctoral research scholar.

To my parents

ACKNOWLEDGEMENTS

The four years of Ph.D. is probably the most challenging phase of my career till date. During this time, I first learnt (and am still learning) to stand on my own feet and also to be so far away from home. I feel priviledged to write a note of thanks to all who have supported and wished me well.

I thank Prof. Tim Healey for teaching me so many things. I can recall I always prepared to my best before meeting him and he would always point to me what lied ahead. It was under his mentorship that I diversified myself by learning mechanics, mathematics, as well as computation. I also grew more independent in thinking. A lesson that I would carry along with me: use more and more of mathematics and less and less of intuition in reaching a conclusion. I am really indebted to him for shaping me into what I am today. I also thank Prof. Wilkins Aquino for his wonderful association during my final year. It was under him that I got introduced to several of the new concepts in the finite element methods.

I thank Prof. Subrata Mukherjee who has many a time been caring to me. It was under his guidance that I got an opportunity to work on carbon nanotubes during my final year. Prof. Mukherjee has been very patient, understanding and almost always available to discuss academic as well as non-academic issues. I also thank Prof. Alexander Vladimirsky who taught me theory and numerics of partial differential equations. I feel very glad to get his taste of numerical mathematics during my early years of Ph.D. I also wish to thank Prof. Herbert Hui who reintroduced me to the concept of objective structures and further thank him for teaching me about fibrils and geckos. I benefited greatly from my interactions and courses with Prof. Charlie Van Loan and learnt to organize things

in matrix way. I thank several of the Cornell faculty whose courses played a valuable role in my educational experience at Cornell. I also benefited from members of the Cornell faculty with whom I worked as a teaching assistant - to them I owe the teaching experience I gained at Cornell.

Finally, I thank my friends at Cornell for motivating me to hang on till the end. I owe greatly to them for making my stay in Ithaca an enriching experience.

TABLE OF CONTENTS

LIST OF TABLES

LIST OF FIGURES

CHAPTER 1

INTRODUCTION

Interest in the special theory of Cosserat rods [1] has surged in recent years, due in large part to its applicability in biophysics, e.g., [3, 20, 43, 44, 58, 59] as well as in other areas such as modeling of cables [23], arteries [21] and carbon nanotubes [5, 22]. A rod, being one-dimensional, provides an excellent and efficient tool for the modeling and analysis of such objects. The goal of this dissertation is to address present theoretical and computational challenges associated with rod theory with an objective to increasing its area of applicability.

One of the challenges lies in developing a general and efficient numerical tool for determination of stability of equilibria. Systematic and reliable numercial methods for computing equilibria of nonlinearly elastic rods are now widely available, e.g., [8, 10, 29, 54] but there is not much of progress with respect to a systematic and reliable numerical approach to determine the stability of static equilibria of rods. For unconstrained rod problems, the determination of stability of equilibria is a direct by-product of an iterative Newtonian solver, i.e., the linearized tangent stiffness matrix carries all required information for the determination of stability [54]. However, in applications, the shear stiffnesses and/or the extensional stiffness are often orders of magnitude greater than the bending and torsional stiffnesses. Accordingly unshearable and/or inextensible rods are the rule rather than the exception. The presence of such constraints (point-wise in nature) or other integral constraints complicates the determination of stability considerably. Some of the earlier works to analyze stability of rods were analytical in nature and hence, were limited to planar or homogeneous/trivial equilibria, e.g., [20, 39, 40]. For conservative problems subjected

to integral constraints and Dirichlet boundary conditions, a numerical implementation of Jacobi's conjugate-point method has been employed with success [33, 43]. Recently that approach has been extended to scalar problems with Neumann boundary conditions [42]. In Chapter 2 of this dissertation, a systematic and reliable computational approach to the determination of stability of equilibria of nonlinearly elastic rods is presented that is general enough to handle constraints - pointwise or integral, non-conservative or conservative loadings, and arbitrary combinations of mixed (well-posed) boundary conditions. Accordingly the usual criterion of linearized dynamics for stability, e.g., [20, 48] is adopted. Beginning with an appropriate spatial weak form of the full dynamical equations of an elastic rod along with the constraint equations, its linearization is obtained about an equilibrium. Then all admissible perturbations of the form $\triangle\boldsymbol{\zeta}(s,t) = \triangle\boldsymbol{\zeta}_0(s)\exp(\omega t)$, where $\triangle\boldsymbol{\zeta}_0$ is the "amplitude" of the perturbation, are sought. Assuming an accurate, discrete representation of an equilibrium, finite element interpolation functions are employed to form a global, generalized eigenvalue problem of the form:

$$\begin{bmatrix} \mathbf{K} & \mathbf{C} \\ \mathbf{C}^T & \mathbf{O} \end{bmatrix} \begin{bmatrix} \mathbf{x} \\ \mathbf{y} \end{bmatrix} = -\omega^2 \begin{bmatrix} \mathbf{M} & \mathbf{O} \\ \mathbf{O} & \mathbf{O} \end{bmatrix} \begin{bmatrix} \mathbf{x} \\ \mathbf{y} \end{bmatrix} \tag{1.1}$$

Here K is the stiffness matrix, which is symmetric for conservative problems, C is the linearized constraint matrix and M is the positive-definite mass matrix. Observe that the matrix on the right hand side of (1.1) is necessarily singular in the presence of constraints, which complicates the numerical computation of eigenvalues. The study of such generalized eigenvalue problems is not new. For example, it arises in the context of stability of steady state flow of incompressible fluids [6]. Efficient numerical methods to compute a few "left-most" eigenvalues of (1.1) are well known; recent developments can be found in [51].

The singularity from the right side of (1.1), essentially due to constraints, complicates as well as "corrupts" the numerical computation of the desired eigenvalues using existing numerical schemes. In Chapter 2 of this dissertation, an efficient numerical algorithm is sought that not only removes the singularity present in (1.1) but at the same time preserves the sparsity in the matrices.

There is another important issue in formulating an integral constrained version for extensible and unshearable rods. Such rods have only pointwise unshearability constraints. For unshearable and inextensible rods, an integral constrained formulation already exists which delivers us with a reduced version of the rod equations. In Chapter 3, a novel integral-constrained variational formulation for extensible and unshearable rods is proposed. The motivation for this problem stems from recent interest in analyzing coupled extension-twist behavior of chiral structures. The proposed formulation also leads to a convenient application of the numerical method developed in Chapter 2.

One of the limitations of the special Cosserat theory of rods lies in assuming rigidity of a rod's cross-section. While this is often a good assumption, rigidity of cross-sections is questionable when modeling hollow tubes such as carbon nanotubes, arteries as well as solid tubes that undergo large axial stretch or bending. Although this issue could be addressed using 2-d shell theory or 3-d continuum theory, these approaches often unnecessarily increase the number of degrees of freedom of the system being modeled. Thus, a challenge remains in capturing the cross-sectional deformations within the confines of a one-dimensional theory in a consistent manner. Chapter 4 of this dissertation addresses this issue. There has been substantial work in this regard. In

the special theory of Cosserat rods, the three directors are constrained to remain orthonormal even after deformation, thus restraining a rod's cross-section to be rigid. A more general rod theory allowing the two cross-sectional directors to deform was proposed in 1966 by Green and Laws [24] and the special theory of Cosserat rods was shown to be a constrained version of this general theory in a later work [25]. The balance equations are also derived there. Like Green and Laws [24], Rubin, in a recent work [52], also proposes a kinematic model that allows the directors to be just linearly independent (neither unit-normed nor orthogonal). Here two of the directors span a rod's cross-section while the third one is tangential to the centerline of a rod and hence is not necessarily perpendicular to its cross-section. It may be mentioned though that keeping the third director perpendicular to a rod's cross-section not only helps to separate in-plane cross-sectional deformation from rigid motion of its cross-section, but it also enables easy identification of strain invariants based on material symmetry of a rod, as shown in a later section. In the works of Hodges [30], cross-sectional deformation is accounted for only through a suitable constitutive law and is not considered explicitly in the one-dimensional equations governing global deformation of a rod. Thus, global deformation of a rod is not allowed to depend on its cross-sectional deformation. As mentioned by him, such a formulation is suitable only if (a) local constraints on the cross-sectional deformation are assumed to be negligible and (b) cross-sectional deformation is unrestrained. In the present Chapter, no such restriction is assumed; infact it is shown later that the proposed formulation does reduce to that of Hodges' when such restrictions are imposed. Recent work by Gould and Burton [22] uses a novel idea of a "rod theory on rod theory" which is restricted to modeling of hollow tubes. Here the authors model cross-sectional deformation using a per-

turbation scheme that yields the most favored shape (energetically) an isolated closed ring would take on when deformed. This idea assumes, however, that any cross-section (closed ring) is isolated from its neighboring cross-sections. In the present author's view, it may be more appropriate to regard a hollow rod as a pack of infinite closed rings (each ring being coupled to its nearest neighbors) where the boundary conditions as well as lateral tractions (if any) influence the shape of a deformed cross-section. To be specific, in addition to lateral traction, deformations such as axial stretch, bending and twist may also dictate the deformed shape of a cross-section. In addition to failing to capture the Poisson type coupling between the cross-sectional stretch and the axial stretch, the theory by Gould and Burton [22] is also restricted to modeling isotropic and linear material behavior. In another work, Antman [1] constraints the third director to be unit-normed as well as orthogonal to the other two directors which span the plane of a cross-section. The two cross-sectional directors are allowed to stretch and become non-orthogonal. Following Antman, in this dissertation also the third director is taken to be unit-normed and perpendicular to the other two cross-sectional directors. In addition, three new field variables are defined in order to capture cross-sectional deformation: two of them allow anisotropic stretching of a cross-section (this lets the cross-sectional directors to not be unit-normed) while the last one allows in-plane cross-sectional shearing (this lets the two cross-sectional directors become non-orthogonal). The kinematics still only allows in-plane deformation, i.e., a plane section remains a plane, thereby excluding the possibility of warping of a cross-section. In essence, in the first step, the two cross-sectional directors stretch and also become non-orthogonal while in the second step, the three directors are allowed to rigidly rotate as in the special Cosserat theory of rods. As opposed to Antman's kinematic setup and

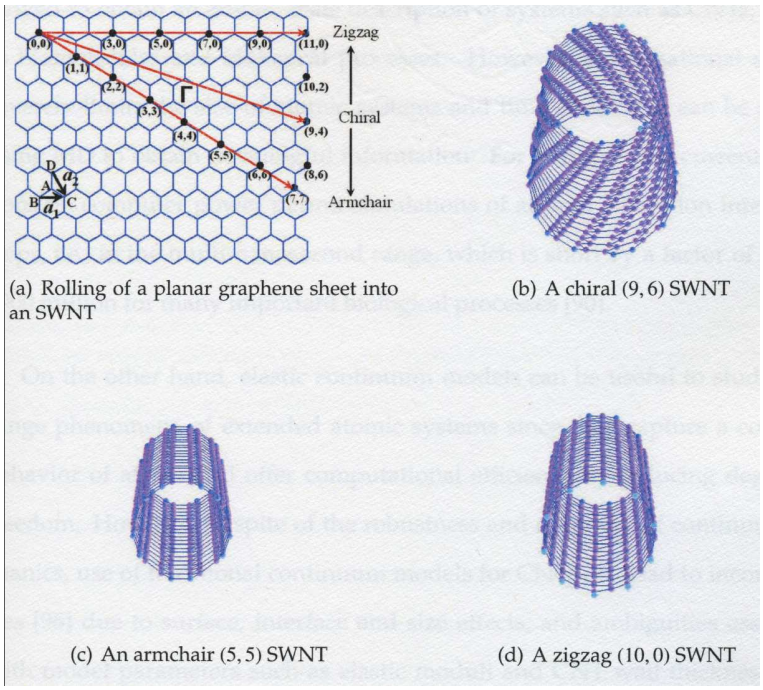

Figure 1.1: Rolling of a planar graphene sheet into Single-walled Carbon Nanotubes (SWCNTs)

the resulting theory [1], this two step decomposition allows convenient application of material symmetry. It also leads to development of a formulation which preserves the strain measures as well as the balance equations of the special Cosserat theory of rods, while introducing three additional cross-sectional strain measures as well as the equilibrium equations corresponding to the three new field variables. Thus the new formulation proposed here appears as a somewhat straightforward extension of the special Cosserat theory of rods.

The last Chapter of this dissertation is concerned with one-dimensional modeling of deformation of single-walled carbon nanotubes (SWCNTs). Carbon nanotubes (CNTs) are nanometer sized cylinders made up of carbon atoms which possess extraordinary electrical, thermal, and mechanical properties. A single-walled carbon nanotube (SWCNT) is a CNT formed from a single atomic layer

comprised of a hexagonal network of carbon atoms that has been rolled up to form a seamless, hollow cylinder (see Fig.1.1), and it is of interest to understand how the underlying atomic structure determines its macroscopic properties. The intriguing properties of CNTs have aroused a strong interest in their possible use in nano-electro-mechanical systems (NEMS) such as nanowires, or as active components in electronic devices such as field-effect transistors. Chapter 5 focusses on computing the elastic moduli of a nanotube, taking into consideration its underlying atomic structure. Elastic continuum models are useful to study long-range phenomena of extended atomic systems since they capture a collective behavior of atoms and offer computational efficiency by reducing the total degrees of freedom. In spite of this, the use of traditional continuum models for CNTs can lead to inconsistencies [61] due to surface, interface and size effects, and ambiguities associated with model parameters such as elastic moduli and CNT wall thickness. In this Chapter, a one-dimensional rod model is used to study the elastic properties of carbon nanotubes. Certainly the ambiguity associated with the wall thickness of a nanotube is no more present when the nanotube is modeled as a rod. A limitation of an earlier approach [5] in this regard has been in assuming rigidity of a nanotube's cross-section. As carbon nanotubes do exhibit large deformation of their cross-sections [49], Gould and Burton [22] develop a rod model with deformable cross-section to model nanotubes. However as mentioned earlier, this model has several limitations and drawbacks. We accordingly employ the rod model proposed in Chapter 4. Although this model cannot capture out-of-plane deformation of a rod's cross-section (such as warping), this deformation mode is expected to be insignificant for hollow/ thin tubes having "closed-face" cross-sections. Atomistic simulations are performed on a representative unit cell of a (9,6) single-walled

chiral carbon nanotube using a density-functional-based tight-binding (DFTB) method [12, 14], maintaining self-consistency in electronic charges (SCC). The unit cell contains 228 carbon atoms with its length being 18.37 angstrom while the atoms are placed at a radial distance of 5.16 angstrom from its axis. The simulation data are used to estimate the parameters involved in the energy expression (4.35). A judicious choice of numerical experiments allows easy determination of the moduli (associated with the deformation of a cross-section) of a nanotube. Some peculiar observations such as coupled Extension-Twist-Cross-sectional shrinkage deformation of this nanotube, as well as rotation of its neighboring cross-sections in alternate directions due to imposed extension, are observed and further explained using the new rod model. Chapter 6 concludes this dissertation, where several directions for future research are discussed.

CHAPTER 2

STABILITY OF EQUILIBRIA OF NONLINEARLY ELASTIC RODS IN THE PRESENCE OF CONSTRAINTS

2.1 Introduction and Outline

In the present Chapter, a generalized approach to stability of static equilibria of nonlinearly elastic rods, subjected to general loading, boundary conditions and constraints (of both point-wise and integral type), based upon the linearized dynamics stability criterion is presented. Discretization of the governing equations leads to a non-standard (singular) generalized eigenvalue problem. A new efficient sparse-matrix-friendly algorithm is presented to determine its few left-most eigenvalues, which, in turn, yields stability/instability information. For conservative problems, the eigenvalue problem arising from the linearized dynamics stability criterion is also shown to be equivalent to that arising in the determination of constrained local minima of the potential energy. The method is illustrated with several examples. The outline of this Chapter is as follows. In Section 2.2, the special theory of nonlinearly elastic Cosserat rods is summarized. In Section 2.3, linearization of the spatial weak form of the full dynamical rod equations about an equilibrium is derived. Section 2.4 deals with the finite dimensional approximation of the linearized weak form and the associated eigenvalue problem (1.1). Here a new algorithm to compute a few left-most eigenvalues of (1.1) is also presented. In Section 2.5 the method is illustrated with some examples of large, spatial buckling of elastic rods. The formulation, as proposed by Healey and Mehta [29], is employed in concert with AUTO [9] to compute equilibria. It should be mentioned that the former has the advantage

of consistently delivering a well-posed nonlinear 2-point boundary value problem in a *linear* space. In the first example, a boundary value problem governing the spatial equilibria of a finite rod with intrinsic curvature [11] is considered. In particular, stability exchange during the helical "perversions" of a straight rod in tension are shown. Then large helical buckled states of a compressed hemitropic rod with clamped ends [28, 50] are shown. The third example is associated with the stability of a spatial cantilevered rod in the shape of a ruler subjected to a lateral load. Finally, a non-conservative follower load problem is considered. In Section 2.6, discretization error and convergence issues are briefly discussed. Section 2.7 concludes this Chapter.

2.2 Brief Description of an Elastic Rod

Let $\{\mathbf{e}_1, \mathbf{e}_2, \mathbf{e}_3\}$ denote a fixed, right-handed, orthonormal basis for $\mathbf{R}^3$. Let us consider a straight rod of unit length occupying a reference configuration parallel to $\mathbf{e}_3$ and s $\in [0, 1]$ denote the arclength coordinate (of the centerline) in the undeformed configuration and **r**(s,t) denote the position vector (with respect to some fixed origin) of the material point originally at "s" in the reference configuration for any given time "t". Similarly, let **R**(s,t) denote the rotation of the cross-section spanned by $\{\mathbf{e}_1, \mathbf{e}_2\}$. The first two unit vectors of the orthonormal field defined by

$$\mathbf{d}_i(s,t) = \mathbf{R}(s,t)\mathbf{e}_i, \quad i = 1, 2, 3 \tag{2.1}$$

are called directors in the special Cosserat theory. The deformed configuration of a rod at any given time "t" is uniquely specified by the field variables **r**(·,t) and **R**(·,t). Henceforth the time variable "t" will be explicitly written only when necessary, and differentiation of a field variable with respect to arclength is de-

noted $\frac{d}{ds} \equiv ()'$ while that with respect to time is denoted $\frac{d}{dt} \equiv \dot{()}$. Unless mentioned otherwise, repeated Latin indices sum from 1 to 3 while repeated Greek indices sum from 1 to 2.

Differentiating equation (2.1) with respect to the arclength coordinate "s" yields:

$$\mathbf{d}_i' = \mathbf{R}'\mathbf{R}^T\mathbf{d}_i, \quad i = 1, 2, 3. \tag{2.2}$$

Let us write

$$\mathbf{r}' = \nu_i\mathbf{d}_i \quad \text{and} \quad \boldsymbol{\kappa} = \kappa_i\mathbf{d}_i. \tag{2.3}$$

Here $\boldsymbol{\kappa}$ is the axial vector of the skew symmetric matrix $\mathbf{R}'\mathbf{R}^T$. The numbers ν_i and κ_i are the "strains" in this theory [1]; ν_1, ν_2 are "shears", ν_3 is the "axial stretch", κ_1, κ_2 are "curvatures", and κ_3 is the "twist". Let $\mathbf{n}$(s) and $\mathbf{m}$(s) denote the internal contact force and internal moment respectively, which act on the cross-section originally at "s" in the reference configuration. Let us also write

$$\mathbf{n} = n_i\mathbf{d}_i, \quad \text{and} \quad \mathbf{m} = m_i\mathbf{d}_i. \tag{2.4}$$

Here n_1, n_2 are "shear forces", n_3 is the "axial force", m_1, m_2 are "bending moments", and m_3 is the "torque" or "twisting moment". For a hyperelastic rod, the existence of a twice-differentiable, scalar-valued stored energy function $W(\nu_1, \nu_2, \nu_3, \kappa_1, \kappa_2, \kappa_3)$ is assumed throughout this Chapter. If we define the triples $\underline{\mathrm{n}} = (n_1, n_2, n_3)$, $\underline{\mathrm{m}} = (m_1, m_2, m_3)$, $\underline{\mathrm{v}} = (\nu_1, \nu_2, \nu_3)$, and $\underline{\mathrm{k}} = (\kappa_1, \kappa_2, \kappa_3)$, then

$$\underline{\mathrm{n}} = \frac{\partial W}{\partial \underline{\mathrm{v}}}, \quad \underline{\mathrm{m}} = \frac{\partial W}{\partial \underline{\mathrm{k}}}. \tag{2.5}$$

Equations (2.5) are the constitutive laws of a rod. We make the physically reasonable assumption that the Hessian, $D^2W(.)$, is a positive-definite matrix for each of its arguments on $\mathbf{R}^2 \times (0, \infty) \times \mathbf{R}^3$. Assuming that the rod is subjected

to a distributed, external body force per unit of undeformed length $\mathbf{b}(s)$ and a distributed, external body couple per unit of undeformed length $\mathbf{g}(s)$, and that the centroid and the center of mass of cross-section coincide, the local form of the balance laws have the form:

$$\mathbf{n}' + \mathbf{b} = \rho A \ddot{\mathbf{r}} \tag{2.6}$$

and

$$\mathbf{m}' + \mathbf{r}' \times \mathbf{n} + \mathbf{g} = \rho[\dot{\mathbf{I}}\mathbf{w}]. \tag{2.7}$$

Here ρ denotes mass per unit volume while "A" denotes area of the cross section at a given arclength "s". Similarly "$\mathbf{I}$" and "$\mathbf{w}$" denote the moment of area tensor and the angular velocity of the cross-section respectively. The following equations represent pointwise constraints for rods (if any):

Unshearability:

$$\nu_\alpha \equiv \mathbf{r}' \cdot \mathbf{Re}_\alpha = 0, \quad \alpha = 1, 2 \tag{2.8}$$

Inextensibility:

$$\nu_3 \equiv \mathbf{r}' \cdot \mathbf{Re}_3 = 1 \tag{2.9}$$

For unshearable and/or inextensible rods, shear forces and/or axial forces, respectively, are the unknown fields. In such cases the balance laws are supplemented with equations (2.8) and/or (2.9), respectively.

2.3 Linearization of the Weak Form

In order for the rod equations to be satisfied pointwise, $\mathbf{r}(\cdot,t)$ and $\mathbf{R}(\cdot,t)$ should be of class C^2. To relax this requirement as well as for numerical convenience, let us deal with a weak form of the rod equations which enables $\mathbf{r}(\cdot,t)$ and $\mathbf{R}(\cdot,t)$ to lie in a relatively weaker space of C^1.

A spatial weak form of the equations is obtained by multiplying each of (2.6)-(2.9) by smooth test functions and then integrating their sum over the length of the rod, as follows:

$$G \equiv \int_0^1 \Big[(\rho A \ddot{\mathbf{r}} - \mathbf{n}') \cdot \boldsymbol{\eta}_0 + \Big(\rho [\dot{\mathbf{I}}\mathbf{w}] - \mathbf{m}' - \mathbf{r}' \times \mathbf{n} \Big) \cdot \boldsymbol{\psi} + [\lambda_\alpha \mathbf{r}' \cdot \mathbf{R}\mathbf{e}_\alpha + \lambda_3 (\mathbf{r}' \cdot \mathbf{R}\mathbf{e}_3 - 1)] \Big] ds = 0 \tag{2.10}$$

for all admissible smooth test functions $\boldsymbol{\eta}(s) \equiv (\boldsymbol{\eta}_0(s), \boldsymbol{\psi}(s))$, $\lambda_\alpha(s)$ and $\lambda_3(s)$. Here $\boldsymbol{\eta}_0$ and $\boldsymbol{\psi}$ correspond to smooth variations of $\mathbf{r}$ and $\mathbf{R}$ respectively, the latter explained more precisely below (after eq. (2.12)). The functions λ_α and λ_3 correspond to smooth varitaions of shear forces n_α and the axial force n_3 respectively. Hence, depending on the boundary conditions, these test functions may vanish at the boundary. The terms corresponding to λ_α and/or λ_3 appear only when the rod is unshearable and/or inextensible, respectively. Let us also assume that no distributive force or couple acts on the rod. Upon integration by parts, one can get: $G = G_{static} + G_{dynamic}$, where

$$G_{static} \equiv \int_0^1 \Big[\mathbf{n} \cdot (\boldsymbol{\eta}_0' - \boldsymbol{\psi} \times \mathbf{r}') + \mathbf{m} \cdot \boldsymbol{\psi}' + \lambda_\alpha \mathbf{r}' \cdot \mathbf{R}\mathbf{e}_\alpha + \lambda_3 (\mathbf{r}' \cdot \mathbf{R}\mathbf{e}_3 - 1) \Big] ds - (\mathbf{n} \cdot \boldsymbol{\eta}_0 + \mathbf{m} \cdot \boldsymbol{\psi}) \Big|_0^1 \tag{2.11}$$

$$G_{dynamic} \equiv \int_0^1 \left(\rho A\ddot{\mathbf{r}} \cdot \boldsymbol{\eta}_0 + \rho[\mathbf{I}\dot{\mathbf{w}}] \cdot \boldsymbol{\psi}\right) ds \tag{2.12}$$

Of course the elasticity laws (2.5) for $\mathbf{m}$ and the non-reactive components of $\mathbf{n}$ (via (2.4)) also need to be incorporated in order to complete (2.11). Note that the last term in (2.11) vanishes in the case of Dirichlet problems (or for free boundary conditions) as the admissible smooth test functions (or forces and moments) vanish at the boundary in such cases.

In order to linearize the weak form, let $\mathbf{r}_\epsilon(s,t) = \mathbf{r}(s) + \epsilon\triangle\mathbf{r}(s,t)$, and $\mathbf{R}_\epsilon(s,t) = exp(\epsilon\triangle\boldsymbol{\Theta}(s,t))\mathbf{R}(s)$ be the time-dependent perturbed configuration of a rod about any equilibrium configuration ($\mathbf{r}$(s), $\mathbf{R}$(s)). Here $exp(\cdot)$ denotes the usual exponential function defined on 3×3 matrices, and $\triangle\boldsymbol{\Theta}(s,t)$ is a smooth, admissible, skew-matrix valued variation. Let $\triangle\boldsymbol{\theta}(s,t)$ denote the unique axial vector field associated with $\triangle\boldsymbol{\Theta}(s,t)$. Note that the admissibility of the vector-valued variation $\boldsymbol{\psi}$ appearing in (2.10)-(2.12) (at the boundary) is the same as that dictated by $\triangle\boldsymbol{\theta}(s,t)$. As in Simo [54], observe that $\mathbf{R}_\epsilon(s,t)$, so defined, is an SO(3)-valued (proper rotation) function. In the presence of unshearability and/or inextensibility, let us also assume perturbation of the shear forces and/or axial force respectively, as follows:

$n_{\alpha,\epsilon}(s,t) = n_\alpha(s) + \epsilon\triangle n_\alpha(s,t), \quad n_{3,\epsilon}(s,t) = n_3(s) + \epsilon\triangle n_3(s,t)$

Let us further assume that the time-dependent perturbations about the equilibrium configurtion are of the form:

$$\triangle\boldsymbol{\zeta}(s,t) = \triangle\boldsymbol{\zeta}_0(s)\exp(\omega t). \tag{2.13}$$

At static equilibrium, $G(\mathbf{r},\mathbf{R},\underline{\mathrm{n}};\boldsymbol{\eta},\boldsymbol{\lambda}) \equiv 0$. Hence, using Taylor's expansion, $G(\mathbf{r}_\epsilon,\mathbf{R}_\epsilon,\underline{\mathrm{n}}_\epsilon;\boldsymbol{\eta},\boldsymbol{\lambda}) = \epsilon DG(\mathbf{r},\mathbf{R},\underline{\mathrm{n}};\boldsymbol{\eta},\boldsymbol{\lambda})\triangle\boldsymbol{\zeta} + o(|\epsilon\triangle\boldsymbol{\zeta}|)$. Upon ignoring the higher order terms, all time dependent perturbed solutions are then given by $DG(.)\triangle\boldsymbol{\zeta} = 0$.

On substituting the perturbation form (2.13), one gets a generalized eigenvalue problem:

$$DG_{static}\triangle\boldsymbol{\zeta}_0 = -\omega^2 DG_{dynamic}\triangle\boldsymbol{\zeta}_0 \tag{2.14}$$

that must be satisfied for all admissible smooth test functions $(\boldsymbol{\eta}, \boldsymbol{\lambda})$. Here $\mu = -\omega^2$ is the corresponding eigenvalue. From (2.13), perturbations grow in time if "ω" has a positive real part. If eigenvalues "μ" of (2.14) are positive, then "ω" always turn out to be purely imaginary. These eigenvalues admit perturbations whose amplitude remain constant in time and hence do not affect stability of a system. On the other hand, presence of a negative eigenvalue admits "ω" with a positive real part, rendering the system unstable. Thus, for conservative/symmetric problems, if the smallest (algebraic)/ left-most eigenvalue is positive, then the corresponding equilibrium configuration is considered as stable. Thus one only needs to look at the left-most spectrum of (2.14). While for non-conservative/asymmetric problems, the presence of either a negative eigenvalue or a complex eigenvalue renders the equilibrium configuration unstable. Therefore in such cases, one should not only check the left-most spectrum but also check for the presence of a complex eigenvalue. The latter can be established by looking for the eigenvalue with the largest imaginary part.

As $G_{dynamic}$ is independent of constraints, it has the same expression for both flexible(constraint-free) as well as constrained rods. Below, the linearized form of G, for both its dynamic and static parts, is shown. For DG_{static}, the linearized integral terms are reported from (2.11) for the three cases of unconstrained, unshearable, and unshearable-inextensible rods in (2.16)-(2.18), respectively, while

the linearized boundary terms from (2.11) are given in (2.19).

$$
\begin{aligned}
DG_{dynamic}\begin{bmatrix}\triangle\mathbf{r}\\ \triangle\boldsymbol{\theta}\end{bmatrix} &\equiv \int_0^1 \rho\left(A\triangle\ddot{\mathbf{r}}\cdot\boldsymbol{\eta_0} + \mathbf{R}\mathbf{I}_0\mathbf{R}^T\triangle\ddot{\boldsymbol{\theta}}\cdot\boldsymbol{\psi}\right)ds \\
\text{or, } DG_{dynamic}\begin{bmatrix}\triangle\mathbf{r}_0\\ \triangle\boldsymbol{\theta}_0\end{bmatrix} &\equiv \omega^2\int_0^1 \rho\begin{bmatrix}A\,\mathbf{I} & \mathbf{O}\\ \mathbf{O} & \mathbf{R}\mathbf{I}_0\mathbf{R}^T\end{bmatrix}\begin{bmatrix}\triangle\mathbf{r}_0\\ \triangle\boldsymbol{\theta}_0\end{bmatrix}\cdot\begin{bmatrix}\boldsymbol{\eta_0}\\ \boldsymbol{\psi}\end{bmatrix}ds
\end{aligned}
\tag{2.15}
$$

Following the notation of Simo [54], let us define

$$
\mathbf{H}_{(6\times6)} = \begin{bmatrix}\frac{\partial^2 W}{\partial \underline{\mathrm{v}}^2} & \frac{\partial^2 W}{\partial \underline{\mathrm{v}}\partial \underline{\mathrm{k}}}\\ \frac{\partial^2 W}{\partial \underline{\mathrm{k}}\partial \underline{\mathrm{v}}} & \frac{\partial^2 W}{\partial \underline{\mathrm{k}}^2}\end{bmatrix},\quad \boldsymbol{\Pi}_{(6\times6)} = \begin{bmatrix}\mathbf{R} & \mathbf{O}\\ \mathbf{O} & \mathbf{R}\end{bmatrix},\quad \mathbf{E}^T_{(6\times6)} = \begin{bmatrix}\mathbf{1}\frac{d}{ds} & \mathbf{r}'\times\\ \mathbf{O} & \mathbf{1}\frac{d}{ds}\end{bmatrix}
$$

Flexible rods:

$$
DG_{static}\begin{bmatrix}\triangle\mathbf{r}_0\\ \triangle\boldsymbol{\theta}_0\end{bmatrix} \equiv \int_0^1 \left[\left(\boldsymbol{\Pi}\mathbf{H}\boldsymbol{\Pi}^T\mathbf{E}^T + \begin{bmatrix}\mathbf{O} & -\mathbf{n}\times\\ \mathbf{O} & -\mathbf{m}\times\end{bmatrix}\right)\begin{bmatrix}\triangle\mathbf{r}_0\\ \triangle\boldsymbol{\theta}_0\end{bmatrix}\cdot\mathbf{E}^T\begin{bmatrix}\boldsymbol{\eta_0}\\ \boldsymbol{\psi}\end{bmatrix} + (\mathbf{n}\times\triangle\mathbf{r}_0')\cdot\boldsymbol{\psi}\right]ds
\tag{2.16}
$$

Unshearable rods:

$$
\mathbf{H}_{(4\times4)} = \begin{bmatrix}\frac{\partial^2 W}{\partial \nu_3^2} & \frac{\partial^2 W}{\partial \nu_3\partial \underline{\mathrm{k}}}\\ \frac{\partial^2 W}{\partial \underline{\mathrm{k}}\partial \nu_3} & \frac{\partial^2 W}{\partial \underline{\mathrm{k}}^2}\end{bmatrix},\quad \boldsymbol{\Pi}_{(6\times4)} = \begin{bmatrix}\mathbf{Re}_3 & \mathbf{O}\\ \mathbf{0} & \mathbf{R}\end{bmatrix},
$$

$$
\begin{aligned}
DG_{static}\begin{bmatrix}\triangle\mathbf{r}_0\\ \triangle\boldsymbol{\theta}_0\\ \triangle n_{1,0}\\ \triangle n_{2,0}\end{bmatrix} &\equiv \int_0^1 \left[\left(\boldsymbol{\Pi}\mathbf{H}\boldsymbol{\Pi}^T\mathbf{E}^T + \begin{bmatrix}\mathbf{O} & -\mathbf{n}\times\\ \mathbf{O} & -\mathbf{m}\times\end{bmatrix}\right)\begin{bmatrix}\triangle\mathbf{r}_0\\ \triangle\boldsymbol{\theta}_0\end{bmatrix}\cdot\mathbf{E}^T\begin{bmatrix}\boldsymbol{\eta_0}\\ \boldsymbol{\psi}\end{bmatrix} + (\mathbf{n}\times\triangle\mathbf{r}_0')\cdot\boldsymbol{\psi}\right]ds \\
&+ \int_0^1\left[\begin{bmatrix}\mathbf{Re}_1 & \mathbf{Re}_2\end{bmatrix}\begin{bmatrix}\triangle n_{1,0}\\ \triangle n_{2,0}\end{bmatrix}\cdot\begin{bmatrix}\mathbf{1}\frac{d}{ds} & \mathbf{r}'\times\end{bmatrix}\begin{bmatrix}\boldsymbol{\eta_0}\\ \boldsymbol{\psi}\end{bmatrix} + \begin{bmatrix}\mathbf{1}\frac{d}{ds} & \mathbf{r}'\times\end{bmatrix}\begin{bmatrix}\triangle\mathbf{r}_0\\ \triangle\boldsymbol{\theta}_0\end{bmatrix}\cdot\begin{bmatrix}\mathbf{Re}_1 & \mathbf{Re}_2\end{bmatrix}\begin{bmatrix}\lambda_1\\ \lambda_2\end{bmatrix}\right]ds
\end{aligned}
\tag{2.17}
$$

Unshearable and Inextensible rods:

$$\mathbf{H}_{(3\times3)} = \frac{\partial^2 W}{\partial \underline{\mathbf{k}}^2}, \quad \mathbf{\Pi}_{(3\times3)} = \mathbf{R}$$

$$DG_{static}\begin{bmatrix} \triangle\mathbf{r}_0 \\ \triangle\boldsymbol{\theta}_0 \\ \triangle\underline{\mathrm{n}}_0 \end{bmatrix} \equiv \int_0^1 \left[\mathbf{\Pi}\mathbf{H}\mathbf{\Pi}^T \triangle\boldsymbol{\theta}_0' \cdot \boldsymbol{\psi}' + \begin{bmatrix} \mathbf{O} & -\mathbf{n}\times \\ \mathbf{O} & -\mathbf{m}\times \end{bmatrix} \begin{bmatrix} \triangle\mathbf{r}_0 \\ \triangle\boldsymbol{\theta}_0 \end{bmatrix} \cdot \mathbf{E}^T \begin{bmatrix} \boldsymbol{\eta_0} \\ \boldsymbol{\psi} \end{bmatrix} + (\mathbf{n} \times \triangle\mathbf{r}_0') \cdot \boldsymbol{\psi} \right] ds$$

$$+ \int_0^1 \left[\mathbf{R}\triangle\underline{\mathrm{n}}_0 \cdot \begin{bmatrix} \mathbf{1}\frac{d}{ds} & \mathbf{r}'\times \end{bmatrix} \begin{bmatrix} \boldsymbol{\eta_0} \\ \boldsymbol{\psi} \end{bmatrix} + \begin{bmatrix} \mathbf{1}\frac{d}{ds} & \mathbf{r}'\times \end{bmatrix} \begin{bmatrix} \triangle\mathbf{r}_0 \\ \triangle\boldsymbol{\theta}_0 \end{bmatrix} \cdot \mathbf{R}\,\boldsymbol{\lambda} \right] ds \tag{2.18}$$

Linearization of boundary terms in (2.11):

$$DG_{static,bdry} = -\left[\frac{\partial \mathbf{n}}{\partial \mathbf{r}} \triangle\mathbf{r}_0 \cdot \boldsymbol{\eta}_0 + \left(\frac{\partial \mathbf{m}}{\partial \mathbf{R}} \triangle\mathbf{\Theta}_0 \mathbf{R} \right) \cdot \boldsymbol{\psi} \right]\Bigg|_0^1 - \left[\left(\frac{\partial \mathbf{n}}{\partial \mathbf{R}} \triangle\mathbf{\Theta}_0 \mathbf{R} \right) \cdot \boldsymbol{\eta}_0 + \frac{\partial \mathbf{m}}{\partial \mathbf{r}} \triangle\mathbf{r}_0 \cdot \boldsymbol{\psi} \right]\Bigg|_0^1 \tag{2.19}$$

In all the expressions above, $\triangle\boldsymbol{\theta}_0$ denotes the axial vector field of the skew-matrix valued field $\triangle\mathbf{\Theta}_0$. From (2.15)-(2), $DG_{dynamic}$ is a symmetric and positive definite operator. The linearized boundary term (2.19) vanishes in the case of dead loading, whereas for live loading it typically makes a non-symmetric contribution to DG_{static}.

2.4 Finite Dimensional Approximation of the Linearized Form and Solution of the corresponding Eigenvalue Problem

The eigenvalue problem (2.14) should be satisfied for all smooth test functions $(\boldsymbol{\eta}, \boldsymbol{\lambda})$. For the purpose of numerical computation, the smooth test functions as well as the spatial perturbations $\left(\triangle\mathbf{r}_0, \triangle\boldsymbol{\theta}_0, \triangle\underline{\mathrm{n}}_0\right)$ are approximated by finite dimensional piecewise linear functions. This leads to a spatial discretization of

(2.14), which is a matrix eigenvalue problem:

$$\begin{bmatrix} \mathbf{K}_{m\times m} & \mathbf{C}_{m\times p} \\ \mathbf{C}^T{}_{p\times m} & \mathbf{O}_{p\times p} \end{bmatrix} \begin{bmatrix} \begin{bmatrix} \triangle\mathbf{r}_0 \\ \triangle\boldsymbol{\theta}_0 \end{bmatrix} \\ \triangle\underline{\mathrm{n}}_0 \end{bmatrix} = \mu \begin{bmatrix} \mathbf{M}_{m\times m} & \mathbf{O} \\ \mathbf{O} & \mathbf{O} \end{bmatrix} \begin{bmatrix} \begin{bmatrix} \triangle\mathbf{r}_0 \\ \triangle\boldsymbol{\theta}_0 \end{bmatrix} \\ \triangle\underline{\mathrm{n}}_0 \end{bmatrix} \tag{2.20}$$

For flexible rods, it reduces to:

$$\mathbf{K}_{m\times m} \begin{bmatrix} \triangle\mathbf{r}_0 \\ \triangle\boldsymbol{\theta}_0 \end{bmatrix} = \mu\, \mathbf{M}_{m\times m} \begin{bmatrix} \triangle\mathbf{r}_0 \\ \triangle\boldsymbol{\theta}_0 \end{bmatrix} \tag{2.21}$$

Here, subscripts denote the dimension of the respective block matrices. The symbols **K** and **M** denote the block tri-diagonal stiffness and mass matrices respectively. The stiffness matrix **K** is symmetric for conservative loadings at static equilibrium [54]. For non-conservative loadings, **K** is non-symmetric, which is due to the linearization of the boundary terms in (2.11). The mass matrix **M** is symmetric and positive-definite, while **C** is a rectangular matrix representing the constraints present in the problem. A sufficient condition for the success of the Lagrange-multiplier method is that the columns of **C** should be linearly independent [57]. The number of columns "p" in **C** equals the total number of discretized constraints present. For example, in the case of pointwise constraints, **C** is block tridiagonal and "p" is of the order of number of discrete points "n" used to represent a rod (e.g. unshearbale rods: $p \approx 2n$, inextensible and unshearable rods: $p \approx 3n$) while for problems with integral constrains, **C** is dense and $p \ll m(\equiv 6n)$. It should be noted from equation (2.20) that the presence of constraints makes the eigenvalue problem singular. In particular, the right-hand side matrix in (2.20) is singular, and hence, the computation of eigenvalues becomes difficult. The eigen-system (2.20) has an interesting property: it has "2p" undesirable eigenvalues that lie at infinity. They are termed spurious eigenvalues. An efficient procedure to compute a few left-most eigen-

values of (2.20) is the Krylov Subspace method. One of the difficulties of using this method for system (2.20) is that the Arnoldi vectors generated during the process get corrupted with spurious eigen directions and the method then converges to or gets corrupted with spurious eigenvalues. One can refer to refs. [18, 56] for the Krylov Subspace method and Arnoldi iterations and refs. [37, 46, 51] for detailed discussions on purification strategies specific to the eigen problem (2.20).

For the reader's convenience, a reduced version of (2.20), also shown in ref. [6], is first presented below that eliminates all the spurious eigenvalues but preserves the remaining finite eigenvalues. Splitting equation (2.20) into two parts, one can get:

$$\begin{gathered} \mathbf{K}\begin{bmatrix} \triangle \mathbf{r}_0 \\ \triangle \boldsymbol{\theta}_0 \end{bmatrix} + \mathbf{C} \triangle \underline{\mathrm{n}}_0 = \mu\, \mathbf{M} \begin{bmatrix} \triangle \mathbf{r}_0 \\ \triangle \boldsymbol{\theta}_0 \end{bmatrix} \\ \mathbf{C}^T \begin{bmatrix} \triangle \mathbf{r}_0 \\ \triangle \boldsymbol{\theta}_0 \end{bmatrix} = \mathbf{0} \end{gathered} \tag{2.22}$$

The Q-R factorization of $\mathbf{C}$ leads to: $\mathbf{C} \equiv \begin{bmatrix} \mathbf{Q1} & \mathbf{Q2} \end{bmatrix} \begin{bmatrix} \mathbf{R1} \\ \mathbf{0} \end{bmatrix} \equiv \mathbf{Q1}\ \mathbf{R1}$. This implies that the columns of **Q1** make an orthonormal basis that spans the subspace formed by columns of $\mathbf{C}$ while columns of **Q2** span the subspace which is the orthogonal complement of that formed by columns of **Q1** or $\mathbf{C}$. Hence, the second part of (2.22) implies that the spatial perturbations of the "basic" unknowns are orthogonal to the subspace formed by columns of **Q1** or, $(\triangle \mathbf{r}_0,\ \triangle \boldsymbol{\theta}_0) = \mathbf{Q2}\ \triangle \boldsymbol{\zeta}_0$. Here, $\triangle \boldsymbol{\zeta}_0$ can be thought of as the generalized coordinates required to represent the constrained system at the linearized level. Substituting this into the first part

of equation (2.22) and premultiplying the same by $\mathbf{Q2}^T$ simplifies it to:

$$\begin{aligned}\left(\mathbf{Q2^T K\ Q2}\right)\triangle\boldsymbol{\zeta}_0 &= \mu\ \left(\mathbf{Q2^T M\ Q2}\right)\triangle\boldsymbol{\zeta}_0 \\ \tilde{\mathbf{K}}\triangle\boldsymbol{\zeta}_0 &= \mu\ \tilde{\mathbf{M}}\triangle\boldsymbol{\zeta}_0\end{aligned} \tag{2.23}$$

In addition to eliminating all the spurious eigenvalues present in (2.20), this reduction step reduces the dimension of the matrix equation from 'm+p' to 'm-p'.

For conservative/symmetric cases, where $\mathbf{K}$ and hence $\tilde{\mathbf{K}}$ are each symmetric, it can be shown that the signs of the eigenvalues are determined only through $\tilde{\mathbf{K}}$ while the projected mass matrix $\tilde{\mathbf{M}}$ only affects the magnitudes of these eigenvalues. Since the stability of a symmetric system is determined only through signs of eigenvalues, one can replace $\tilde{\mathbf{M}}$ with an identity matrix as shown below.

$$\left(\mathbf{Q2^T K\ Q2}\right)\triangle\boldsymbol{\zeta}_0 = \mu\ \mathbf{I}\triangle\boldsymbol{\zeta}_0 \tag{2.24}$$

One arrives at the same eigenvalue problem (2.24) if one starts from the minimum-potential-energy formulation instead of linearized dynamics. In the former case, $\mathbf{K}$ is the discrete 2nd variation operator of the constrained potential energy. Thus, eq.(2.24) establishes an equivalence between the minimum-potential-energy method and the linearized stability method for conservative problems. Indeed, the former is based solely on statics and hence does not take into cognizance the effect of the mass matrix.

Since the new matrices $\tilde{\mathbf{K}}$ and $\tilde{\mathbf{M}}$, also called the projected stiffness and mass matrices, respectively, become dense, (2.23) is an inefficient reduction for numerical computation of eigenvalues. However, a new algorithm that can exploit this reduction in a sparse-matrix-friendly way is proposed as shown in the following subsection. A limitation of this algorithm is further shown at the end.

2.4.1 An Efficient Algorithm to compute Eigenvalues of the Reduced Problem

As noted earlier, $\tilde{\mathbf{K}}$ should not be formed explicitly since one loses sparsity of the matrices present in (2.20). Because computational efficiency of the current eigensolvers (e.g., Arnoldi Iteration procedure) depends crucially on efficient computation of the matrix-vector product, one does not need to form $\tilde{\mathbf{K}}$ explicitly if the matrix-vector product can be efficiently carried out without explicitly forming it. To begin with, one need not even form **Q2** explicitly but utilize its structure as follows.

Let us say we have integral constraints in the system, the number of constraints being 3. Then $\mathbf{C}$ is an m $\times$ 3 dense matrix. Further, let $\mathbf{v}_i$ be the vector required to annihilate all the entries below the i^{th} row in the i^{th} column of $\mathbf{C}$ during the Q-R factorization of $\mathbf{C}$ (via householder transformation). Then,

$$\mathbf{Q} = \left(\mathbf{I}_m - 2\mathbf{v}_1\mathbf{v}_1^T\right)\begin{bmatrix} 1 & \mathbf{0} \\ \mathbf{0} & \left(\mathbf{I}_{m-1} - 2\mathbf{v}_2\mathbf{v}_2^T\right) \end{bmatrix}\begin{bmatrix} \mathbf{I}_2 & \mathbf{0} \\ \mathbf{0} & \left(\mathbf{I}_{m-2} - 2\mathbf{v}_3\mathbf{v}_3^T\right) \end{bmatrix} \tag{2.25}$$

or,

$$\mathbf{Q} = \left(\mathbf{I}_m - 2\mathbf{v}_1\mathbf{v}_1^T\right)\left(\mathbf{I}_m - 2\tilde{\mathbf{v}}_2\tilde{\mathbf{v}}_2^T\right)\left(\mathbf{I}_m - 2\tilde{\mathbf{v}}_3\tilde{\mathbf{v}}_3^T\right) \tag{2.26}$$

Here, $\tilde{\mathbf{v}}_2 = \begin{bmatrix} 0 \\ \mathbf{v}_2 \end{bmatrix}$ and $\tilde{\mathbf{v}}_3 = \begin{bmatrix} 0 \\ 0 \\ \mathbf{v}_3 \end{bmatrix}$

Further, $\mathbf{Q2}\ \mathbf{x} \equiv \mathbf{Q}\begin{bmatrix} 0 \\ 0 \\ 0 \\ \mathbf{x} \end{bmatrix}$. Hence, using the structure of $\mathbf{Q}$, one can form $\mathbf{Q2}\,\mathbf{x}$ efficiently in O(m) steps. Similarly, one can also form the product $\mathbf{Q2}^T\mathbf{x}$ and hence $\left(\mathbf{Q2}^T\mathbf{KQ2}\right)\mathbf{x}$ in O(m) steps. In case of pointwise constraints, $\mathbf{C}$ is block tri-diagonal, therefore one can use Given's rotation to compute its Q-R factorization in O(m) steps. One can then exploit the structure of the $\mathbf{Q}$ matrix along similar lines as above, to efficiently compute $\left(\mathbf{Q2}^T\mathbf{KQ2}\right)\mathbf{x}$.

It is also possible to accelerate convergence to the left-most eigenvalues via a "shift-invert" transformation (2.27) or a Cayleigh transformation (2.28), e.g., [46]. This is necessary when the left-most eigenvalues are clustered or not well separated.

$$(\tilde{\mathbf{K}} - \alpha_1\mathbf{I})^{-1}\mathrm{x} = \theta\,\mathrm{x} \tag{2.27}$$

$$(\tilde{\mathbf{K}} - \alpha_1\mathbf{I})^{-1}(\tilde{\mathbf{K}} - \alpha_2\mathbf{I})\mathrm{x} = \theta\,\mathrm{x} \tag{2.28}$$

For example, in the case of the Cayleigh transformation, the transformed eigenvalues θ are related to the original eigenvalues μ via $\theta = (\mu - \alpha_1)^{-1}(\mu - \alpha_2)$. Hence, the desired eigenvalues (close to α_1) are amplified and become well separated. In particular: $\mathrm{Re}(\mu) \geq (\leq)\frac{1}{2}(\alpha_1 + \alpha_2) \Leftrightarrow |\theta| \leq (\geq)1$. Here, α_1 is taken to be smaller than α_2. But, chosing the optimal shift parameters α_1 and α_2 a priori is not easy, as one needs to know the location of the left-most eigenvalues. In addition, one also needs to form the matrix-vector product:

$(\tilde{\mathbf{K}} - \alpha_1 \mathbf{I})^{-1}$x or $\left(\mathbf{Q2}^T (\mathbf{K} - \alpha_1 \mathbf{I})\, \mathbf{Q2}\right)^{-1}$ x efficiently. A formula for the inverse of the "shifted-projected matrix" $\left(\mathbf{Q2}^T (\mathbf{K} - \alpha_1 \mathbf{I})\, \mathbf{Q2}\right)$ is derived below to facilitate this computation.

Let, A = K - α_1I. Then, $(Q^T AQ)(Q^T A^{-1} Q) = I$

or,

$$\begin{bmatrix} Q1^T AQ1 & Q1^T AQ2 \\ Q2^T AQ1 & Q2^T AQ2 \end{bmatrix} \begin{bmatrix} Q1^T A^{-1} Q1 & Q1^T A^{-1} Q2 \\ Q2^T A^{-1} Q1 & Q2^T A^{-1} Q2 \end{bmatrix} = I \qquad (2.29)$$

Multiplying the 2nd row with the 2nd column and upon some algebraic manipulation, one can find:

$$\left(Q2^T AQ2\right)^{-1} = \left(Q2^T A^{-1} Q2\right)\left[I - \left(Q2^T AQ1\right)\left(Q1^T A^{-1} Q2\right)\right]^{-1} \qquad (2.30)$$

Further, using the Shermann Morrison formula to find the inverse of $I - \left(Q2^T AQ1\right)\left(Q1^T A^{-1} Q2\right)$ and using the identity $I = Q1Q1^T + Q2Q2^T$, one arrives at:

$$\left(Q2^T AQ2\right)^{-1} = \left(Q2^T A^{-1} Q2\right) - \left(Q2^T A^{-1} Q1\right)\left(Q1^T A^{-1} Q1\right)^{-1}\left(Q1^T A^{-1} Q2\right) \qquad (2.31)$$

In order to use the formula (2.31) to efficiently compute the matrix-vector product, the inverse of $\left(Q1^T A^{-1} Q1\right)$ is required. For problems with integral constraints (let us say 3), the matrix $\left(Q1^T A^{-1} Q1\right)$ is of dimension 3. So, one can explicitly compute its inverse and use the same in the formula (2.31). A step by step algorithm is shown below as to how the matrix-vector product is implemented with the formula (2.31):

1. Compute the factorization of A.
2. AinvQ1 = A\Q1, AinvQ2x = A\(Q2 x).
3. $\left(Q2^T AQ2\right)^{-1}$ x = $Q2^T \left(\text{AinvQ2x} - \text{AinvQ1}\left(\left(Q1^T \text{AinvQ1}\right)^{-1}\left(Q1^T \text{AinvQ2x}\right)\right)\right)$

For problems with point-wise constraints, $\left(Q1^T A^{-1} Q1\right)$ has dimension of the order of "n" and hence the formula (2.31) is of no use. Due to this limitation, the following two cases need be analyzed using the large singular eigen problem as presented efficiently in ref. [51]:

1. Point-wise constrained conservative problems having clustered left-most eigenvalues

2. Point-wise constrained non-conservative problems (as in Example 5.4 below)

2.5 Examples

In this section, several examples are presented with the proposed methodology. In the first three examples, new stability results are obtained. In the last (non-conservative) case, the algorithm is tested against a classical result. First the static equilibria are computed using the approach of Healey and Mehta [29]. Once an equilibrium is computed, the associated stiffness matrix **K** and the constraint matrix **C** are assembled using the finite element procedure. Then, the algorithm developed is used to deduce stability. As mentioned earlier, the mass matrix **M** is formed only for non-conservative problems. In order to accelerate convergence for problems with clustered left-most eigenvalues, use of the Cayleigh transformation is advocated. In all the examples, the continuation is started with a stable solution and then we move towards the unstable regime as the parameter is varied. Thus, to begin with, the left-most eigenvalues, being positive, are also the smallest magnitude eigenvalues. This enables use of the "shift-invert" transformation (with zero shift parameter) to compute the two smallest magnitude eigenvalues. This, in turn, provides information about the

region where the left-most eigenvalues lie. Then, we can set: $\alpha_1 = \frac{\mu_1+\mu_2}{2}$ and $\alpha_2 = 2\mu_2 - \alpha_1$ as parameters of the Cayleigh transformation [51] during the continuation process. Here, μ_1 and μ_2 are the two left-most eigenvalues which evolve with the continuation algorithm. For this particular choice, all the desired eigenvalues $\mu < \mu_2$ are transformed to $|\theta| > 1$.

MATLAB's EIGS() function is used to compute the smallest magnitude eigenvalue using the "shift-invert" strategy in the initial step and the largest magnitude eigenvalues of the Cayleigh transformed system during the continuation process. For the examples below, their stability diagrams are shown where the stable branches are shown as solid thick line while the unstable branches are shown as dotted lines. The number of negative eigenvalues for each of the branches are also shown alongside the respective branches.

2.5.1 Perversion of a "Telephone Cord"

In the first example, stability of helical solutions and so-called perversions or helical-reversal solutions exhibited by a rod of finite length with intrinsic curvature, e.g. a telephone cord, is shown. Please refer to ref. [45] for an analytical study of the perversion solutions of an infinite rod and to ref. [11] for a systematic study of the class of finite-length rod problems considered here. Let us assume an unshearable, inextensible rod with initial curvature κ_0 about the $\mathbf{e}_1$ axis. Its constitutive laws are summarized in Table 2.1. The intrinsic curvature κ_0 is related to the length of the rod "L" via $N\frac{2\pi}{\kappa_0} = L$ where "N" corresponds to the number of turns in the cord. For numerical simulation, let us assign the intrinsic curvature κ_0 to be 3π which corresponds to N = 1.5. At s=0, the rod is clamped

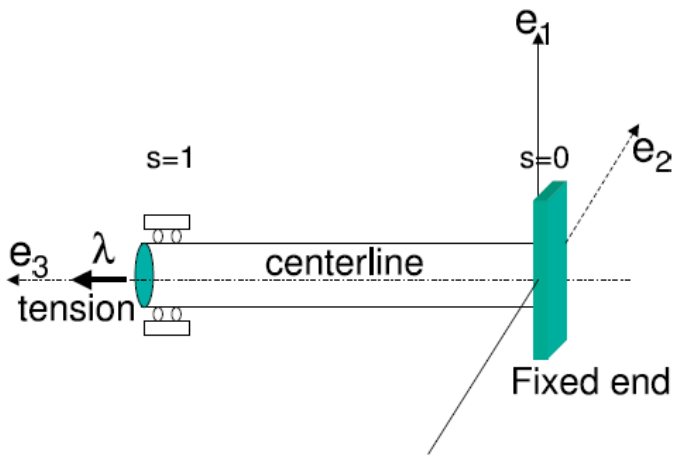

Figure 2.1: Schematic of a Telephone Cord shown in its stressed configuration with the boundary conditions

while at s=1, it is clamped against rotation and transverse displacements. Axial tension is also imposed at the end s = 1 as shown in Fig.2.1. The left-most eigenvalues in this example are not clustered. Hence, no Cayleigh transformation strategy is needed to accelerate convergence to the left-most eigenvalue. Boundary conditions for the rod are as follows:

$$\begin{aligned} &\mathbf{r}(0) = \mathbf{0},\ \mathbf{R}(0) = \mathbf{I} \text{ (the identity)} \\ &r_1(1) = 0,\ r_2(1) = 0,\ n_3(1) = \lambda,\ \mathbf{R}(1) = \mathbf{I} \end{aligned} \tag{2.32}$$

It should be noted that unshearability and inextensibility are the pointwise con-

Table 2.1: Constitutive Laws for a Telephone Cord

Unshearable	$\nu_1 = 0, \nu_2 = 0$
Inextensible	$\nu_3 = 1$
Bending moments	$m_1 = \kappa_1, m_2 = \kappa_2 - \kappa_0$
Twisting moment	$m_3 = \kappa_3$

straints. Hence there are 9 unknowns at each of the interior nodes of the discretized rod: 3 each for perturbations in the center-line displacement, rotation

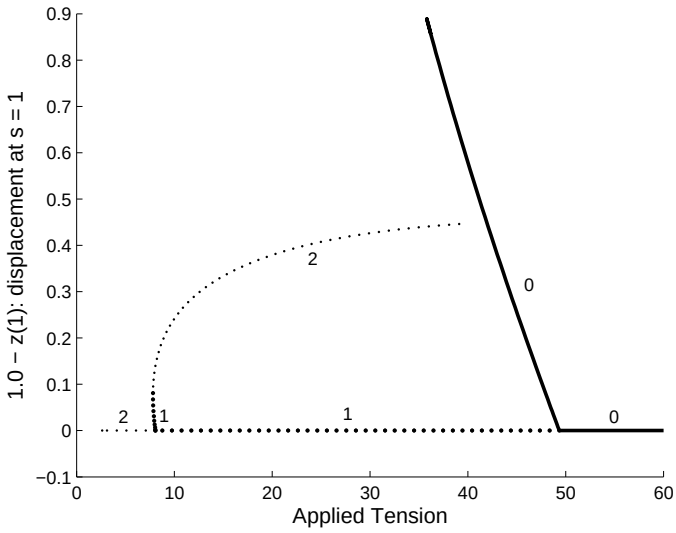

Figure 2.2: Stability diagram for a Telephone Cord as applied Tension is being varied

and the internal force. In order to be compatible with the given boundary conditions, perturbation in the axial force must vanish at s=1. Assuming that the rod is discretized into "n" elements, the number of unknowns corresponding to the perturbation variables are as follows:

$\triangle \mathbf{r}_0$: 3n-2, $\triangle \boldsymbol{\theta}_0$: 3n-3, $\triangle \underline{n}_0$: 3n+2.

Accordingly, the dimension of the matrices involved are as follows:

K: (6n-5) × (6n-5) & **C**: (6n-5) × (3n+2)

And, the dimension of the reduced system in equation (2.23) is (3n-7)×(3n-7).

Numerical Results

Fig.2.2 shows the stability diagram for a telephone cord. The reference configuration(straight state) is not its natural configuration. Therefore the diagram shows it to be unstable when the tension applied at one of its ends is low, whereas it is stable for high enough values of tension. Beginning from the high tension side, as tension is decreased, a subcritical pitchfork bifurcation is ob-

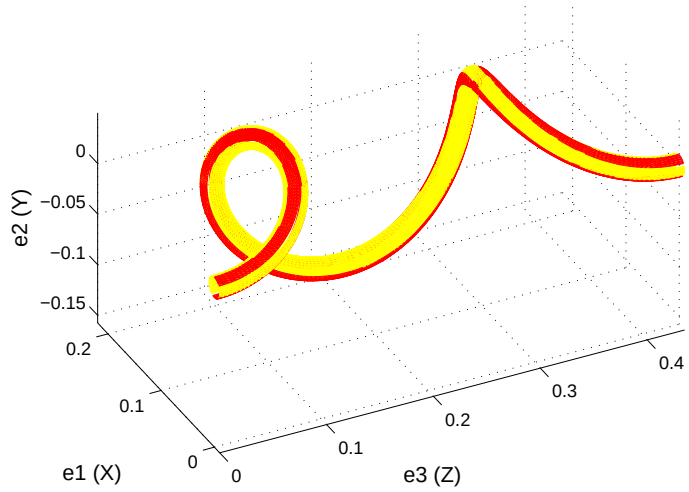

Figure 2.3: A typical non-trivial stable configuration of a Telephone Cord

served. The cord is stable along the non-trivial branch originating from this point, whereas along the trivial branch, one of the positive eigenvalues becomes negative. As the magnitude of tension is kept to decrease, another bifurcation is observed, which is unstable. A turning point is also observed as one moves along this second bifurcating branch - hence the increase from 1 to 2 negative eigenvalues. Stability results along the trivial branch agree with the local analysis presented in ref. [11]. Fig.2.3 shows a typical stable configuration of a telephone cord along the first stable non-trivial branch. Observe that the cord goes from a left-handed helix to a right-handed one in going along the positive z-axis - hence the terminology “perversion”.

2.5.2 Stability of a Compressed “Cable” or a “DNA Strand”

The next example is of an unshearable hemitropic rod (see Table 2.2 for its constitutive laws). Hemitropy is a natural model of long filaments with helical

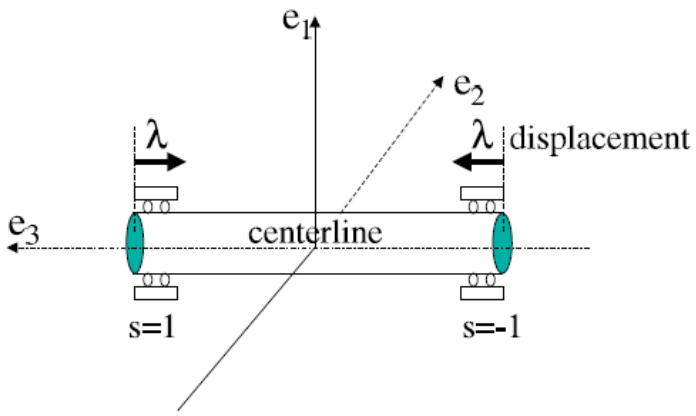

Figure 2.4: Schematic of a compressed rod shown in its reference configuration with boundary conditions at the two ends

micro-structure in the relaxed state [28]. The two ends of the rod are "clamped" against rotation and displacements, while the axial displacements of the two end points are prescribed through the parameter λ as shown in Fig.2.4.

$$\begin{gathered} \mathrm{r}_\alpha(-1) = 0, \alpha = 1,2, \quad \mathrm{r}_3(-1) = (-1+\lambda)L \\ \mathbf{R}(-1) = \mathbf{I} \end{gathered} \tag{2.33}$$

$$\begin{gathered} \mathrm{r}_\alpha(1) = 0, \alpha = 1,2, \quad \mathrm{r}_3(1) = (1-\lambda)L \\ \mathbf{R}(1) = \mathbf{I} \end{gathered} \tag{2.34}$$

Table 2.2: Constitutive Laws of a Hemitropic Rod

Unshearable	$\nu_1 = 0, \nu_2 = 0$
Axial force	$n_3 = g(\nu_3) + A\kappa_3$
Bending moments	$m_1 = C\kappa_1, m_2 = C\kappa_2$
Twisting moment	$m_3 = B\kappa_3 + A(\nu_3 - 1)$

Here the aim is to establish stability of the static solutions as the parameter

λ is increased from zero (where the rod is assumed to be in its reference configuration). The bifurcation analysis for the unshearable case has been studied in ref. [50]. All the solutions of a compressed rod are shown to have a certain "flip" $\mathbf{Z}^2$ isotropy subgroup. Also, due to rotational symmetry, this problem admits a family of connected solutions. This makes computation of an equilibrium solution difficult. Healey and Mehta [29] exploit the complete symmetry to deduce an equivalent set of boundary conditions which admit only isolated solutions. One can further generate all the connected solutions by rotating the obtained isolated solution about the $\mathbf{e}_3$ axis. For details, please refer to refs. [29, 50]. It should be noted that hemitropic rods have point-wise unshearability constraints. Hence, there are 8 unknowns at each of the nodes: 3 each for $\triangle\mathbf{r}_0$ and $\triangle\boldsymbol{\theta}_0$ and 2 for $\triangle n_{\alpha,0}$, perturbation in shear forces. Of these unknowns, $\triangle\mathbf{r}_0$ and $\triangle\boldsymbol{\theta}_0$ vanish at the boundaries. Hence, the size of the matrices involved are as follows:

K: 6(n-1) $\times$ 6(n-1), **C**: 6(n-1) $\times$ 2(n+1)

Accordingly, the reduced problem (2.23) is of dimension 4(n-2) $\times$ 4(n-2).

The left-most eigenvalues in this example are clustered. Therefore, the "shift-invert"/ Cayleigh transformation strategy is required to accelerate convergence. But, as mentioned earlier, in order to use the algorithm to accelerate convergence, integral constraints are needed. An integral-constrained version for an unshearable rod is proposed below. To the best of the author's knowledge, this is the first such formulation for unshearable and extensible rods.

For unshearable rods $\mathbf{r}' = \nu_3\mathbf{R}\mathbf{e}_3$. This suggests thinking of $(\nu_3, \mathbf{R})$, rather than $(\mathbf{r}, \mathbf{R})$, as the configuration variables. Now, unshearability is already inherent

in the new formulation. But one also gets a new set of 3 integral constraints as follows:

$$\begin{aligned} &\int_{-1}^{1} \mathbf{r}' \, ds \equiv 2\,(1-\lambda)\, L\mathbf{e}_3 \\ \text{or,} \quad &\int_{-1}^{1} \left[\nu_3 \mathbf{R}\mathbf{e}_3 - (1-\lambda)\, L\mathbf{e}_3\right] \, ds \equiv \mathbf{0} \end{aligned} \tag{2.35}$$

Equation (2.35) basically says that the two ends of a rod should always remain $2(1-\lambda)L$ distance apart along $\mathbf{e}_3$. An expression for the total potential energy of the rod, Φ, using the new formulation, can be written as:

$$\Phi\left(\nu_3, \mathbf{R}\right) \equiv \int_{-1}^{1} W\left(\nu_3, \underline{\mathrm{k}}\right) \, ds - \mathbf{n} \cdot \int_{-1}^{1} \left[\nu_3 \mathbf{R}\mathbf{e}_3 - (1-\lambda)\, L\mathbf{e}_3\right] \, ds \tag{2.36}$$

Here $\mathbf{n}$ is the constant Lagrange multiplier vector which enforces the integral constraint (2.35). With the new formulation, one now has 4 unknowns at every node as opposed to 8 in the earlier case. Here, the strain variable ν_3 is the new unknown variable along with the configuration variable $\mathbf{R}$. It can therefore be called a "mixed" variational formulation. The first variation of the energy expression (2.36) with respect to $(\nu_3, \mathbf{R})$ provides us with a new set of Euler-Lagrange equations while discretization of its second variation leads to the stiffness and the constraint matrices. This formulation is analyzed in more detail in the next Chapter. The dimension of the matrices with this new formulation for determination of stability are as follows:

K: 4n-2 × 4n-2, **C**: 4n-2 × 3

Accordingly, the reduced problem (2.23) is of dimension 4n-5 × 4n-5. Also, now **Q1** is of dimension 4n-2 × 3. Hence one can use the formula (2.31) to accelerate convergence to the left-most eigenvalues.

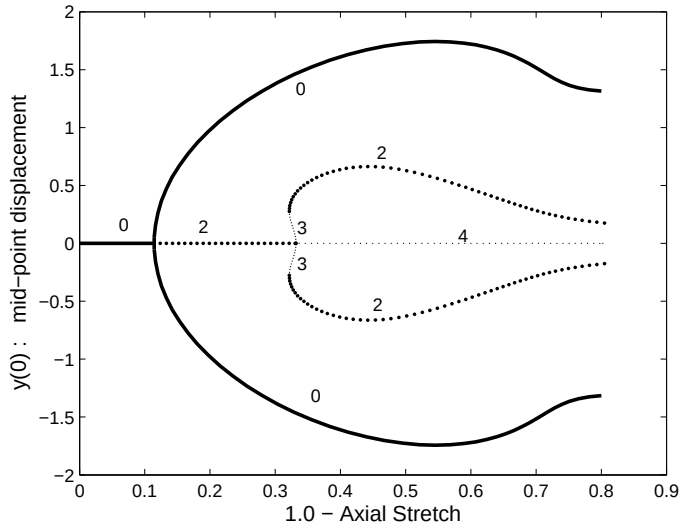

Figure 2.5: Stability diagram for a Compressed Hemitropic rod as the rod is being compressed

Numerical Results

Parameters of the rod for numerical simulation are as follows:

Half length of the rod $(L) = 3,\ g(\nu_3) = 10(\nu_3 - 1),\ A = -3,\ C = 1,\ B = 1$

Fig.2.5 shows the stability diagram of the compressed hemitropic rod. It shows two bifurcation points along the trivial branch. The first bifurcation point is a supercritical pitch-fork. All the eigenvalues are positive before the first bifurcation. After each bifurcation along the trivial branch, two of the positive eigenvalues become negative. There exists an eigenvalue of zero magnitude along all the non-trivial branches since this problem admits an orbit of connected non-trivial solutions. The first non-trivial branch is a stable branch. Along the second non-trivial branch, the number of negative eigenvalues is three as one moves off the trivial branch. Then, as the turning point is reached, one of the negative eigenvalues becomes positive while the remaining eigenvalues have their signs unchanged. Fig.2.6 shows a typical configuration of the rod along the stable

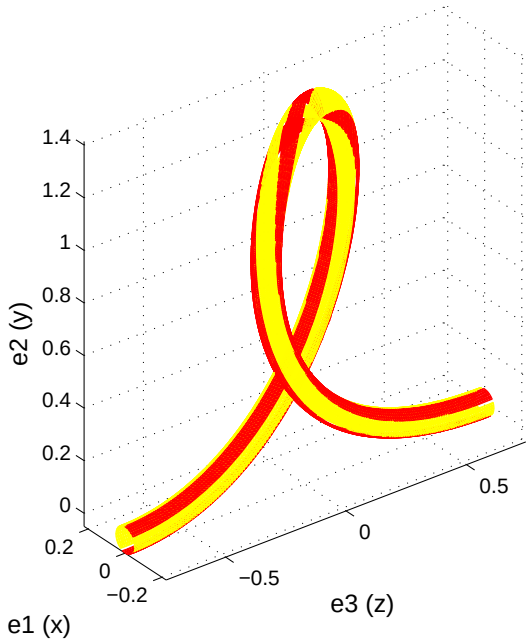

Figure 2.6: A typical stable configuration of a Hemitropic Rod along the 1st non-trivial branch

non-trivial branch.

2.5.3 Stability of a "Ruler" subjected to a lateral end load

In this example, stability of a ruler subjected to a lateral load, the direction of the load being fixed in the global coordinate system, is investigated. By a "ruler", a straight prismatic rod is assumed which has one bending stiffness much larger than the other. As shown in Fig.2.7, the ruler is clamped at one of its ends, while it is free to rotate as well as displace at the other end. The constitutive laws for the rod are shown below in Table 2.3. In particular, observe that one bending stiffness is an order of magnitude larger than the other.

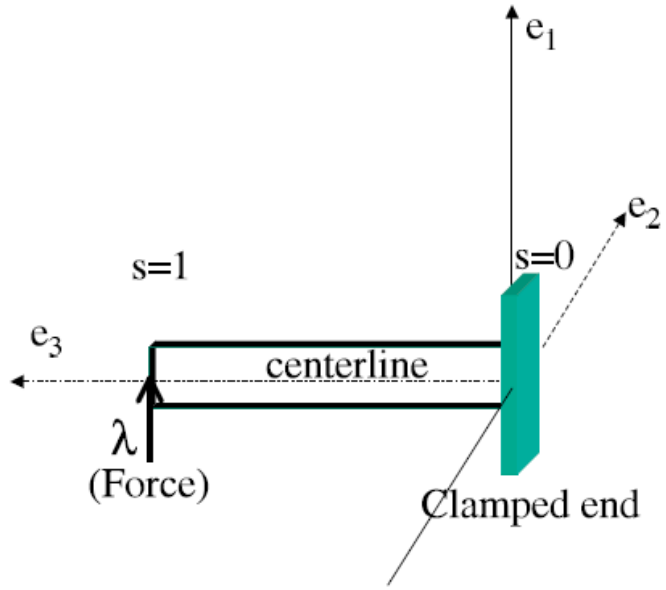

Figure 2.7: A Ruler shown in the reference configuration with the boundary conditions

The rod has pointwise unnshearability constraint. Hence, as in the previous

Table 2.3: Constitutive Laws for a Ruler

Unshearable	$\nu_1 = 0, \nu_2 = 0$
Axial force	$n_3 = 20\log(\nu_3)$
Bending moments	$m_1 = \kappa_1, m_2 = 10\kappa_2$
Twisting moment	$m_3 = \kappa_3$

example, one can again think of $(\nu_3, \mathbf{R})$ as the configuration variables and thus avoid pointwise constraints to facilitate the use of (2.31) in order to accelerate convergence. There is an additional constraint on $(\nu_3, \mathbf{R})$ at s=1. The axial force dictated by the constitutive laws must be compatible with the applied lateral load. An expression for the constrained potential energy is given below for this

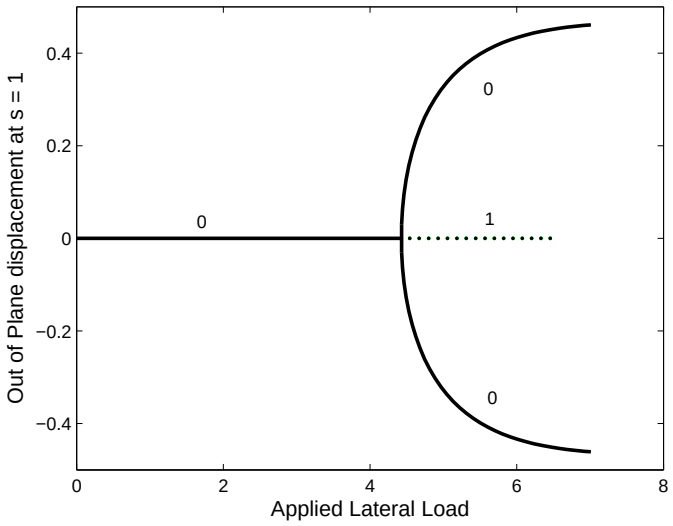

Figure 2.8: Stability diagram for a Ruler as the applied lateral load is increased

particular case:

$$\Phi(\nu_3, \mathbf{R}) \equiv \int_0^1 W\left(\nu_3, \underline{k}\right) ds \; - \; \lambda \mathbf{e}_2 \cdot \int_0^1 \nu_3 \mathbf{R}\mathbf{e}_3 \, ds \; - \; \gamma \left(\frac{\partial W}{\partial \nu_3} - \lambda \mathbf{e}_2 \cdot \mathbf{R}\mathbf{e}_3 \right) \Bigg|_{s=1} \tag{2.37}$$

Here λ is the magnitude of applied lateral force while γ is a scalar Lagrange multiplier. The dimension of the matrices involved are as follows:

K: (4n+3)×(4n+3), **C**: (4n+3)×1

One can observe from the stability diagram in Fig.2.8 that the ruler exhibits a stable planar solution until a critical load is reached where it bifurcates out of the plane. After this bifurcation, the planar solution turns unstable while the non-planar solution becomes stable. Fig.2.9 shows a typical non-planar stable solution for a ruler.

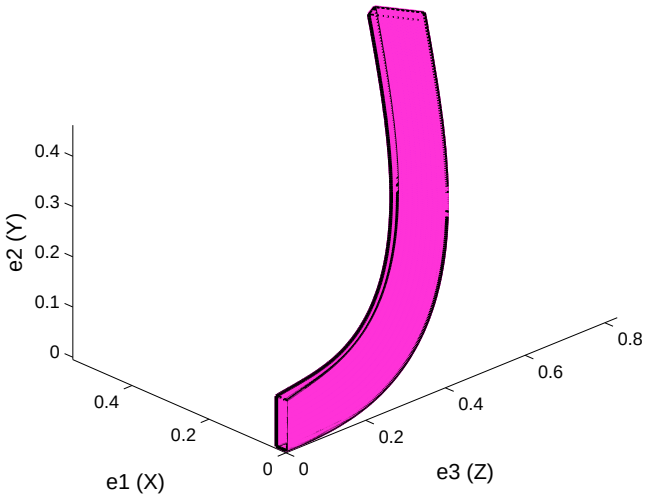

Figure 2.9: A typical non-planar stable configuration of a Ruler along the non-trivial branch

2.5.4 Follower Load Problem (Non-conservative)

The last example concerns problems with non-conservative loadings. The same "ruler", as in the last example, is investigated but here it is assumed to be unshearable as well as inextensible. The constitutive laws are shown in Table 2.4.

As shown in Fig.2.10, the rod is clamped on one end while a compressive

Table 2.4: Constitutive Laws for a Ruler with a tangential follower Load

Unshearable	$\nu_1 = 0, \nu_2 = 0$
Inextensible	$\nu_3 = 1$
Bending moments	$m_1 = \kappa_1, m_2 = 10\kappa_2$
Twisting moment	$m_3 = \kappa_3$

force acts at the other end. The applied force follows the ruler tangentially as it deforms. This generates a non-symmetric stiffness matrix. The problem of the stability of the straight state for this problem is a well known paradigm [2].

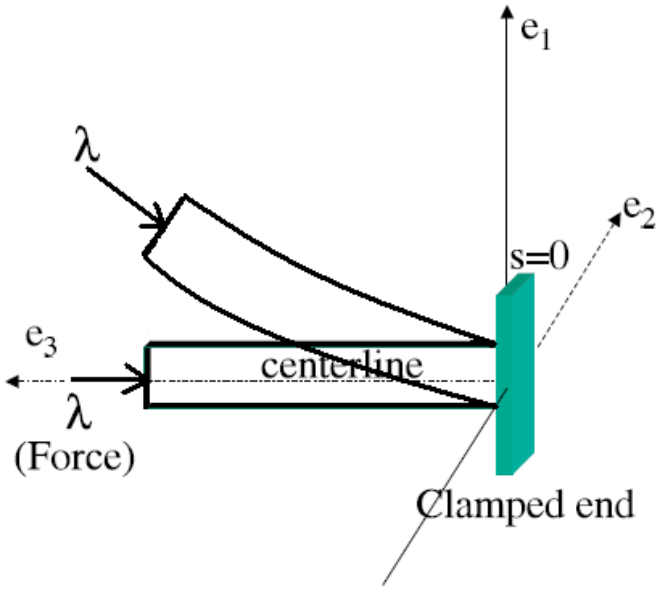

Figure 2.10: Schematic of a Ruler clamped at one end and with a follower load at the other end

Interestingly, it only admits straight static solutions while the non-trivial (non-straight) solutions are dynamic in nature. Thus only the stability of the trivial (straight) solution is studied as the tangential compressive force is varied. Since the stiffness matrix **K** is non-symmetric, the mass matrix **M** is required for the stability analysis. Since the constraints are pointwise in nature and the left-most eigenvalues are clustered, the large singular eigen problem (2.20) is used for stability analysis. This example has interesting eigen properties. At zero load the stiffness matrix **K** is symmetric and hence all the eigenvalues are real and positive. As the compressive load is increased, **K** becomes non-symmetric but its eigenvalues still remain real and positive. In particular, the left-most eigenvalues grow more positive. However, the loss of stability here arises from the birth of complex eigenvalues.

As the desired eigenvalues are also the smallest magnitude eigenvalues, one

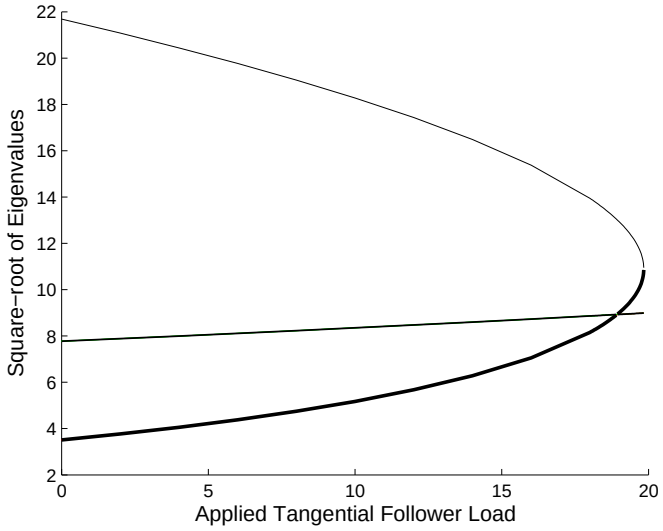

Figure 2.11: Evolution of the 3 left-most eigenvalues along the straight configuration

can use the "shift-invert" strategy on the eigen problem (2.20) as shown below:

$$\begin{bmatrix} \mathbf{K} & \mathbf{C} \\ \mathbf{C}^T & \mathbf{O} \end{bmatrix}^{-1} \begin{bmatrix} \mathbf{M} & \mathbf{O} \\ \mathbf{O} & \mathbf{O} \end{bmatrix} \begin{bmatrix} \begin{bmatrix} \triangle \mathbf{r}_0 \\ \triangle \boldsymbol{\theta}_0 \end{bmatrix} \\ \triangle \underline{\mathrm{n}}_0 \end{bmatrix} = \mu^{-1} \begin{bmatrix} \begin{bmatrix} \triangle \mathbf{r}_0 \\ \triangle \boldsymbol{\theta}_0 \end{bmatrix} \\ \triangle \underline{\mathrm{n}}_0 \end{bmatrix} \tag{2.38}$$

Fig.2.11 depicts evolution of the three left-most eigenvalues as the load is varied. (Note that this is not a bifurcation diagram.) Observe that the 1st and 3rd eigenvalues approach each other as the load is increased until, at a critical load, they coalesce and then become complex (the latter not shown). As mentioned earlier, complex eigenvalues indicate that the straight solution becomes unstable. This is also known as a Hamiltonian-Hopf bifurcation, e.g., [38]. The value of the critical load obtained here (19.9 in magnitude) compares well with the critical load formula ($\frac{2\pi^2 \mathrm{EI}_1}{\mathrm{L}^2} \approx 19.74$) given in ref. [2].

2.6 A Note on Discretization Error and Convergence

This algorithm requires an "accurate" represention of a static equilibrium. In general, this representation is in discrete form, coming from a numerical solver. It already inherits discretization error. Then the global stiffness matrix **K**, mass matrix **M** and constraint matrix **C** are formed. This requires the use of finite element interpolation functions and integration over each of the finite elements. Thus, another error is introduced while forming these matrices.

First a family of solutions $\{u_k\}$ is generated using the approach of Healey and Mehta [29] until $\frac{\|u_k - u_{k-1}\|}{\|u_k\|} < tol$, indicating "convergence". Here, the subscript "k" corresponds to the order of refinement (number of elements used to generate equilibria) while $\|.\|$ denotes the L^2 norm. For all the examples presented, the equilibrium solution converged within 150 elements. Once a converged solution has been obtained, linear shape functions and the mid-point integration rule are used for element integration during the Finite Element Assembly process to form the global matrices. The proposed algorithm further requires the columns of the constraint matrix **C** to be linearly independent. To check this, first the smallest singular value σ_{min} of **C** is found. As entries in the **C** matrix are of the order of element size "h", σ_{min} is dependent on "h". Therefore, linear independency of the columns of **C** is checked by looking at the ratio $\frac{\sigma_{min}}{\mathrm{h}}$. A small value for $\frac{\sigma_{min}}{\mathrm{h}}$ signifies that the columns of **C** are nearly dependent. Table 2.5 shows the ratio $\frac{\sigma_{min}}{\mathrm{h}}$ for different values of element size "h" in the second example 5.2 on "Stability of a Compressed Cable or DNA Strand".

Table 2.5: Smallest singular value (normalized by element size) as a function of the element size

Element size(h)	$\frac{\sigma_{min}}{\mathrm{h}}$
0.12	0.2105
0.06	0.2079
0.04	0.2219
0.03	0.2220

2.7 Concluding Remarks

A generalized computational approach to stability of static equilibria of nonlinearly elastic rods is presented. Based upon linearized dynamics, stability of static equilibria of a rod subjected to general boundary conditions, loadings and constraints - pointwise and/or integral type are obtained. It may be remarked again that any approach based upon Jacobi's conjugate-point method is necessarily limited to stability analysis of conservative problems with Dirichlet boundary conditions (or possibly Neumann boundary conditions [42]) and in the possible presence of integral constraints. The proposed method also provides information about unstable eigen directions which may be utilized to stabilize a system via a suitable feedback control mechanism.

An efficient sparse-matrix-friendly algorithm is also presented to solve the associated eigenvalue problem. As mentioned at the end of Section 2.4, the algorithm has some limitations which can be overcome provided we have an efficient formula for the inverse of a "projected matrix" for the point-wise constrained case. However, the presented algorithm has an advantage over other existing algorithms when applicable. Not only do we work efficiently with a

reduced dimensional problem, but no purification strategy is required as all the spurious eigenvalues are eliminated initially. The computational cost associated with the proposed algorithm is of the same order (O(n)) as that presented in ref. [43], while the approach presented herewith is applicable to a much broader class of problems.

The method was illustrated in the context of four examples. Of these, only the first, Example 5.1 "Perversion of a Telephone Cable" is directly amenable to the conjugate-point method. In the context of Example 5.2, a new "mixed" variational formulation is also presented for a general class of extensible, unshearable rods. This delivers a reduced representation for such rods, which is attractive for numerical computation of equilibria as well as for stability analysis. Indeed, the formulation converts the pointwise unshearability constraints into integral type. Thus, with the new formulation in hand, it is also possible to analyze the second Example 5.2 "Stability of a Compressed Cable or DNA Strand" via the conjugate-point approach [43]. The same cannot be said for the other two Examples 5.3 and 5.4 - the former becuase of the boundary conditions and the latter due to the non-conservative loading.

In the last Example 5.4, the "shift-invert" strategy with a real shift parameter could capture the eigenvalues with "sufficiently" small imaginary parts. Indeed, here the critical load, at which the real eigenvalues first "collide" and then become complex, is only investigated. But, in general, a complex shift may be required to capture the eigenvalues with large imaginary parts [47]. Finally, the non-symmetric stiffness matrix, arising due to linearization of the boundary terms, is connected to its symmetric part via a low ranked matrix. This low rank

connection could be beneficial in developing an algorithm which could exploit the niceties of symmetric problems and yet solve the non-symmetric problem.

CHAPTER 3

A NEW FORMULATION FOR UNSHEARABLE AND EXTENSIBLE RODS

3.1 Introduction and Outline

In Kirchoff rod theory, the centerline displacement of a rod can be expressed purely in terms of the rotation variables. This lets the total number of degrees of freedom to be only three for such rods. But, such reduction is not trivial when extensibility is also included. In this chapter, a new "mixed" variational principle is presented for unshearable rods that lets the total number of degrees of freedom to be four. Recent interests in extensible rods, hemitropic rods in particular [28], would benefit from this reduction. The outline of this Chapter is as follows. In Section 3.2, the new (reduced) Euler Lagrange equations are derived using a mixed variational principle. In Section 3.3, the weak form of the Euler Lagrange equations are presented along with the linearization of the weak form. The linearized weak form is compared with the corresponding form derived using the pointwise unshearability constraint and their equivalence is established. This lets both numerical computation of the equilibria as well as their stability analysis to be deduced via the reduced formulation. Finally in Section 3.4, stability is analyzed analytically along the trivial branch of a compressed hemitropic rod.

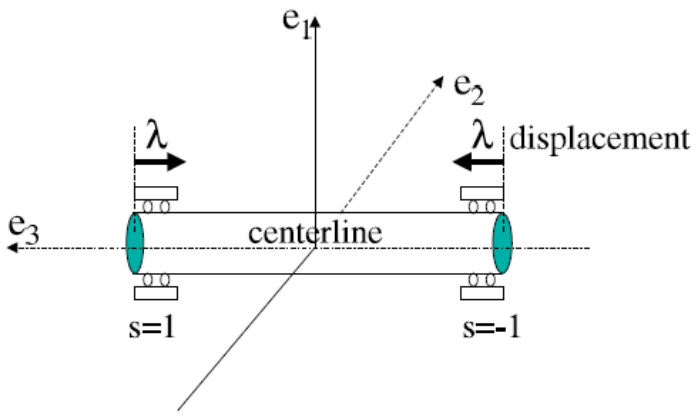

Figure 3.1: An extensible and unshearable rod shown in its reference configuration

3.2 Derivation

Let us take the example of an extensible rod that is clamped at the two ends against rotation as well as displacement. The axial displacements of the two end points are prescribed through the parameter λ as shown in the Fig.3.1.

$$\begin{gathered} \mathrm{r}_\alpha(-1) = 0, \alpha = 1, 2, \quad \mathrm{r}_3(-1) = (-1 + \lambda) L \\ \mathbf{R}(-1) = \mathbf{I} \end{gathered} \tag{3.1}$$

$$\begin{gathered} \mathrm{r}_\alpha(1) = 0, \alpha = 1, 2, \quad \mathrm{r}_3(1) = (1 - \lambda) L \\ \mathbf{R}(1) = \mathbf{I} \end{gathered} \tag{3.2}$$

Such rods have point-wise unshearability constraints. Hence, there are 8 unknowns: 3 each for centerline displacement and the rotation variable and 2 for the Lagrange multipliers (shear forces) that enforce unshearability. Since $\mathbf{r}' = \nu_3 \mathbf{R}\mathbf{e}_3$, this suggests thinking of $(\nu_3, \mathbf{R})$, rather than $(\mathbf{r}, \mathbf{R})$, as the configuration variables. Now unshearability is already inherent in the former. One does get a

Table 3.1: Constitutive Laws of an Extensible and Unshearable Rod

Unshearable	$\nu_1 = 0, \nu_2 = 0$
Axial force	$n_3 = g(\nu_3) + A\kappa_3$
Bending moments	$m_1 = C\kappa_1, m_2 = C\kappa_2$
Twisting moment	$m_3 = B\kappa_3 + A(\nu_3 - 1)$

new set of 3 integral constraints as follows:

$$\begin{aligned} &\int_{-1}^{1} \mathbf{r}' \, ds \equiv 2(1-\lambda) L \mathbf{e}_3 \\ \text{or,} \quad &\int_{-1}^{1} \left[\nu_3 \mathbf{R}\mathbf{e}_3 - (1-\lambda) L \mathbf{e}_3\right] \, ds \equiv \mathbf{0} \end{aligned} \tag{3.3}$$

Equation (3.3) basically says that the two ends of a rod should always remain $2(1-\lambda)L$ distance apart along $\mathbf{e}_3$. An expression for the total potential energy of the rod, Φ, using the new formulation, can be written as:

$$\Phi(\nu_3, \mathbf{R}) \equiv \int_{-1}^{1} W\left(\nu_3, \underline{\mathrm{k}}\right) ds - \mathbf{n} \cdot \int_{-1}^{1} \left[\nu_3 \mathbf{R}\mathbf{e}_3 - (1-\lambda) L \mathbf{e}_3\right] \, ds \tag{3.4}$$

Here $\mathbf{n}$ is the constant Lagrange multiplier vector which enforces the integral constraint (3.3). With the new formulation, one now has 4 unknowns at every node as opposed to 8 in the earlier case. Here, the strain variable ν_3 is the new unknown variable along with the configuration variable $\mathbf{R}$. It is therefore called a "mixed" variational formulation. The first variation of the energy expression (3.4) with respect to $(\nu_3, \mathbf{R})$ provides us with a new set of Euler-Lagrange equations:

$$\begin{aligned} &\frac{\partial W}{\partial \nu_3} - \mathbf{n} \cdot \mathbf{R}\mathbf{e}_3 = 0 \\ &\left(\mathbf{R}\frac{\partial W}{\partial \underline{\mathrm{k}}}\right)' + \nu_3 \mathbf{R}\mathbf{e}_3 \times \mathbf{n} = \mathbf{0} \\ &\textbf{BC:} \quad \mathbf{R}(-1) = \mathbf{R}(1) = \mathbf{I} \end{aligned} \tag{3.5}$$

Equation (3.5)-(1) can also be obtained by integrating the corresponding static version of (2.6) and further projecting the integrated form along the $\mathbf{Re}_3$ axis. It should be noted that there is no boundary condition on the axial stretch ν_3. Equations (3.5) along with the integral constraint equation (3.3) forms a closed mathematical system for analytical/ numerical solution of such rods. Upon comparison with (2.7), the Lagrange multiplier $\mathbf{n}$ in (3.5) is actually the constant internal force acting on a cross-section.

Now we derive the linearized form of the Euler lagrange equations which may be used for both numerical computation of the equilibrium configurations via a finite element procedure as well as for stability analysis as illustrated in the previous Chapter.

3.3 Weak Form of the equations

The weak form of the static Euler Lagrange equations (3.5) along with the integral constraint equation (3.3) delivers us with G_{static} as shown below.

$$\begin{aligned} G_{static} \equiv & \int_{-1}^{1} \left[\left(\frac{\partial W}{\partial \nu_3} - \mathbf{n} \cdot \mathbf{Re}_3 \right) \beta + \mathbf{m} \cdot \boldsymbol{\psi}' - \mathbf{n} \cdot (\boldsymbol{\psi} \times \nu_3 \mathbf{Re}_3) \right] ds \\ & - \boldsymbol{\lambda} \cdot \int_{-1}^{1} \left(\nu_3 \mathbf{Re}_3 - (1-\lambda) L \mathbf{e}_3 \right) ds = 0 \end{aligned} \tag{3.6}$$

for all admissible smooth test functions $\beta(s), \boldsymbol{\psi}(s)$ and the vector $\boldsymbol{\lambda}$. Here β and ψ correspond to smooth variations of ν_3 and $\mathbf{R}$, respectively, while the vector $\boldsymbol{\lambda}$ corresponds to a variation in the constant internal force $\mathbf{n}$. To linearize the weak form (3.6), let $\nu_{3,\epsilon}(s) = \nu_3(s) + \epsilon \triangle \nu_3(s)$ and $\mathbf{R}_\epsilon = exp(\epsilon \triangle \boldsymbol{\Theta}(s)) \mathbf{R}(s)$ as before. Further,

let $\mathbf{n}_\epsilon = \mathbf{n} + \epsilon\triangle\mathbf{n}$. The linearized form then looks as follows:

$$
\begin{aligned}
DG_{static}\begin{bmatrix}\triangle\nu_3\\ \triangle\boldsymbol{\theta}\\ \triangle\mathbf{n}\end{bmatrix} \equiv \int_{-1}^{1}\Bigg[\mathbf{H}\begin{bmatrix}\triangle\nu_3\\ \mathbf{R}^T\triangle\boldsymbol{\theta}'\end{bmatrix}\cdot\begin{bmatrix}\beta\\ \mathbf{R}^T\boldsymbol{\psi}'\end{bmatrix} + \begin{bmatrix}\mathbf{0} & -\mathbf{n}\times\\ \mathbf{0} & -\mathbf{m}\times\end{bmatrix}\begin{bmatrix}\triangle\nu_3\\ \triangle\boldsymbol{\theta}\end{bmatrix}\cdot\begin{bmatrix}\beta\mathbf{Re}_3\\ \boldsymbol{\psi}'\end{bmatrix} \\
- [(\triangle\nu_3\mathbf{Re}_3 + \nu_3\triangle\boldsymbol{\theta}\times\mathbf{Re}_3)\times\mathbf{n}]\cdot\boldsymbol{\psi}\Bigg]ds - \\
\int_{-1}^{1}\Bigg[\begin{bmatrix}(\mathbf{Re}_3)^T\\ \nu_3\mathbf{Re}_3\times\end{bmatrix}\triangle\mathbf{n}\cdot\begin{bmatrix}\beta\\ \boldsymbol{\psi}\end{bmatrix} + \begin{bmatrix}\triangle\nu_3\\ \triangle\boldsymbol{\theta}\end{bmatrix}\cdot\begin{bmatrix}(\mathbf{Re}_3)^T\\ \nu_3\mathbf{Re}_3\times\end{bmatrix}\boldsymbol{\lambda}\Bigg]ds
\end{aligned}
\tag{3.7}
$$

Here $\mathbf{H}$ is as defined in (2.17) (in Chapter 2). The discrete form of the first integral in (3.7) leads to the stiffness matrix $\mathbf{K}$ while the discrete form of the remaining terms leads to the constraint matrix $\mathbf{C}$. The two matrices can then be used both for numerical computation of equilibria as well as for the purpose of stability analysis, as illustrated in Chapter 2. A natural question arises whether the stability results obtained using the integral constraint formulation (3.7) and the pointwise constraint formulation (2.17) of the previous Chapter are the same. In order to explore this comparison, let $\mathbf{r}'_\epsilon = \nu_{3,\epsilon}\,\mathbf{R}_\epsilon\mathbf{e}_3$. Hence,

$$
\mathbf{r}' + \epsilon\triangle\mathbf{r}' = \nu_3\mathbf{Re}_3 + \epsilon\,(\triangle\nu_3\mathbf{Re}_3 + \nu_3\triangle\boldsymbol{\theta}\times\mathbf{Re}_3) + \mathrm{O}(\epsilon^2) \tag{3.8}
$$

or,

$$
\triangle\mathbf{r}' = \triangle\nu_3\mathbf{Re}_3 + \nu_3\triangle\boldsymbol{\theta}\times\mathbf{Re}_3 + \mathrm{O}(\epsilon) \tag{3.9}
$$

Further,

$$
\begin{aligned}
\triangle\nu_3 &= \mathbf{R}^T\,(\triangle\mathbf{r}' - \triangle\boldsymbol{\theta}\times\nu_3\mathbf{Re}_3)\cdot\mathbf{e}_3 + \mathrm{O}(\epsilon)\\
\text{Similarly,}\quad \beta &= \mathbf{R}^T\,(\boldsymbol{\eta}'_0 - \boldsymbol{\psi}\times\nu_3\mathbf{Re}_3)\cdot\mathbf{e}_3 + \mathrm{O}(\epsilon)
\end{aligned}
\tag{3.10}
$$

Substituting (3.9) and (3.10) into (3.7) and further noting that $DG_{static} = \frac{dG}{d\epsilon}\Big|_{\epsilon=0}$, observe that the higher order terms from (3.9) and (3.10) vanish when substituted in (3.7). Upon further rearrangement of terms, a straightforward manipulation shows that the first integral in the expression (3.7) is equal to the first

integral in the expression (2.17). Furthermore, the second integral expression in both (2.17) and (3.7) enforce the appropriate linearized constraint on the perturbation variables thus restraining the later to lie in the same constrained space. Hence the operator DG_{static} from the two different formulations are the same. For a given discretization of the rod, the stability results computed by the projected stiffness matrices (cf. (2.24)) formed using the two different formulations would not match exactly (discretization errors introduced would be different corresponding to the two different representations). In particular, the critical parameter level at which instability occurs could differ a little but even this difference would approach zero in the limit as the number of the discretized elements in the rod approaches infinity. Consequently, one may deduce linearized dynamic stability from the reduced formulation (3.7).

3.4 Stability Analysis along the trivial branch

Now we analyze stability of a compressed rod in its straight state equilibrium configuration as the compression parameter λ is varied. Second variation of (3.4) about the trivial solution ($\nu_3(s) = 1 - \lambda, \mathbf{R}(s) = \mathbf{I}$) is: $\delta^2\Phi\left[\triangle\nu_{3,0}\ , \triangle\boldsymbol{\theta}_0\right] = \delta^2\Phi_1 + \delta^2\Phi_2$ where,

$$\begin{aligned}
\delta^2\Phi_1 &= \int_{-1}^{1} \begin{bmatrix} g' & A \\ A & B \end{bmatrix} \begin{bmatrix} \triangle\nu_{3,0} \\ \triangle\theta_{3,0} \end{bmatrix} \cdot \begin{bmatrix} \triangle\nu_{3,0} \\ \triangle\theta_{3,0} \end{bmatrix} dx \\
\delta^2\Phi_2 &= \int_{-1}^{1} c\left(\triangle\theta'_{1,0}{}^2 + \triangle\theta'_{2,0}{}^2\right) + (1-\lambda)\, g\left(\triangle\theta^2_{1,0} + \triangle\theta^2_{2,0}\right) \\
&\quad - \lambda A\left(\triangle\boldsymbol{\theta}'_0 \times \triangle\boldsymbol{\theta}_0\right) \cdot \mathbf{e}_3 \ ds
\end{aligned} \tag{3.11}$$

The perturbations $(\triangle\nu_{3,0},\ \triangle\boldsymbol{\theta}_0)$ should satisfy the following linearized constraints and the boundary conditions:

$$\begin{gathered}\int_{-1}^{1}\triangle\nu_{3,0}\equiv\int_{-1}^{1}\triangle\theta_{\alpha,0}=0\\ BC:\triangle\boldsymbol{\theta}_0(-1)\equiv\triangle\boldsymbol{\theta}_0(1)=[0,0,0]\end{gathered}\tag{3.12}$$

The associated Jacobi equations [16] of (3.11) satisfying (3.12) can be found either through integration by parts of (3.11) or by linearization of the Euler-Lagrange equations (3.5) as shown below. The same Jacobi equations were also obtained in [50] using a formulation based on pointwise unshearability constraint.

$$\begin{gathered}A\triangle\nu'_{3,0}+B\triangle\theta''_{3,0}=0\\ \triangle\theta''_{3,0}=0\end{gathered}\tag{3.13}$$

$$\begin{bmatrix}\triangle\theta''_{1,0}\\ \triangle\theta''_{2,0}\end{bmatrix}-\lambda A\begin{bmatrix}0&1\\-1&0\end{bmatrix}\begin{bmatrix}\triangle\theta'_{1,0}\\ \triangle\theta'_{2,0}\end{bmatrix}-g(1-\lambda)\begin{bmatrix}\triangle\theta_{1,0}\\ \triangle\theta_{2,0}\end{bmatrix}=\begin{bmatrix}\triangle\theta'_{1,0}\\ \triangle\theta'_{2,0}\end{bmatrix}_{-1}^{1}\equiv\text{constant}\tag{3.14}$$

The solution to the above Jacobi equations must satisfy (3.12). These Jacobi equations do not admit solutions for all the values of the parameter λ. These solutions correpond to the non-trivial solutions at bifurcation points along the trivial branch. It should be noted that $\delta^2\Phi_1$ depends on only $(\triangle\nu_{3,0},\ \triangle\theta_{3,0})$ whereas $\delta^2\Phi_2$ depends on $\triangle\theta_{\alpha,0}$. This means $\delta^2\Phi_1$ and $\delta^2\Phi_2$ are independent of each other. As $\delta^2\Phi_1$ is always positive, one can show that the sign of the second variation $\delta^2\Phi$ depends only on $\delta^2\Phi_2$. Hence, in order to determine stability, one needs to only look at the Jacobi equation (3.14).

Let $\boldsymbol{\theta}\equiv\begin{bmatrix}\triangle\theta_{1,0}\\ \triangle\theta_{2,0}\end{bmatrix}$ for simplicity of notation. Taking a dot product on both sides of the equation (3.14) by $\boldsymbol{\theta}$, we get: $\boldsymbol{\theta}''\cdot\boldsymbol{\theta}+\lambda A(\boldsymbol{\theta}'\times\boldsymbol{\theta})\cdot\mathbf{e}_3-g(1-\lambda)|\theta|^2=\boldsymbol{\theta}'\Big|_{-1}^{1}\cdot\boldsymbol{\theta}$

Now, integrating on both the sides and using the linearized constraints (3.12),

we get:

$$\int |\boldsymbol{\theta}'|^2 + g\,(1-\lambda)\,|\boldsymbol{\theta}|^2 = \lambda A \int (\boldsymbol{\theta}' \times \boldsymbol{\theta}) \cdot \mathbf{e}_3 \tag{3.15}$$

Following Hoffman et al. [33], we can also write equation (3.14) as:

$\mathbf{S}_\lambda \boldsymbol{\theta} \equiv (\mathbf{S1} + \mathbf{S2}_\lambda)\,\boldsymbol{\theta} = \boldsymbol{\theta}'\Big|_{-1}^{1}$

where, $\mathbf{S1}\boldsymbol{\theta} \equiv \boldsymbol{\theta}''$ and $\mathbf{S2}_\lambda \boldsymbol{\theta} \equiv -\lambda A \begin{bmatrix} 0 & 1 \\ -1 & 0 \end{bmatrix} \boldsymbol{\theta}' - g\,(1-\lambda) \begin{bmatrix} 1 & 0 \\ 0 & 1 \end{bmatrix} \boldsymbol{\theta}$

Following are the properties of the $\mathbf{S}$ operator for all admissible $\boldsymbol{\theta}_i$ satisfying (3.12):

1. $\delta^2\Phi_2 \equiv \int_{-1}^{1} \mathbf{S}_\lambda \boldsymbol{\theta} \cdot \boldsymbol{\theta}\, dx \equiv \langle \mathbf{S}_\lambda \boldsymbol{\theta}, \boldsymbol{\theta} \rangle$
2. $\langle \mathbf{S}_\lambda \boldsymbol{\theta}_1, \boldsymbol{\theta}_2 \rangle \equiv \langle \mathbf{S}_\lambda \boldsymbol{\theta}_2, \boldsymbol{\theta}_1 \rangle$

If $\boldsymbol{\theta}_i$ is also a solution to equation (3.14) at parameter value λ_i, then

3. $\langle \mathbf{S}_\lambda \boldsymbol{\theta}_1, \boldsymbol{\theta}_2 \rangle \equiv \langle (\mathbf{S2}_\lambda - \mathbf{S2}_{\lambda_1})\,\boldsymbol{\theta}_1, \boldsymbol{\theta}_2 \rangle$ and $\langle \mathbf{S2}_{\lambda_1} \boldsymbol{\theta}_1, \boldsymbol{\theta}_2 \rangle \equiv \langle \mathbf{S2}_{\lambda_2} \boldsymbol{\theta}_2, \boldsymbol{\theta}_1 \rangle$
4. If $g = -\frac{\lambda}{1-\lambda}$, then $\left\langle \mathbf{S}_\lambda \boldsymbol{\theta}_i, \boldsymbol{\theta}_j \right\rangle \equiv \delta_{ij}$, or $\mathbf{S}$ can be diagonalized by the eigensolutions $\boldsymbol{\theta}_i$

Assuming that $\boldsymbol{\theta}_i$, which are solutions to equation (3.14) at parameter values λ_i, form a basis for the space of functions defined by (3.12), any general admissible perturbation can then be written as: $\boldsymbol{\theta} = \sum_{i=0}^{\infty} \alpha_i \boldsymbol{\theta}_i$. Let us choose a particular constitive law: $g = -\frac{\lambda}{1-\lambda}$, then using property (4) of the $\mathbf{S}$ operator:

$$\begin{aligned}
\left\langle \mathbf{S}_\lambda \sum \boldsymbol{\alpha}_i \theta_i, \sum \boldsymbol{\alpha}_j \theta_j \right\rangle &= \sum |\alpha_i|^2 \langle \mathbf{S}_\lambda \boldsymbol{\theta}_i, \boldsymbol{\theta}_i \rangle = \sum |\alpha_i|^2 \langle (\mathbf{S2}_\lambda - \mathbf{S2}_{\lambda_i})\,\boldsymbol{\theta}_i, \boldsymbol{\theta}_i \rangle \\
&= \sum |\alpha_i|^2 \int (\lambda_i - \lambda) \left(|\boldsymbol{\theta}_i|^2 + A\,(\boldsymbol{\theta}_i' \times \boldsymbol{\theta}_i) \cdot \mathbf{e}_3 \right) \\
&= \sum |\alpha_i|^2 \int (\lambda_i - \lambda) \left(|\boldsymbol{\theta}_i|^2 - |\boldsymbol{\theta}_i|^2 + \lambda^{-1} |\boldsymbol{\theta}_i'|^2 \right) \\
&= \sum |\alpha_i|^2 \int \left(\frac{\lambda_i}{\lambda} - 1 \right) |\boldsymbol{\theta}_i'|^2
\end{aligned}$$

This estimate says that if $\lambda < \lambda_1$, where λ_1 is the first bifurcation point, then the static solution is stable. It also says that as we increase the parameter λ, the

number of unstable directions keep increasing as a bifurcation point is crossed. A more rigorous analysis is required to deduce stability results for any general constitutive law. One can certainly deduce the same via a numerical procedure as outlined in Chapter 2.

CHAPTER 4

A GEOMETRICALLY EXACT ROD MODEL INCLUDING IN-PLANE CROSS-SECTIONAL DEFORMATION

4.1 Introduction and Outline

In this Chapter, a novel approach for nonlinear, three dimensional deformation of a rod is presented that allows in-plane cross-sectional deformation. The approach is based on the concept of multiplicative decomposition, i.e., the deformation of a rod's cross-section is performed in two steps: pure in-plane cross-sectional deformation followed by its rigid motion. This decomposition, in turn, allows straightforward extension of the special Cosserat theory of rods (having rigid cross-section) to a new formulation that also allows in-plane cross-sectional deformation. A complete set of static equilibrium equations along with the boundary conditions necessary for analytical/ numerical solution of the aforementioned deformation problem is then derived. A variational approach to solve the relevant boundary value problem is also presented. Later symmetry arguments are used to derive invariants of the objective strain measures for transversely isotropic rods as well as for rods with inbuilt handedness (hemitropy) such as dna, carbon nanotubes etc. The invariants derived impose restrictions on the form of the strain energy density leading to a simplified form of quadratic strain energy density that exhibits some interesting physically relevant coupling between the different modes of deformation. The outline of this Chapter is as follows. In Section 4.2, the kinematic assumptions used in the proposed theory are discussed in detail and the objective strain measures are further derived. In Section 4.3, a complete set of equilibrium equations are de-

rived along with the necessary boundary conditions in order to analytically/ numerically solve for an equilibrium configuration. Physical description of the stress resultants corresponding to the new cross-sectional strain measures are also provided. This is followed by a variational formulation to solve the balance equations in Section 4.4. Section 4.5 determines restrictions on the 2^{nd} partials of the strain energy density due to application of strong ellipticity from the 3-d continuum theory. In Section 4.6, the concept of material symmetry is applied to derive invariants of the objective strain measures which facilitates in deriving the most general expression for quadratic strain energy in Section 4.7. This is carried out for both transversely isotropic and hemitropic rods. Strong ellipticity is again applied on this specific form of energy density to find additional constraints on the parameters involved. Section 4.8 concludes this Chapter.

4.2 Kinematic Assumptions and the Objective Strain Measures

Let $\{\mathbf{e}_1, \mathbf{e}_2, \mathbf{e}_3\}$ denote a fixed, right-handed, orthonormal basis for $\mathbf{R}^3$ and $\mathbf{X} \equiv (\tilde{\mathbf{X}}, s)$ denote the coordinate of a material point of a rod in its straight state reference configuration while $\mathbf{x}$ denote the coordinate in the deformed configuration of a material point lying at $\mathbf{X}$ in the reference configuration. Here $\tilde{\mathbf{X}} \equiv (X_1, X_2)$ denotes cross-sectional coordinates while s denotes arc-length of the centerline of a rod lying along $\mathbf{e}_3$ in its straight state reference configuration. In this Chapter, the Greek symbol α runs from 1 to 2 unless specified. Furthermore, unless mentioned otherwise, repeated Latin indices sum from 1 to 3 while repeated Greek indices sum from 1 to 2.

As mentioned earlier, in addition to rigid body motion, a cross-section is also

allowed to undergo in-plane cross-sectional deformation with a restriction that any straight line element in a cross-section remains straight even when deformed. Out of plane deformation such as warping is not allowed. The deformation map can now be written as:

$$\mathbf{x}(\mathbf{X}) = \mathbf{r}(s) + X_\alpha \mathbf{d}_\alpha(s) \tag{4.1}$$

Here $\mathbf{r}(.)$ represents displacement of the centerline of a rod while $\mathbf{d}_\alpha$ represents the two cross-sectional directors. The two directors $\mathbf{d}_\alpha$ spanning a cross-section are allowed to become non-orthogonal after deformation. To facilitate this, the deformation map for the directors can be written as:

$$\mathbf{d}_i(s) = \mathbf{R}(s)\mathbf{U}(s)\mathbf{e}_i, \quad \text{for } i = 1 \text{ to } 3 \tag{4.2}$$

The mapping (4.2) is decomposed as a product of 3-d rigid body rotation of a cross-section ($\mathbf{R}$) and in-plane cross-sectional deformation ($\mathbf{U}$). Here $\mathbf{U}$ has a special matrix form in the given coordinate system as shown in (4.4). This form lets the third director $\mathbf{d}_3$ to be unit-normed and perpendicular to the other two directors. It may be noted that the cross-sectional directors $\mathbf{d}_\alpha$ track the deformation of two line elements in the cross-section of a rod that are orthonormal in the straight state reference configuration (possibly the two principal axes) while the director $\mathbf{d}_3$ is fictitious in nature and does not necessarily track any material line element. However, as illustrated in Fig.4.1, this decomposition as introduced in (4.2) is not unique. In order for the directors to attain the final deformation stage, only the product $\mathbf{RU}$ needs be fixed while $\mathbf{R}$ and $\mathbf{U}$ themselves could be arbitrary upto any rotation about an axis perpendicular to the rod's cross-section. For example $\mathbf{RU} = (\mathbf{RQ})(\mathbf{Q}^T\mathbf{U})$ where $\mathbf{Q}$ is any arbitrary rotation of a cross-section about an axis perpendicular to it (twisting of a rod). It should be mentioned that this arbitrariness associated with multiplicative decomposition also occurs in the theory of elastoplasticity [36] and in the theory of tissue

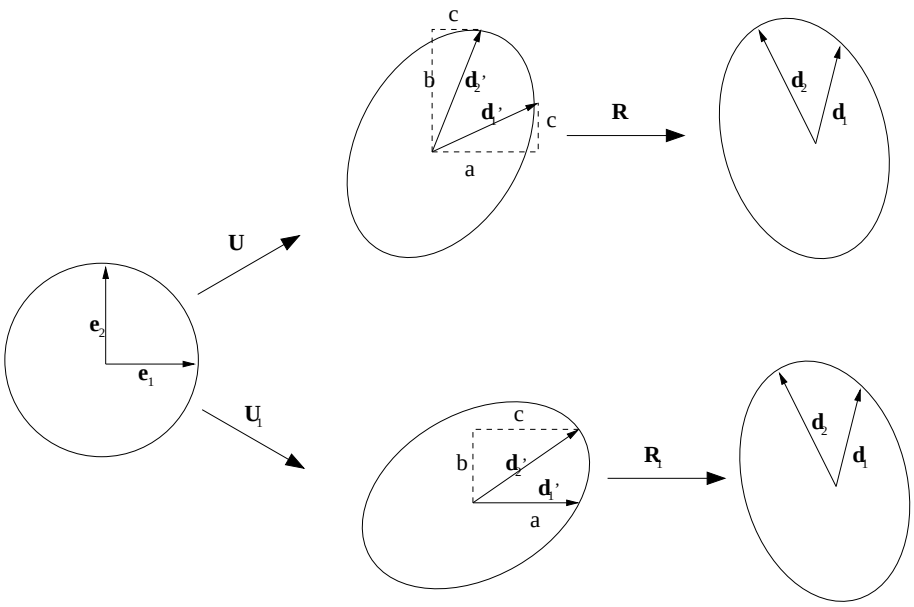

Figure 4.1: A typical cross-section of a rod undergoing in-plane cross-sectional deformation followed by rigid rotation: two possible decompositions

growth [19]. Here this arbitrariness is removed by choosing **U** to be symmetric (top of Fig.4.1). This choice of **R** and **U**, which also corresponds to the unique polar decomposition of the "deformation gradient" of a cross-section, further allows convenient application of material symmetry in a later section. With the aid of Fig.4.1 one can now write:

$$\mathbf{x}(\mathbf{X}) = \mathbf{r}(s) + X_\alpha \mathbf{R}(s)\mathbf{U}(s)\mathbf{e}_\alpha \tag{4.3}$$

The matrix form of **U**, as shown below, is symmetric and positive definite.

$$\mathbf{U}(s) = \begin{bmatrix} a(s) & c(s) & 0 \\ c(s) & b(s) & 0 \\ 0 & 0 & 1 \end{bmatrix} \tag{4.4}$$

From expression (4.3), the shape of a deformed cross-section is only determined by the $X_\alpha \mathbf{U}\mathbf{e}_\alpha$ part of the mapping since **r** and **R** only allow rigid translation

and rigid rotation, respectively, of a cross-section. The tensor **U** being symmetric, its eigenvectors define the two directions along which a cross-section stretches maximally or minimally (the magnitude of the stretch depends on the respective eigenvalue). In particular, this allows a circular cross-section to become an ellipse with its axes alligned along the eigenvectors of **U**. Thus, components of **U** (as shown in (4.4)) define the shape of a deformed cross-section. Here c is a scalar representing in-plane cross-sectional shearing or "degree of non-orthogonality" of the cross-sectional directors. Orientation of the axes of ellipses (in case of initially circular cross-sections) is also governed by c. In case when c is zero, a and b are the scalars that represent stretching of the two cross-sectional directors. The discarded non-symmetric choice for the matrix form of **U**, corresponding to the bottom of Fig.4.1, is shown below for completeness.

$$\mathbf{U}(s) = \begin{bmatrix} a(s) & c(s) & 0 \\ 0 & b(s) & 0 \\ 0 & 0 & 1 \end{bmatrix} \tag{4.5}$$

Now the deformation gradient can be written as:

$$\mathbf{F} \equiv \nabla \mathbf{x} = [\mathbf{r}' + X_\alpha \{\mathbf{R}'\mathbf{U} + \mathbf{R}\mathbf{U}'\}\mathbf{e}_\alpha] \otimes \mathbf{e}_3 + \mathbf{R}\mathbf{U}\mathbf{e}_\alpha \otimes \mathbf{e}_\alpha \tag{4.6}$$

or

$$\mathbf{F} = \mathbf{R}\left[\underline{\mathrm{v}} \otimes \mathbf{e}_3 + X_\alpha \{\mathbf{K}\mathbf{U} + \mathbf{U}'\}\mathbf{e}_\alpha \otimes \mathbf{e}_3 + \mathbf{U}\mathbf{e}_\alpha \otimes \mathbf{e}_\alpha\right] \tag{4.7}$$

Here $\underline{\mathrm{v}} = \mathbf{R}^T\mathbf{r}'$ is a 3-vector, the first two components of which represent shear while the third component represents axial stretch, $\mathbf{K} = \mathbf{R}^T\mathbf{R}'$ is a skew symmetric matrix whose axial vector $\underline{\mathrm{k}}$ is a 3-vector, the first two components of which represent components of local curvature while the third component represents twist. It should be mentioned though that unlike in the case of the special Cosserat rod theory, here the shears v_α are not the components of $\mathbf{r}'$ along

the cross-sectional directors $\mathbf{d}_\alpha$ but rather along $\mathbf{Re}_\alpha$. The same applies to the first two components of the axial vector $\underline{k}$.

From expression (4.7), it may be seen that the objective part of the deformation gradient $\mathbf{F}$ depends on the following quantities: $\underline{v}, \mathbf{KU}, \mathbf{U}, \mathbf{U}'$. Hence they also define the objective strain measures. Let us define $\underline{z} = \begin{bmatrix} a \\ b \\ c \end{bmatrix}$ and $\underline{z}' = \begin{bmatrix} a' \\ b' \\ c' \end{bmatrix}$. Hence $\underline{v}$ and $\underline{k}$ denote the usual bulk strains as in the Cosserat rod theory while $\underline{z}$ and $\underline{z}'$ denote the new strain measures corresponding to in-plane cross-sectional deformation. Local injectivity of the deformation gradient ($det(\mathbf{F}) > 0$) puts restriction(s) on the range of values the objective strain measures can take. To find the restriction(s) explicitly, the deformation gradient $\mathbf{F}$ from expression (4.7) is written in matrix form below:

$$\mathbf{F} = \mathbf{R}\begin{bmatrix} a & c & * \\ c & b & * \\ 0 & 0 & e \end{bmatrix}, \quad \text{where, } e = X_1(ck_1 - ak_2) + X_2(bk_1 - ck_2) + v_3 \tag{4.8}$$

Here '*' denotes the matrix components whose explicit expressions are not required for application of local injectivity. At the origin of a cross-section ($X_1 = X_2 = 0$), local injectivity thus implies $v_3(ab - c^2) > 0$. For hollow rods which have no material point at the origin of a cross-section, the same condition can be derived by invoking injectivity at two points on the cross-section symmetrically placed about the origin. As the axial stretch $v_3 > 0$, local injectivity physically implies that the directors must form a right-handed triad even when deformed.

Invoking hyperelasticity and material objectivity, one can write down the ex-

pression for strain energy density per unit of undeformed length as:

$$\begin{aligned} W(s) &= \int_{\Omega} \tilde{W}(\mathbf{F}, s) d\Omega \\ &= \int_{\Omega} \tilde{W}(\underline{v}, \mathbf{K}\mathbf{U}, \mathbf{U}, \mathbf{U}', s) d\Omega \\ &= \Phi(\underline{v}, \underline{k}, \underline{z}, \underline{z}', s) \end{aligned} \tag{4.9}$$

Here $\Phi(.)$ is the strain energy density expression obtained by integrating over the cross-section Ω of a rod.

4.3 Equations of Equilibrium and the Required Boundary Conditions

From the previous section, the total number of unknown field variables is found to be 9: 3 corresponding to the centerline displacement $\mathbf{r}$, 3 corresponding to rigid rotation of the cross-section $\mathbf{R}$ and 3 for in-plane cross-sectional deformation $\underline{z}$. Thus one needs a total of 9 equations. The first 6 are the usual linear momentum balance and the angular momentum balance equations as in the special Cosserat rod theory. They are found to have the same form as in the special Cosserat rod theory and are shown below.

$$\begin{aligned} \mathbf{LMB}: \ \mathbf{n}' + \mathbf{f} = \mathbf{0} \\ \mathbf{AMB}: \ \mathbf{m}' + \mathbf{r}' \times \mathbf{n} + \mathbf{g} = \mathbf{0} \end{aligned} \tag{4.10}$$

Here $\mathbf{n} = \mathbf{R}\frac{\partial \Phi}{\partial \underline{v}}$ and $\mathbf{m} = \mathbf{R}\frac{\partial \Phi}{\partial \underline{k}}$ denote the internal contact force and the internal moment respectively acting at a cross-section, while $\mathbf{f}$ and $\mathbf{g}$ denote the distributed force and the distributed couple per unit of undeformed length respectively, acting along the length of a rod. These six ordinary differential equations

(ODEs), being of 2^{nd} order in the kinematic field variables, require a set of 12 boundary conditions which may be prescribed either through the values of $\mathbf{r}$, $\mathbf{R}$ or through the values of $\mathbf{n}$, $\mathbf{m}$ at the two ends of a rod. It may be mentioned that these six equations could get coupled to the remaining three equations (to be derived below) through the constitutive laws of a rod or through the boundary conditions.

To derive the remaining three equations, let us first find the stress resultants conjugate to the in-plane cross-sectional strains $\underline{z}$ and $\underline{z}'$. An expression for the time rate of change of the deformation gradient $\mathbf{F}$ is shown below.

$$\dot{\mathbf{F}} = \dot{\mathbf{R}}\mathbf{R}^T\mathbf{F} + \mathbf{R}[\dot{\underline{v}} \otimes \mathbf{e}_3 + X_\alpha\{\dot{\mathbf{K}}\mathbf{U} + \mathbf{K}\dot{\mathbf{U}} + \dot{\mathbf{U}}'\}\mathbf{e}_\alpha \otimes \mathbf{e}_3 + \dot{\mathbf{U}}\mathbf{e}_\alpha \otimes \mathbf{e}_\alpha] \tag{4.11}$$

If $\mathbf{P}$ is the 1^{st} Piola-Kirchoff stress tensor, then the rate of change of strain energy per unit of undeformed length equals:

$$\begin{aligned}\dot{W} &= \int_\Omega \mathbf{P} : \dot{\mathbf{F}} d\Omega \\ &= \int_\Omega tr\{\mathbf{P}\mathbf{F}^T\hat{\mathbf{W}}\} + \mathbf{R}\dot{\underline{v}} \cdot \int_\Omega \mathbf{P}\mathbf{e}_3 + \mathbf{R}\dot{\underline{k}} \cdot \int_\Omega (X_\alpha \mathbf{R}\mathbf{U}\mathbf{e}_\alpha \times \mathbf{P}\mathbf{e}_3) \\ &+ \dot{\mathbf{U}}'\mathbf{e}_\alpha \cdot \mathbf{R}^T \int_\Omega X_\alpha \mathbf{P}\mathbf{e}_3 - \dot{\mathbf{U}}\mathbf{e}_\alpha \cdot \left\{\underline{k} \times \mathbf{R}^T \int_\Omega X_\alpha \mathbf{P}\mathbf{e}_3 - \mathbf{R}^T \int_\Omega \mathbf{P}\mathbf{e}_\alpha\right\}\end{aligned} \tag{4.12}$$

The 1^{st} term involving the trace operator vanishes since $\mathbf{P}\mathbf{F}^T$ is a symmetric tensor proportional to the Cauchy stress tensor while $\hat{\mathbf{W}} = \dot{\mathbf{R}}\mathbf{R}^T$ is a skew symmetric tensor. Further noting that $\mathbf{P}\mathbf{e}_i$ is the traction acting on a plane whose normal points towards $\mathbf{e}_i$, one can write down the strain energy rate in a simplified form as:

$$\dot{W} = \mathbf{n} \cdot \mathbf{R}\dot{\underline{v}} + \mathbf{m} \cdot \mathbf{R}\dot{\underline{k}} + Q_1\dot{a}' + Q_2\dot{b}' + Q_3\dot{c}' + q_1\dot{a} + q_2\dot{b} + q_3\dot{c} \tag{4.13}$$

Here Q_i and q_i are the stress resultants cojugate to the in-plane cross-sectional strains. Assuming hyperelasticity and using (4.9), the strain energy rate can also

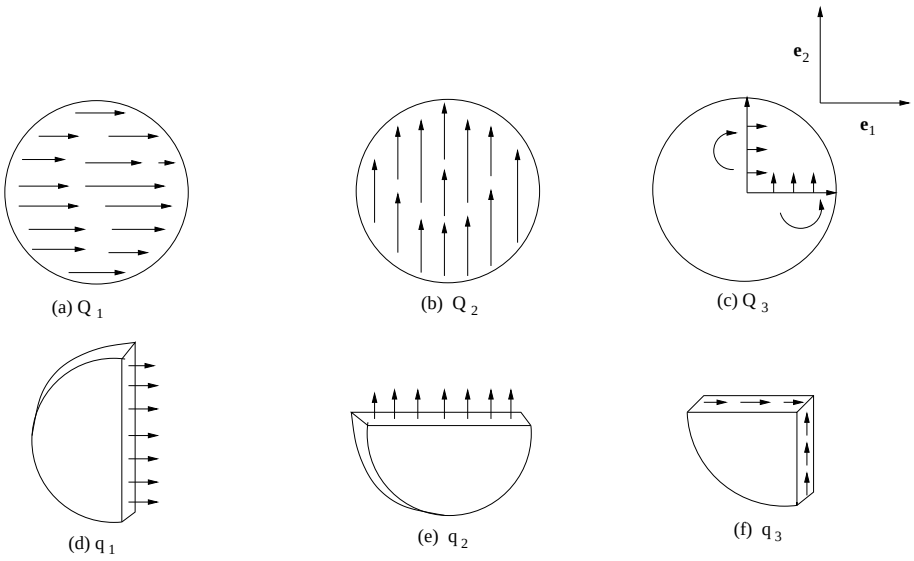

Figure 4.2: A pictorial representation of the tractions generating the stress resultants conjugate to the in-plane cross-sectional strain measures

be wrritten as:

$$\dot{W} = \mathbf{R}\frac{\partial \Phi}{\partial \underline{v}} \cdot \mathbf{R}\dot{\underline{v}} + \mathbf{R}\frac{\partial \Phi}{\partial \underline{k}} \cdot \mathbf{R}\dot{\underline{k}} + \frac{\partial \Phi}{\partial a'}\dot{a}' + \frac{\partial \Phi}{\partial b'}\dot{b}' + \frac{\partial \Phi}{\partial c'}\dot{c}' + \frac{\partial \Phi}{\partial a}\dot{a} + \frac{\partial \Phi}{\partial b}\dot{b} + \frac{\partial \Phi}{\partial c}\dot{c} \quad (4.14)$$

Comparing (4.13) and (4.14), it is observed that the stress resultants can be represented in terms of derivatives of the strain energy density function $\Phi(.)$. Expressions for Q_i and q_i are shown below now along with their physical meanings, which have been derived upon comparing (4.12) and (4.13).

$$Q_1 = \int_\Omega X_1 \mathbf{e}_1 . \left(\mathbf{R}^T \mathbf{P} \mathbf{e}_3\right) \quad (4.15)$$

Thus Q_1 is the X_1-weighted integral of the shear traction acting on a cross-sectional plane along the $\mathbf{e}_1$ direction and is a penalty/ stress resultant conjugate to a'.

$$Q_2 = \int_\Omega X_2 \mathbf{e}_2 . \left(\mathbf{R}^T \mathbf{P} \mathbf{e}_3\right) \quad (4.16)$$

Q_2 has the similar physical meaning as Q_1 above. Fig.4.2(a) and 4.2(b) show the shear tractions responsible for generating Q_1 and Q_2 respectively.

$$Q_3 = \int_\Omega X_1 \mathbf{e}_2 . \left(\mathbf{R}^T \mathbf{P} \mathbf{e}_3 \right) + X_2 \mathbf{e}_1 . \left(\mathbf{R}^T \mathbf{P} \mathbf{e}_3 \right) \tag{4.17}$$

The 1^{st} term in Q_3 above corresponds to the twisting moment generated due to shear traction acting along the $\mathbf{e}_2$ direction while the 2^{nd} term corresponds to the twisting moment generated due to shear traction acting along the $\mathbf{e}_1$ direction. In order to obtain the net twisting moment, the 2nd term should have a negative sign but the net resultant would then correspond to the stress resultant conjugate to twisting of a cross-section. As Q_3 is conjugate to c′, the positive sign for the 2nd term makes sense as they together act against any non-uniformity in the in-plane cross-sectional shear (non-orthogonality of the directors $\mathbf{d}_\alpha$) along the length of a rod. Fig.4.2(c) illustrates the same pictorially.

From the definition of Q_i, they represent the first moments of shear traction acting on a cross-sectional plane. Clearly, if the shear traction in a cross-sectional plane is distributed in such a way that the net shear force can be placed at the centroid of a cross-section, then all Q_i would vanish. This is somewhat related to the concept of shear center but not equivalent. To be more precise, coincidence of the shear center and the centroid of a cross-section does not mean vanishing of any of the three Q_i.

Next, we have

$$q_1 = -\mathbf{e}_1 \cdot \left\{ \underline{k} \times \mathbf{R}^T \int_\Omega X_1 \mathbf{P} \mathbf{e}_3 \right\} + \int_\Omega \mathbf{e}_1 . \left(\mathbf{R}^T \mathbf{P} \mathbf{e}_1 \right) \tag{4.18}$$

The 1^{st} term in the expression for q_1 above is of higher order for small enough strain values and may be neglected. Interpretation of the 2nd term is more interesting. In particular, as illustrated in Fig.4.2(d), the normal traction or the

$\mathbf{e}_1$-component of the traction acting on a plane perpendicular to the $\mathbf{e}_1$ axis is now being integrated. Although this normal traction does not act on the cross-sectional plane, it is being integrated over the cross-sectional plane. This is a little strange but careful reflection reveals that this normal traction should actually be integrated over the volume between two neighboring cross-sections which are apart by an infinitesimal length. But in order to get the strain energy rate per unit of undeformed length, one needs to divide by this infinitesimal length and hence the entire process is equivalent to integration over the surface of a cross-section.

$$q_2 = -\mathbf{e}_2 \cdot \left\{ \underline{k} \times \mathbf{R}^T \int_\Omega X_2 \mathbf{P}\mathbf{e}_3 \right\} + \int_\Omega \mathbf{e}_2 . \left(\mathbf{R}^T \mathbf{P}\mathbf{e}_2 \right) \tag{4.19}$$

q_2 has similar meaning as q_1 above and is illustrated in Fig.4.2(e).

$$\begin{aligned} q_3 = &- \left[\mathbf{e}_2 \cdot \left\{ \underline{k} \times \mathbf{R}^T \int_\Omega X_1 \mathbf{P}\mathbf{e}_3 \right\} + \mathbf{e}_1 \cdot \left\{ \underline{k} \times \mathbf{R}^T \int_\Omega X_2 \mathbf{P}\mathbf{e}_3 \right\} \right] \\ &+ \int_\Omega \left[\mathbf{e}_2 . \left(\mathbf{R}^T \mathbf{P}\mathbf{e}_1 \right) + \mathbf{e}_1 . \left(\mathbf{R}^T \mathbf{P}\mathbf{e}_2 \right) \right] \end{aligned} \tag{4.20}$$

Here again the 1^{st} two terms are of higher order while the remaining terms are of importance for small strain conditions. Instead of integrating the normal traction as for q_1 and q_2, the shear tractions acting on the $\mathbf{e}_1$ and $\mathbf{e}_2$ plane are now being integrated. As illustrated in Fig.4.2(f), these shear tractions try to change the angle between the two cross-sectional directors, thus they generate in-plane cross-sectional shear.

Below one of the new equilibrium equations is derived by differentiating Q_1 and using the 3-d equilibrium equation $(\mathbf{P}\mathbf{e}_i)_{,i} + \rho_0 \mathbf{b} = \mathbf{0}$. Here ρ_0 is the density

of the 3-d continuum while **b** is the body force per unit of undeformed volume.

$$\begin{aligned} Q_1' &= \mathbf{e}_1 \cdot \left[-\underline{k} \times \mathbf{R}^T \int_\Omega X_1 \mathbf{P}\mathbf{e}_3 + \mathbf{R}^T \int_\Omega X_1 \left(\mathbf{P}\mathbf{e}_3\right)_{,3} \right] \\ &= \mathbf{e}_1 \cdot \left[-\underline{k} \times \mathbf{R}^T \int_\Omega X_1 \mathbf{P}\mathbf{e}_3 - \mathbf{R}^T \int_\Omega X_1 \left\{ \left(\mathbf{P}\mathbf{e}_\alpha\right)_{,\alpha} + \rho_0 \mathbf{b} \right\} \right] \\ &= \mathbf{e}_1 \cdot \left[-\underline{k} \times \mathbf{R}^T \int_\Omega X_1 \mathbf{P}\mathbf{e}_3 + \mathbf{R}^T \int_\Omega \mathbf{P}\mathbf{e}_1 \right] - \mathbf{e}_1 \cdot \mathbf{R}^T \left[\int_{\partial\Omega} X_1 \mathbf{P}\boldsymbol{\nu} + \int_\Omega X_1 \rho_0 \mathbf{b} \right] \end{aligned} \tag{4.21}$$

or,

$$Q_1' - q_1 + r_1 = 0 \tag{4.22}$$

Here $\boldsymbol{\nu}$ is an outward normal to $\partial\Omega$, the lateral surface of a rod, while $r_1 = \mathbf{e}_1 \cdot \mathbf{R}^T \left[\int_{\partial\Omega} X_1 \mathbf{P}\boldsymbol{\nu} + \int_\Omega X_1 \rho_0 \mathbf{b} \right]$ is the distributed "force" per unit of undeformed length. By definition, in the absence of body force and lateral traction, r_1 would vanish. It should be noted that (4.22) is an ODE of 2^{nd} order in a and hence it requires two additional boundary conditions which may be provided through the values of a and/or Q_1 at the two ends of a rod. The remaining two equations are of the same form as (4.22) and are shown below:

$$Q_2' - q_2 + r_2 = 0 \tag{4.23}$$

$$Q_3' - q_3 + r_3 = 0 \tag{4.24}$$

Here $r_2 = \mathbf{e}_2 \cdot \mathbf{R}^T \left[\int_{\partial\Omega} X_2 \mathbf{P}\boldsymbol{\nu} + \int_\Omega X_2 \rho_0 \mathbf{b} \right]$ while $r_3 = \mathbf{e}_2 \cdot \mathbf{R}^T \left[\int_{\partial\Omega} X_1 \mathbf{P}\boldsymbol{\nu} + \int_\Omega X_1 \rho_0 \mathbf{b} \right] + \mathbf{e}_1 \cdot \mathbf{R}^T \left[\int_{\partial\Omega} X_2 \mathbf{P}\boldsymbol{\nu} + \int_\Omega X_2 \rho_0 \mathbf{b} \right]$.

If we write $\underline{Q} = \begin{bmatrix} Q_1 \\ Q_2 \\ Q_3 \end{bmatrix}$, $\underline{q} = \begin{bmatrix} q_1 \\ q_2 \\ q_3 \end{bmatrix}$ and $\underline{r} = \begin{bmatrix} r_1 \\ r_2 \\ r_3 \end{bmatrix}$, the three additional equations can be written in compact form as:

$$\begin{aligned} \underline{Q}' - \underline{q} + \underline{r} &= \mathbf{0} \\ \text{or, } \left(\frac{\partial \Phi}{\partial \underline{z}'} \right)' - \frac{\partial \Phi}{\partial \underline{z}} + \underline{r} &= \mathbf{0} \end{aligned} \tag{4.25}$$

Thus (4.10) and (4.25) together constitute a complete set of nine 2^{nd} order ordinary differential equations necessary to solve for the 9 unknown field variables. It also requires a total of 18 boundary conditions. The set of ODEs can be conveniently solved numerically using a slightly modified version of the numerical scheme presented by Healey & Mehta [29].

Assuming (a) there is not much of non-uniformity in the cross-sectional strains so that $\underline{z}'$ could be assumed to be negligible all along the length of a rod and further (b) lateral traction and body forces are absent so that the cross-sectional deformation could be unrestrained, then the first and last terms from equations (4.25) would drop out and equations (4.25) would reduce to the algebraic equations:

$$\frac{\partial \Phi}{\partial \underline{z}} \approx \mathbf{0} \tag{4.26}$$

Thus the extra differential equations (4.25) would not be needed to solve for the cross-sectional deformation but only the algebraic equations (4.26) would be needed along with the equations of linear and angular momentum balance (4.10). Similar assumptions were made for determining the cross-sectional deformation in the work of Hodges [30, 31, 32].

4.4 Variational Formulation to Solve the System of ODEs

Equations (4.10) and (4.25) being of 2^{nd} order, the basic unknowns $\mathbf{r}(s)$, $\mathbf{R}(s)$ and $\underline{z}(s)$ must lie in the space of C^2 functions. In order to relax this requirement as well as for numerical convenience, a weak form of the equilibrium equations is derived which enables the unknowns to lie in a relatively weaker space of C^1.

$\mathbf{R}$(s), being a SO(3) map, can also be realized as rotation about an axis by a certain angle. Let $\boldsymbol{\theta}(s)$ be a vector which is directed along this axis of rotation and let $|\boldsymbol{\theta}|$ denote the angle of rotation. Further, let $\boldsymbol{\Theta}(s)$ be a skew symmetric matrix whose axial vector is $\boldsymbol{\theta}(s)$. Then, $\mathbf{R}(s) = exp(\boldsymbol{\Theta}(s))$. Assuming absence of lateral traction or body force, one arrives at the following "spatial" weak form:

$$G \equiv \int_0^1 \mathbf{n}' \cdot \boldsymbol{\eta}_0 + (\mathbf{m}' + \mathbf{r}' \times \mathbf{n}) \cdot \boldsymbol{\psi} + \left(\underline{\mathrm{Q}}' - \underline{\mathrm{q}}\right) \cdot \boldsymbol{\lambda}\, ds \tag{4.27}$$

Here, $\boldsymbol{\eta}(s) \equiv (\boldsymbol{\eta}_0(s), \boldsymbol{\psi}(s), \boldsymbol{\lambda}(s))$ are the admissible test functions (arbitrarily smooth). $\boldsymbol{\eta}_0$ and $\boldsymbol{\psi}$ correspond to smooth variations of $\mathbf{r}$ and $\boldsymbol{\theta}$ respectively, whereas $\boldsymbol{\lambda}$ corresponds to smooth varitaion in the cross-sectional strain measure $\underline{\mathrm{z}}$. Depending on the boundary conditions, these test functions may vanish at the boundary. Upon integration by parts, one gets:

$$G \equiv \int_0^1 \left[\mathbf{n} \cdot (\boldsymbol{\eta}_0' - \boldsymbol{\psi} \times \mathbf{r}') + \mathbf{m} \cdot \boldsymbol{\psi}' + \underline{\mathrm{Q}} \cdot \boldsymbol{\lambda}' + \underline{\mathrm{q}} \cdot \boldsymbol{\lambda}\right] ds - \left(\mathbf{n} \cdot \boldsymbol{\eta}_0 + \mathbf{m} \cdot \boldsymbol{\psi} + \underline{\mathrm{Q}} \cdot \boldsymbol{\lambda}\right)\Big|_0^1 \tag{4.28}$$

The boundary terms in the expression (4.28) do not show up in case of Dirichlet problems (or free boundary problems) as the admissible smooth test functions (or the stress resultants) vanish at the boundary in such cases. It should be noted that the boundary terms in the expression (4.28) could render DG, the linearized part of G or the tangent stiffness operator, non-symmetric in the case of non-conservative problems [35, 54].

In order to linearize the weak form, let:
$\boldsymbol{\phi}_\epsilon(s) = \left(\mathbf{r}(s) + \epsilon\triangle\mathbf{r}(s),\ \exp(\epsilon\triangle\boldsymbol{\theta}(s))\mathbf{R}(s),\ \underline{\mathrm{z}}(s) + \epsilon\triangle\underline{\mathrm{z}}(s)\right)$ be the perturbed configuration of a rod about any configuration $\boldsymbol{\phi}(s) = \left(\mathbf{r}(s),\ \mathbf{R}(s),\ \underline{\mathrm{z}}(s)\right)$. Hence, using Taylor's expansion:

$$G(\boldsymbol{\phi}_\epsilon, \boldsymbol{\eta}) = G(\boldsymbol{\phi}, \boldsymbol{\eta}) + \epsilon DG(\boldsymbol{\phi}, \boldsymbol{\eta})\left[\triangle\boldsymbol{\phi}\right] + o\left(|\epsilon\triangle\boldsymbol{\phi}|\right). \tag{4.29}$$

The discrete form of expression (4.29) formed via the finite element procedure is convenient for numerical computation of static equilibria through Newton's iteration method. Below an expression for the tangent stiffness operator is shown whose derivation follows along the lines of Simo & Vu-Quoc [54]. Following their notation [54], let us define:

$$\tilde{\mathbf{C}}_{(9\times9)} = \begin{bmatrix} \frac{\partial^2\Phi}{\partial \underline{\mathrm{v}}^2} & \frac{\partial^2\Phi}{\partial \underline{\mathrm{v}}\partial \underline{\mathrm{k}}} & \frac{\partial^2\Phi}{\partial \underline{\mathrm{v}}\partial \underline{\mathrm{z}}'} \\ \frac{\partial^2\Phi}{\partial \underline{\mathrm{k}}\partial \underline{\mathrm{v}}} & \frac{\partial^2\Phi}{\partial \underline{\mathrm{k}}^2} & \frac{\partial^2\Phi}{\partial \underline{\mathrm{k}}\partial \underline{\mathrm{z}}'} \\ \frac{\partial^2\Phi}{\partial \underline{\mathrm{z}}'\partial \underline{\mathrm{v}}} & \frac{\partial^2\Phi}{\partial \underline{\mathrm{z}}'\partial \underline{\mathrm{k}}} & \frac{\partial^2\Phi}{\partial \underline{\mathrm{z}}'^2} \end{bmatrix}, \quad \Pi_{(6\times6)} = \begin{bmatrix} \mathbf{R} & \mathbf{0} \\ \mathbf{0} & \mathbf{R} \end{bmatrix}, \quad \mathbf{E}^T_{(6\times6)} = \begin{bmatrix} \mathbf{1}\frac{d}{ds} & \mathbf{r}'\times \\ \mathbf{0} & \mathbf{1}\frac{d}{ds} \end{bmatrix}$$

$$\mathbf{Cz}_{(9\times3)} = \begin{bmatrix} \frac{\partial^2\Phi}{\partial \underline{\mathrm{v}}\partial \underline{\mathrm{z}}} \\ \frac{\partial^2\Phi}{\partial \underline{\mathrm{k}}\partial \underline{\mathrm{z}}} \\ \frac{\partial^2\Phi}{\partial \underline{\mathrm{z}}'\partial \underline{\mathrm{z}}} \end{bmatrix}, \quad \mathbf{C}_{(12\times12)} = \begin{bmatrix} \tilde{\mathbf{C}} & \mathbf{Cz} \\ \mathbf{Cz}^T & \frac{\partial^2\Phi}{\partial \underline{\mathrm{z}}^2} \end{bmatrix}$$

Thus:

$$\begin{aligned} DG(\boldsymbol{\phi},\boldsymbol{\eta})\,[\triangle\boldsymbol{\phi}] \equiv \int_0^1 & \begin{bmatrix} \mathbf{E}\Pi & \mathbf{0}_{(6\times3)} & \mathbf{0}_{(6\times3)} \\ \mathbf{0}_{(3\times6)} & \mathbf{1}\frac{d}{ds} & \mathbf{1} \end{bmatrix} \mathbf{C} \begin{bmatrix} \mathbf{E}\Pi & \mathbf{0}_{(6\times3)} & \mathbf{0}_{(6\times3)} \\ \mathbf{0}_{(3\times6)} & \mathbf{1}\frac{d}{ds} & \mathbf{1} \end{bmatrix}^T \triangle\boldsymbol{\phi}\cdot\boldsymbol{\eta} \\ & + \begin{bmatrix} \mathbf{0} & -\mathbf{n}\times \\ \mathbf{0} & -\mathbf{m}\times \end{bmatrix} \begin{bmatrix} \triangle\mathbf{r}_0 \\ \triangle\boldsymbol{\theta}_0 \end{bmatrix} \cdot \mathbf{E}^T \begin{bmatrix} \boldsymbol{\eta_0} \\ \boldsymbol{\psi} \end{bmatrix} + (\mathbf{n}\times\triangle\mathbf{r}_0')\cdot\boldsymbol{\psi}\, ds \end{aligned} \tag{4.30}$$

The tangent stiffness operator (4.30) resembles structurally, to a large extent, the one presented by Simo [54] for Cosserat rod theory and hence the numerical scheme presented there can easily be extended and adopted for the proposed theory.

For convenience, the linearization of the boundary terms is not shown in the expression (4.30) above. Further, upon substituting $\boldsymbol{\eta} = \triangle\boldsymbol{\phi}$ in expression (4.30), one obtains the 2^{nd} variation of the total potential energy associated with the rod, eigenvalues of which contain stability information. As shown later, strong ellipticity guarantees positive definiteness of the matrix $\tilde{\mathbf{C}}$ ensuring well-posedness

of the strong form of the equilibrium equations (4.10) and (4.25). Positive definiteness of $\tilde{\mathbf{C}}$ is also a necessary (but not sufficient) condition for an equilibrium configuration to be stable [35]. This is also known as Legendre's Condition in the calculus of variations pertaining to a necessary condition for a quadratic functional to be non-negative [16].

4.5 Strong Ellipticity

From 3-d continuum theory, strong ellipticity implies positive definiteness of the elasticity tensor along any rank-1 direction. In mathematical form it implies:

$$[\mathbf{a}\otimes\mathbf{b}]\cdot\frac{\partial^2\tilde{\mathrm{W}}}{\partial\mathbf{F}^2}(.)\cdot[\mathbf{a}\otimes\mathbf{b}]\geq 0\ \forall\ \mathbf{a},\ \mathbf{b}\neq\mathbf{0} \tag{4.31}$$

Upon using (4.9):

$$\begin{aligned}\frac{\partial\Phi}{\partial \mathrm{v}_i}&\equiv\int_\Omega\frac{\partial\tilde{\mathrm{W}}}{\partial\mathbf{F}}(\mathbf{F}):\frac{\partial\mathbf{F}}{\partial \mathrm{v}_i}\,ds\\&\equiv\int_\Omega\frac{\partial\tilde{\mathrm{W}}}{\partial\mathbf{F}}(\mathbf{F}):[\mathbf{R}\mathbf{e}_i\otimes\mathbf{e}_3]\,ds\\ \text{and, }\frac{\partial^2\Phi}{\partial \mathrm{v}_i\partial \mathrm{v}_j}&\equiv\int_\Omega[\mathbf{R}\mathbf{e}_i\otimes\mathbf{e}_3]\cdot\frac{\partial^2\tilde{\mathrm{W}}}{\partial\mathbf{F}^2}(\mathbf{F})\cdot[\mathbf{R}\mathbf{e}_i\otimes\mathbf{e}_3]\,ds\end{aligned} \tag{4.32}$$

Similarly, one can form 2^{nd} partials of $\Phi(.)$ with respect to the other strain measures. If we now choose $\mathbf{a}=\mathrm{l}_i\mathbf{R}\mathbf{e}_i+\mathrm{m}_i\mathbf{R}\mathbf{e}_i\times X_\alpha\mathbf{R}\mathbf{U}\mathbf{e}_\alpha+\mathrm{n}_1X_1\mathbf{R}\mathbf{e}_1+\mathrm{n}_2X_2\mathbf{R}\mathbf{e}_2+\mathrm{n}_3\{X_1\mathbf{R}\mathbf{e}_2+X_2\mathbf{R}\mathbf{e}_1\}$ and $\mathbf{b}=\mathbf{e}_3$, then, upon a lengthy but straightforward algebraic manipulation [26], one can show that:

$$\int_\Omega[\mathbf{a}\otimes\mathbf{b}]\cdot\frac{\partial^2\tilde{\mathrm{W}}}{\partial\mathbf{F}^2}(.)\cdot[\mathbf{a}\otimes\mathbf{b}]\,\mathrm{d}\Omega=\begin{Bmatrix}\underline{\mathrm{l}}\\ \underline{\mathrm{m}}\\ \underline{\mathrm{n}}\end{Bmatrix}^T\begin{bmatrix}\frac{\partial^2\Phi}{\partial\underline{\mathrm{v}}^2}&\frac{\partial^2\Phi}{\partial\underline{\mathrm{v}}\partial\underline{\mathrm{k}}}&\frac{\partial^2\Phi}{\partial\underline{\mathrm{v}}\partial\underline{\mathrm{z}}'}\\ \frac{\partial^2\Phi}{\partial\underline{\mathrm{k}}\partial\underline{\mathrm{v}}}&\frac{\partial^2\Phi}{\partial\underline{\mathrm{k}}^2}&\frac{\partial^2\Phi}{\partial\underline{\mathrm{k}}\partial\underline{\mathrm{z}}'}\\ \frac{\partial^2\Phi}{\partial\underline{\mathrm{z}}'\partial\underline{\mathrm{v}}}&\frac{\partial^2\Phi}{\partial\underline{\mathrm{z}}'\partial\underline{\mathrm{k}}}&\frac{\partial^2\Phi}{\partial\underline{\mathrm{z}}'^2}\end{bmatrix}\begin{Bmatrix}\underline{\mathrm{l}}\\ \underline{\mathrm{m}}\\ \underline{\mathrm{n}}\end{Bmatrix}\geq\ 0,\ \forall\ \underline{\mathrm{l}},\ \underline{\mathrm{m}},\ \underline{\mathrm{n}}\neq\ \mathbf{0} \tag{4.33}$$

Thus, the associated matrix in (4.33)(defined as $\tilde{\mathbf{C}}$ in the preceding section) should be positive definite at all values of strain measures. It should be noted that strong ellipticity does not put any restriction on partials of $\Phi(.)$ with respect to $\underline{z}$. However, as shown later, one does get additional restrictions on partials of $\Phi(.)$ with respect to $\underline{z}$ at the straight state reference configuration. This puts additional restrictions on the quadratic form of the strain energy density (usually valid for small strain conditions) for which the matrix of 2^{nd} partials of $\Phi(.)$ with respect to the strain measures is constant, i.e., the matrix $\mathbf{C}$ (defined in the preceding section) is independent of the current strain values.

4.6 Material Symmetry

Now material symmetry of a rod is exploited to extract invariants of the objective strain measures which put restrictions on the form of the strain energy density $\Phi(.)$. For comprehensive treatment of material symmetry applied to the special Cosserat rod theory, please refer to [28].

4.6.1 Hemitropy

For chiral rods with inbuilt handedness and having a straight state stress free reference configuration, the relevant material symmetry group contains all the proper orthogonal rotations with the axis of rotation aligned along the rod's axis (typically $\mathbf{e}_3$). Such rods are also called hemitropic [27, 50]. Hemitropy thus implies that for all proper $\mathbf{Q} \in O(2)$ preceding a given deformation gradient $\mathbf{F}$, the strain energy density remains unchanged. In matrix form $\mathbf{Q}$ =

$\begin{bmatrix} \cos(\theta) & -\sin(\theta) & 0 \\ \sin(\theta) & \cos(\theta) & 0 \\ 0 & 0 & 1 \end{bmatrix}$, which denotes rotation by an angle θ about the $\mathbf{e}_3$ axis. Let us see how the deformation gradient and hence the objective strain measures transform under this pre-rotation.

$$\begin{aligned} &\mathbf{x} \to \mathbf{r}(s) + X_\alpha \mathbf{R}(s)\mathbf{U}(s)\mathbf{Q}\mathbf{e}_\alpha \\ &\mathbf{F} \to \mathbf{R}\left[\underline{\mathrm{v}} \otimes \mathbf{e}_3 + X_\alpha\{\mathbf{KUQ} + \mathbf{U}'\mathbf{Q}\}\mathbf{e}_\alpha \otimes \mathbf{e}_3 + \mathbf{UQ}\mathbf{e}_\alpha \otimes \mathbf{e}_\alpha\right] \\ \text{or, } &\mathbf{F} \to \mathbf{RQ}\left[\mathbf{Q}^T\underline{\mathrm{v}} \otimes \mathbf{e}_3 + X_\alpha\{\mathbf{Q}^T\mathbf{KUQ} + \mathbf{Q}^T\mathbf{U}'\mathbf{Q}\}\mathbf{e}_\alpha \otimes \mathbf{e}_3 + \mathbf{Q}^T\mathbf{UQ}\mathbf{e}_\alpha \otimes \mathbf{e}_\alpha\right] \end{aligned} \tag{4.34}$$

Please note that it is difficult to deduce invariants of **KU** as a single entity since **KU** is a full 3×3 non-symmetric matrix while **Q** corresponds to all rotations restricted to the $\mathbf{e}_1$-$\mathbf{e}_2$ plane. One can however deal with **K** and **U** separately. It is possible though that one may miss some invariants of **KU** that cannot be found when **K** and **U** are dealt with separately. But, the advantage of having picked the director $\mathbf{d}_3$ perpendicular to the cross-section as well as picking a symmetric choice for **U** earlier can now be seen. The first choice leads to a form of **U** and **U**′ where their restriction to the $\mathbf{e}_1$-$\mathbf{e}_2$ plane is decoupled from the $\mathbf{e}_3$ axis and hence use of the symmetry group of **Q** restricted to rotations in the $\mathbf{e}_1$-$\mathbf{e}_2$ plane gets easier to handle. Having a symmetric form of **U** and **U**′ further helps in using standard results. Now, under the rotation **Q**:

- $\underline{\mathrm{v}} \to \mathbf{Q}^T\underline{\mathrm{v}}$
- $\mathbf{KU} \to \mathbf{Q}^T\mathbf{KUQ} \equiv \mathbf{Q}^T\mathbf{KQQ}^T\mathbf{UQ}$
  - $\mathbf{K} \to \mathbf{Q}^T\mathbf{KQ}$ or $\underline{\mathrm{k}} \to \det(\mathbf{Q})\mathbf{Q}^T\underline{\mathrm{k}}$ (see [28] for details)
  - $\mathbf{U} \to \mathbf{Q}^T\mathbf{UQ}$
- $\mathbf{U}' \to \mathbf{Q}^T\mathbf{U}'\mathbf{Q}$.

Define $\mathbf{h} = \begin{bmatrix} v_1 \\ v_2 \end{bmatrix}$, $\mathbf{s} = \begin{bmatrix} k_1 \\ k_2 \end{bmatrix}$, $\mathbf{H} = \begin{bmatrix} a & c \\ c & b \end{bmatrix}$, $\mathbf{S} = \begin{bmatrix} a' & c' \\ c' & b' \end{bmatrix}$, $\mathbf{Q} = \begin{bmatrix} \cos(\theta) & -\sin(\theta) \\ \sin(\theta) & \cos(\theta) \end{bmatrix}$.

Thus for all $\theta \in [0, 2\pi]$: $\mathbf{h} \to \mathbf{Q}^T\mathbf{h}$, $\mathbf{s} \to \mathbf{Q}^T\mathbf{s}$, $\mathbf{H} \to \mathbf{Q}^T\mathbf{H}\mathbf{Q}$, $\mathbf{S} \to \mathbf{Q}^T\mathbf{S}\mathbf{Q}$, $v_3 \to v_3$, $k_3 \to k_3$.

So, we have two vectors **h**, **s** and two symmetric tensors **H**, **S** that rotate or transform through the same rotation tensor **Q**. The invariants corresponding to the two vectors **h** and **s** are their respective norms, their dot-product and cross-product, i.e., $\mathbf{h} \cdot \mathbf{h}$, $\mathbf{s} \cdot \mathbf{s}$, $\mathbf{h} \cdot \mathbf{s}$, $(\mathbf{h} \times \mathbf{s}) \cdot \mathbf{e}_3$.

From standard results of linear algebra, invariants of a second-order symmetric tensor in $\mathbf{R}^2$ under $\mathbf{O}(2)$ are its trace and determinant. Thus, for the two second-order symmetric tensors **H** and **S**, the invariants are: tr(**H**), tr(**S**), tr(**HS**), det(**H**), det(**S**).

Interestingly, as the two vectors and the two tensors rotate in a similar way, there are invariants denoting coupling between them, i.e., quadratic inner product of the vectors with respect to the tensors also remain invariant. These invariants turn out to be of higher order than the quadratic ones: $\mathbf{h} \cdot \mathbf{H}\mathbf{h}$, $\mathbf{h} \cdot \mathbf{S}\mathbf{h}$, $\mathbf{s} \cdot \mathbf{S}\mathbf{s}$, $\mathbf{s} \cdot \mathbf{H}\mathbf{s}$, $\mathbf{h} \cdot \mathbf{H}\mathbf{S}\mathbf{h}$ ... These invariants are neglected as we limit ourselves to finding an expression for the quadratic strain energy density in this dissertation.

Thus, following are the invariants of strain measures of quadratic order or below for hemitropic rods: v_3, k_3, $\mathbf{h} \cdot \mathbf{h}$, $\mathbf{s} \cdot \mathbf{s}$, $\mathbf{h} \cdot \mathbf{s}$, $(\mathbf{h} \times \mathbf{s}) \cdot \mathbf{e}_3$, tr(**H**), tr(**S**), tr(**HS**), det(**H**), det(**S**).

4.6.2 Transverse Isotropy

Let us deduce now the invariants of strain measures for the case of transversely isotropic rods. Here, in addition to all proper rotations about $\mathbf{e}_3$, reflections about the $\mathbf{e}_1$ or $\mathbf{e}_2$ axes are allowed. This puts additional constraints on the invariants already found in the previous subsection. In particular for $\mathbf{Q} = \begin{bmatrix} -1 & 0 & 0 \\ 0 & 1 & 0 \\ 0 & 0 & 1 \end{bmatrix} : \underline{v} \to \begin{bmatrix} -v_1 \\ v_2 \\ v_3 \end{bmatrix}, \underline{k} \to \begin{bmatrix} k_1 \\ -k_2 \\ -k_3 \end{bmatrix}$

Thus: $\mathbf{h} \cdot \mathbf{s} \to -\mathbf{h} \cdot \mathbf{s}$, $k_3 \to -k_3$. Hence, they must appear either as their even powers or as their product in the expression for quadratic strain energy density. All other invariants of quadratic order or below remain unchanged under reflection. Thus, following are the invariants of quadratic order or below pertaining to transverse isotropy: v_3, k_3^2, $\mathbf{h} \cdot \mathbf{h}$, $\mathbf{s} \cdot \mathbf{s}$, $(\mathbf{h} \times \mathbf{s}) \cdot \mathbf{e}_3$, tr($\mathbf{H}$), tr($\mathbf{S}$), tr($\mathbf{HS}$), det($\mathbf{H}$), det($\mathbf{S}$).

Note that $(\mathbf{h} \cdot \mathbf{s})^2$ and $(\mathbf{h} \cdot \mathbf{s})k_3$ are invariants of higher order and hence not included in the list above.

4.6.3 Flip Symmetry

Let us investigate the ramifications of symmetry transformation under rotation about the $\mathbf{e}_2$ axis, i.e. under the rotation matrix $\mathbf{G} = \begin{bmatrix} -1 & 0 & 0 \\ 0 & 1 & 0 \\ 0 & 0 & -1 \end{bmatrix}$. Rods that are homogeneous in the straight state reference configuration satisfy this sym-

metry. It is found that all the quadratic invariants remain unchanged except $(\mathbf{h} \times \mathbf{s}) \cdot \mathbf{e}_3 \rightarrow -(\mathbf{h} \times \mathbf{s}) \cdot \mathbf{e}_3$, $tr(\mathbf{S}) \rightarrow -tr(\mathbf{S})$ and $tr(\mathbf{HS}) \rightarrow -tr(\mathbf{HS})$. Hence these invariants must exist as their even powers or in their product form.

But $\{(\mathbf{h} \times \mathbf{s}) \cdot \mathbf{e}_3\}^2 = (\mathbf{h} \cdot \mathbf{h})(\mathbf{s} \cdot \mathbf{s}) - (\mathbf{h} \cdot \mathbf{s})^2$. Hence $\{(\mathbf{h} \times \mathbf{s}) \cdot \mathbf{e}_3\}^2$ is no more an independent invariant [28]. The modified invariants (of upto quadratic order) satisfying flip symmetry are $\{tr(\mathbf{S})\}^2$, $\{tr(\mathbf{HS})\}^2$ and $tr(\mathbf{S})tr(\mathbf{HS})$. Furthermore, the last two invariants reduce to the first one at the reference configuration.

4.6.4 Quadratic Combinations of Invariants

Based on the results in the previous subsection, for rods satisfying hemitropy and flip symmetry, the following invariants are of quadratic order or below: v_3, k_3, $v_\alpha v_\alpha$, $k_\alpha k_\alpha$, $v_\alpha k_\alpha$, $a+b$, $(a'+b')^2$, $ab-c^2$, $a'b'-(c')^2$, $(aa'+bb'+cc')^2$, $(a'+b')(aa'+bb'+cc')$.

For rods satisfying transverse isotropy and flip symmetry, the following invariants are of quadratic order or below: v_3, k_3^2, $v_\alpha v_\alpha$, $k_\alpha k_\alpha$, $a+b$, $(a'+b')^2$, $ab-c^2$, $a'b'-(c')^2$, $(aa'+bb'+cc')^2$, $(a'+b')(aa'+bb'+cc')$.

It is noted again that there are more invariants but of higher order. It will be interesting to find a complete set of them to deduce strain energy density of higher order for non-linear material modeling purposes.

4.7 Quadratic Expression of Strain Energy Density and Restrictions on Parameters Involved

Here expressions for the quadratic form of strain energy density $\Phi(.)$ are shown for both hemitropic and transversely isotropic rods. Its derivation is based upon Taylor's expansion (of upto quadratic order in the objective strain measures) at the stress free straight state reference configuration. The derivation is lengthy but straightforward and requires careful use of the chain rule since strain energy density is expressed as a function of the strain invariants while the derivatives of strain energy density are computed with respect to the objective strain measures. As this energy expression has been derived at the stress free reference configuration, the 1^{st} partials of $\Phi(.)$ with respect to the objective strain measures accordingly vanish. It is mentioned again that only the invariants of quadratic order or below affect this expression. It is for this reason that a complete set of these invariants were shown in the previous section while leaving the set of invariants of higher orders incomplete.

4.7.1 Hemitropic and Transversely Isotropic Rods

For hemitropic rods satisfying flip symmetry, we have following expression for the quadratic strain energy density that contains 12 parameters:

$$\Phi_{hemi}(.) = \frac{1}{2}\Big[\mathrm{A}\kappa_\alpha\kappa_\alpha + \mathrm{B}\kappa_3^2 + \mathrm{C}\nu_\alpha\nu_\alpha + \mathrm{D}(\nu_3-1)^2 + 2\mathrm{E}(\nu_3-1)\kappa_3 + 2\mathrm{F}\nu_\alpha\kappa_\alpha + 2\mathrm{G}(\nu_3-1)\left(\frac{a+b}{2}-1\right) + 2\mathrm{H}\kappa_3\left(\frac{a+b}{2}-1\right) + \mathrm{I}\left(\frac{a+b}{2}-1\right)^2 + \mathrm{J}\left\{(a-1)(b-1)-c^2\right\} + \mathrm{K}\left(\frac{a'+b'}{2}\right)^2 + \mathrm{L}\left(a'b'-c'^2\right)\Big] \tag{4.35}$$

For transversely isotropic rods satisfying flip symmetry, the quadratic energy expression as shown below contains 9 parameters. The terms corresponding to coupling between extension and twist, coupling between shear and bending as well as the one correspoding to coupling between twist and cross-sectional stretch are absent here as they arise only for chiral rods.

$$\Phi_{iso}(.) = \frac{1}{2}\Big[\mathrm{A}\kappa_\alpha\kappa_\alpha + \mathrm{B}\kappa_3^2 + \mathrm{C}\nu_\alpha\nu_\alpha + \mathrm{D}(\nu_3-1)^2 + 2\mathrm{G}(\nu_3-1)\left(\frac{a+b}{2}-1\right) + \mathrm{I}\left(\frac{a+b}{2}-1\right)^2 + \mathrm{J}\left\{(a-1)(b-1)-c^2\right\} + \mathrm{K}\left(\frac{a'+b'}{2}\right)^2 + \mathrm{L}\left(a'b'-c'^2\right)\Big] \tag{4.36}$$

Physical meanings of the coefficients appearing in the energy expressions (4.35) and (4.36) are as follows:

- A: bending modulus
- B: twist modulus
- C: shear modulus

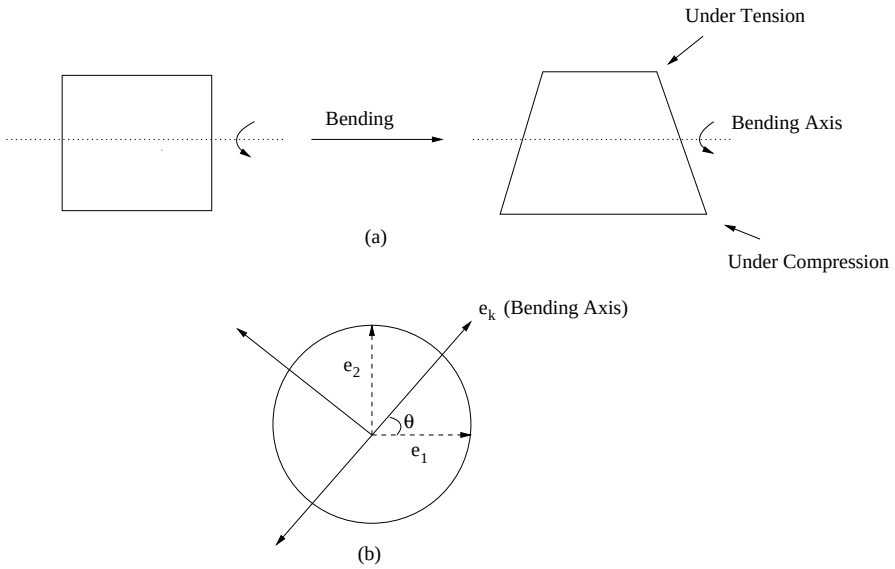

Figure 4.3: Deformation of a cross-section due to bending alone: (a) a rectangle becoming trapezoid (b) a circular cross-section with its bending axis $\mathbf{e}_k$

- D: axial stretch modulus
- E: coupling coefficient between extension and twist
- F: coupling coefficient between shear and bending
- G: Poisson coupling between axial stretch and average cross-sectional stretch
- H: Poisson type coupling between twist and average cross-sectional stretch
- I: average cross-sectional stretch/ cross-sectional size modulus
- J: cross-sectional area change (of 2^{nd} order) modulus
- K, L: penalty for variation in the cross-sectional strains *a*, *b* and *c* along the length of a rod

4.7.2 Ovalization of Cross-Sections due to Bending

Cross-sections also deform due to local bending of a rod. In this regard, one is reminded of a rectangular cross-section becoming a trapezoid (ovalization as in Fig.4.3) from elementary strength of materials. Below is an expression for how a point on a cross-section $\tilde{\mathbf{X}}$ changes its co-ordinate to $\tilde{\mathbf{x}}$ due to bending alone.

$$\tilde{\mathbf{x}} = \left[\mathbf{I} + \mu(\tilde{\mathbf{X}} \cdot \mathbf{e}_k^{\perp})\mathbf{e}_k \otimes \mathbf{e}_k\right]\tilde{\mathbf{X}} \quad \text{(no summation in k)} \tag{4.37}$$

Here $\mathbf{e}_k = \frac{k_\alpha \mathbf{e}_\alpha}{k_1^2+k_2^2}$ is the bending axis, $\mathbf{e}_k^{\perp}$ is perpendicular to it while μ is a parameter proportional to the local curvature. From expression (4.37), a point on the cross-section displaces along the bending axis proportional to its distance from the bending axis. Now, a straight line in the undeformed cross-section no more remains straight. Thus the model fails to capture this effect accurately. The model does allow for anisotropic stretching of the cross-section though. In addition, the cross-sectional strain c can be suitably chosen to orient the resulting ellipse (in case of initially circular cross-section) to fit optimally with a cross-section deformed due to bending. Thus, the model can capture ovalization of a cross-section due to bending in a phenomenological sense. Here, as μ is proportional to the local curvature, the resulting strain developed would also be proportional to the local curvature. Assuming linearity, the strain energy involved in this effect would then be of quadratic order in local curvature. Thus, the physical meaning of A in the expressions (4.35) and (4.36) above should be accordingly modified.

4.7.3 Cross-sectional Strain c and Poisson's Ratio

It should be noted that there is no term in the energy expression that explicitly depends on c. c basically defines orientation of the deformed (elliptical) cross-section which in itself is not expected to influence strain energy density. Furthermore $ab - c^2$, being the determinant of the matrix $\mathbf{U}$, signifies deformed area of a rectangle of unit area in the undeformed cross-section. But, $(a-1)(b-1) - c^2 = (ab - c^2 - 1) - (a + b - 2)$, thus the linearized portion of the change in area is subtracted from the total area change.

In the context of an isotropic rod (with no lateral traction imposed), when a rod is stretched axially, it leads to isotropic and "free shrinkage" of its cross-section. Thus we do not expect $\underline{q}$ (the corresponding stress resultants) to develop. Mathematically it implies $\frac{\partial \Phi}{\partial a} = 0$ or $\frac{a-1}{\nu_3 - 1} = -\frac{G}{I+J}$. This also being the definition of Poisson's ratio, $\frac{G}{I+J}$ defines Poisson's ratio for isotropic rods.

The term corresponding to coupling between extension and twist has been a subject of study by several researchers [4, 13, 60]. Extension and twist properties have also been separately studied in the context of carbon nanotubes [34]. The term corresponding to Poisson type coupling between twist and cross-sectional stretch were reported earlier in the context of carbon nanotubes [4] as well as for tail sheath of bacteriophage T4 [13]. Here this coupling was derived based on mathematical arguments. Often we also assume a rod to be unshearable but extensible [35, 7]. In that case, the terms corresponding to C and F would drop out from expressions (4.35) and (4.36).

4.7.4 Restrictions from Strong Ellipticity

Now restrictions due to strong ellipticity are shown for the parameters involved in the quadratic form of strain energy density just derived. As shown in Section 4.5, the matrix $\tilde{\mathbf{C}}$ must be positive definite at all values of strain measures, in particular it implies $\tilde{\mathbf{C}}$ is also positive definite at the reference configuration. Below is an expression for $\mathbf{C}$ in matrix form:

$$\mathbf{C}_{hemi} = \begin{bmatrix} \begin{bmatrix} C & 0 & 0 \\ 0 & C & 0 \\ 0 & 0 & D \end{bmatrix} & \begin{bmatrix} F & 0 & 0 \\ 0 & F & 0 \\ 0 & 0 & E \end{bmatrix} & \mathbf{[0]} & \begin{bmatrix} 0 & 0 & 0 \\ 0 & 0 & 0 \\ \frac{G}{2} & \frac{G}{2} & 0 \end{bmatrix} \\ \begin{bmatrix} F & 0 & 0 \\ 0 & F & 0 \\ 0 & 0 & E \end{bmatrix} & \begin{bmatrix} A & 0 & 0 \\ 0 & A & 0 \\ 0 & 0 & B \end{bmatrix} & \mathbf{[0]} & \begin{bmatrix} 0 & 0 & 0 \\ 0 & 0 & 0 \\ \frac{H}{2} & \frac{H}{2} & 0 \end{bmatrix} \\ \mathbf{[0]} & \mathbf{[0]} & \begin{bmatrix} \frac{K}{4} & \frac{K}{4}+\frac{L}{2} & 0 \\ \frac{K}{4}+\frac{L}{2} & \frac{K}{4} & 0 \\ 0 & 0 & -L \end{bmatrix} & \mathbf{[0]} \\ \begin{bmatrix} 0 & 0 & \frac{G}{2} \\ 0 & 0 & \frac{G}{2} \\ 0 & 0 & 0 \end{bmatrix} & \begin{bmatrix} 0 & 0 & \frac{H}{2} \\ 0 & 0 & \frac{H}{2} \\ 0 & 0 & 0 \end{bmatrix} & \mathbf{[0]} & \begin{bmatrix} \frac{I}{4} & \frac{I}{4}+\frac{J}{2} & 0 \\ \frac{I}{4}+\frac{J}{2} & \frac{I}{4} & 0 \\ 0 & 0 & -J \end{bmatrix} \end{bmatrix} \tag{4.38}$$

The matrix $\mathbf{C}_{iso}$ can accordingly be put in matrix form by setting E = F = H = 0 in the expression (4.38). Positive definiteness of $\tilde{\mathbf{C}}_{hemi}$ implies:

1. A>0, B>0, C>0, D>0, K> 0, L<0
2. AC-F^2 >0
3. BD-E^2 >0

4. K> |L|

We now look at the partials of $\Phi(.)$ with respect to z_α at the reference configuration.

$$\begin{aligned}\frac{\partial \Phi}{\partial z_\alpha} &= \int_\Omega \frac{\partial \tilde{W}}{\partial \mathbf{F}}(\mathbf{F}) : \frac{\partial \mathbf{F}}{\partial z_\alpha}\, ds \\ &= \int_\Omega \frac{\partial \tilde{W}}{\partial \mathbf{F}}(\mathbf{F}) : [X_\alpha \mathbf{RKe}_\alpha \otimes \mathbf{e}_3 + \mathbf{Re}_\alpha \otimes \mathbf{e}_\alpha]\, ds \quad \text{(no sum on } \alpha)\end{aligned} \tag{4.39}$$

At **F**=**I** (reference configuration), **K**=**0**. Therefore:

$$\begin{aligned}\frac{\partial \Phi}{\partial z_\alpha} &= \int_\Omega \frac{\partial \tilde{W}}{\partial \mathbf{F}}(\mathbf{F} = \mathbf{I}) : [\mathbf{Re}_\alpha \otimes \mathbf{e}_\alpha]\, ds \quad \text{(no sum on } \alpha) \\ \text{And, } \frac{\partial^2 \Phi}{\partial z_\alpha^2} &= \int_\Omega [\mathbf{Re}_\alpha \otimes \mathbf{e}_\alpha] \cdot \frac{\partial^2 \tilde{W}}{\partial \mathbf{F}^2}(\mathbf{F} = \mathbf{I}) \cdot [\mathbf{Re}_\alpha \otimes \mathbf{e}_\alpha]\, ds \quad \text{(no sum on } \alpha) \\ &> 0 \quad \text{(by strong ellipticity)}\end{aligned} \tag{4.40}$$

For quadratic energy expressions (4.35) and (4.36), this implies $I > 0$.

It is difficult to deduce restrictions on the coefficient J mathematically but we imagine a physical experiment where we apply uniform lateral traction throughout the length of a straight rod such that $\frac{a+b}{2} = 1$ but $a < 1$ and $b > 1$. Further, no other strain is allowed to develop. If such an experiment can be performed, it will only activate the term containing J in the strain energy expression. We expect the strain energy developed to be positive, which implies $J < 0$.

4.8 Conclusions

A mathematically consistent extension to standard Cosserat rod theory is developed that can incorporate in-plane cross-sectional deformation. It is envisioned

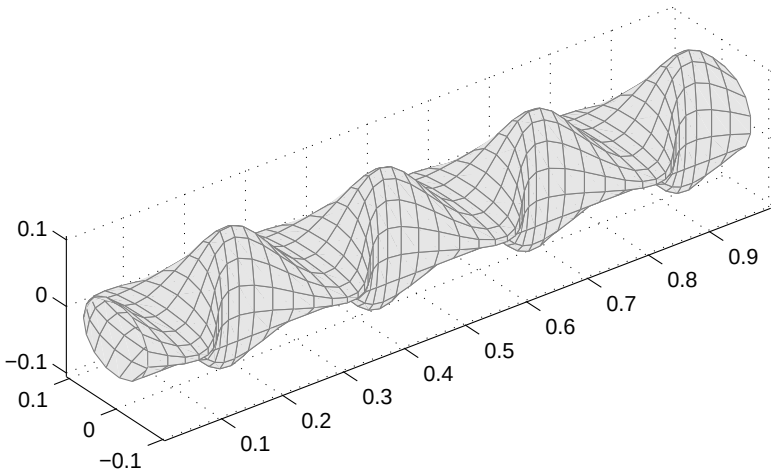

Figure 4.4: Surface deformation of an initially hollow circular cylinder: $a = 1 + 0.7\sin(.5\pi s),\ b = 1 - 0.7\sin(.5\pi s),\ c = 0$

that the proposed theory efficiently bridges the gap between rod theory and cylinderical shell theory, in cases where the effect of warping is negligible. The proposed theory is applicable to solid rods too.

A limitation of the theory lies in the fact it allows a circular cross-section to only become elliptical. However, a careful selection of cross-sectional strains a and b could result in a rather complex shaped wavy deformed surface as shown in Fig.4.4 (the deformed surface resembles that of a single walled carbon nanotube deformed by a compressive axial force, as reported in Fig.1 of [49]). We also have the additional strain measure c to rotate the axes of ellipses along the length of a rod that could make the deformed surface even more exotic. The most general form of the quadratic strain energy density was also derived which can be used by researchers for capturing cross-sectional deformation in dna, nanotubes, col-

lagen, arteries etc using the one-dimensional model. Restrictions on the parameters involved are also derived. A complete set of nine ODEs as well as the corresponding variational formulations were derived for numerical computation of equilibrium shapes for the proposed model. A current research project at Cornell involves using this model to capture deformation (including that of the cross-section) of carbon nanotubes.

There are several opportunities for future research. In this Chapter, the emphasis was only on the quadratic invariants of strain measures. One could find a complete set of the higher order invariants in order to deduce energy expressions of higher order. As reported by Healey [28], upto quadratic form of strain energy density, a hemitropic rod is equivalent to rod-like structures having a finite number of helices such as collagen, dna or carbon nanotubes. But, to derive higher order energy expressions, one has to use symmetry group (e.g., dihedral-helical symmetry [28]) pertaining to the specific molecule or nanotube. A specific example could be to model strain-dependent coupling between extension and twist as reported by Upamanyu et al. [60] for chiral filaments. One could also extend the present model for dynamic analysis. This will require deriving inertia terms for the set of the nine ODEs derived here.

A rod model incorporating only the warping effect was proposed by Simo and Vu-Quoc [55]. It would be a nice step ahead to bridge the present model with that of Simo and Vu-Quoc's in a consistent manner, thus coming up with a more general rod model.

CHAPTER 5

ONE-DIMENSIONAL MODELING OF DEFORMATION OF SINGLE-WALLED CARBON NANOTUBES

5.1 Outline

This Chapter is concerned with one-dimensional elastic modeling of a single-walled carbon nanotube. The outline of this Chapter is as follows. First, parameters of the energy expression (4.35) are estimated using the atomistic simulation data in Section 5.2. In Section 5.3, usefulness of the new rod model proposed in Chapter 4 is demonstrated as it is able to explain some of the peculiar atomistic simulation data corresponding to the axial stretching of a SWCNT. A somewhat unexplored coupling between twist and cross-sectional shrinkage for chiral nanotubes is also established. The parameters evaluated from Section 5.2 are then used to estimate the radial modulus of a carbon nanotube and the estimated value is further compared with that of a continuum isotropic and thick hollow tube (having same size as the nanotube) in Section 5.4. Section 5.5 concludes this Chapter.

5.2 Estimation of the Rod parameters for a (9,6) SWCNT

For convenience, an expression for the strain energy density (4.35) for chiral rods is repeated below:

$$\Phi_{hemi}(.) = \frac{1}{2}\Big[\mathrm{A}\kappa_\alpha\kappa_\alpha + \mathrm{B}\kappa_3^2 + \mathrm{C}\nu_\alpha\nu_\alpha + \mathrm{D}(\nu_3-1)^2 + 2\mathrm{E}(\nu_3-1)\kappa_3 + 2\mathrm{F}\nu_\alpha\kappa_\alpha + \\ 2\mathrm{G}(\nu_3-1)\left(\frac{a+b}{2}-1\right) + 2\mathrm{H}\kappa_3\left(\frac{a+b}{2}-1\right) + \mathrm{I}\left(\frac{a+b}{2}-1\right)^2 + \\ \mathrm{J}\left\{(a-1)(b-1)-c^2\right\} + \mathrm{K}\left(\frac{a'+b'}{2}\right)^2 + \mathrm{L}\left(a'b'-c'^2\right)\Big] \tag{5.1}$$

It contains 12 parameters out of which only the first six (A-F) appear in the special Cosserat theory of rods [28]. These parameters were estimated for a (9,6) SWCNT in [5] but, there the nanotube's cross-section was assumed to be rigid. Here we do not assume rigidity of its cross-section and focus on computing the remaining parameters present in (5.1) (ideally when the rigidity of a cross-section is relaxed, the first six parameters (A-F) should also be re-evaluated but this has not been done in the present work). Of the remaining six, four of them (I-L) are purely related to the cross-sectional deformation while the terms corresponding to G and H signify coupling between deformation of a cross-section with axial stretch and twist respectively. In order to evaluate the parameters I, J, K and L, a judicious set of deformations is chosen for atomistic simulation so that none of the other terms in (5.1) are activated. This is definitely desirable from the perspective of numerics as the final estimates would be less prone to numerical error. Below we show this desired set of deformations.

1. Gradually first stretch then compress the cross-section of a nanotube uniformly along its length such that $a = 1 + \alpha \neq 1$ and $b = 1$. It turns a

circular cross-section into an ellipse and one can exactly compute where the atoms should be positioned. Also, atoms should be constrained from any induced axial stretch ($\nu_3 = 1$) or twist ($k_3 = 0$). This strategy will only activate the term corresponding to the coefficient I in (5.1).

2. Gradually deform the cross-section uniformly along its length such that $a + b = 2$ or $a = 1 + \alpha$ and $b = 1 - \alpha$. (Again, atoms should not be displaced axially neither be allowed to twist). This activates only the term involving J.

3. Gradually deform the cross-sections non-uniformly keeping $a + b = 2$. Here, a sine function is used to induce non-uniformity during the deformation, i.e., $a = 1 + \alpha \sin(\pi s/L_0)$ and $b = 1 - \alpha \sin(\pi s/L_0)$, where s is the arclength of an undeformed unit cell of a nanotube and L_0 is the length of the undeformed unit cell of the same nanotube. This activates only the terms involving J and L.

4. Gradually deform the cross-sections so that $a = b = 1 + \alpha \sin(\pi s/L_0)$. Here, the cross-sections remain circular. This activates the terms involving I, J, K and L.

These four sets of simulations, when performed in the same sequence, allows us to estimate all these four coefficients. It may be mentioned here that the positions of all the atoms, after the deformation, are already known a priori. For each of the four simulations, the unit cell of nanotube is deformed incrementally in small steps and for each of these deformation steps, atomistic simulation data provides us with the associated total inter-atomic energy which is then compared with the continuum energy expression (5.1) to estimate the activated parameters. Now we show plots of how these four parameters vary as a

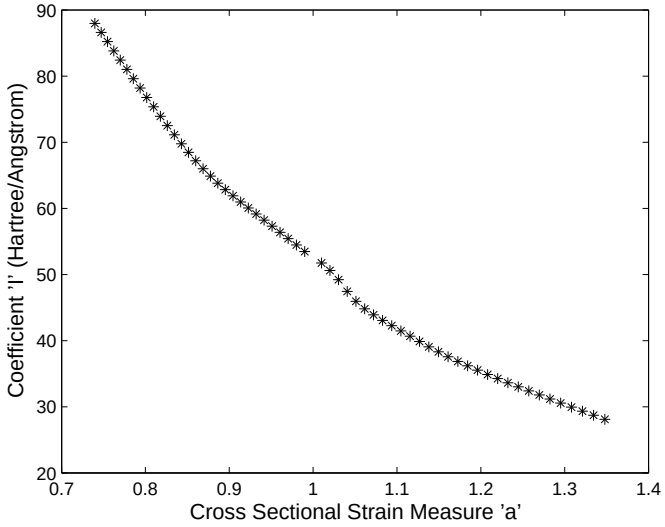

Figure 5.1: Variation in the Coefficient 'I' as a function of the Cross-sectional Strain measure 'a': simulation #1

function of the deformation steps.

Fig.5.1 shows how the coefficient I varies as a function of the deformation steps as outlined in simulation #1. As evident from the figure, it shows a higher value for the compressed regime and a lower value for the stretched regime. This is due to asymmetry in the energy diagram (Fig.5.2) about the reference configuration. This is typical of several atomic potentials (e.g. Lennard-Jones) where stretching of a bond causes less increase in energy than the same amount of compression does. Clearly, the quadratic energy model (5.1) fails to capture this effect and a higher order term gets activated even at a small strain level. Note that a materially linear object with quadratic strain energy density would have constant (not strain-dependent) coefficients in an energy expression such as (5.1).

Fig.5.3 shows how the coefficient J varies as a nanotube's cross-section is de-

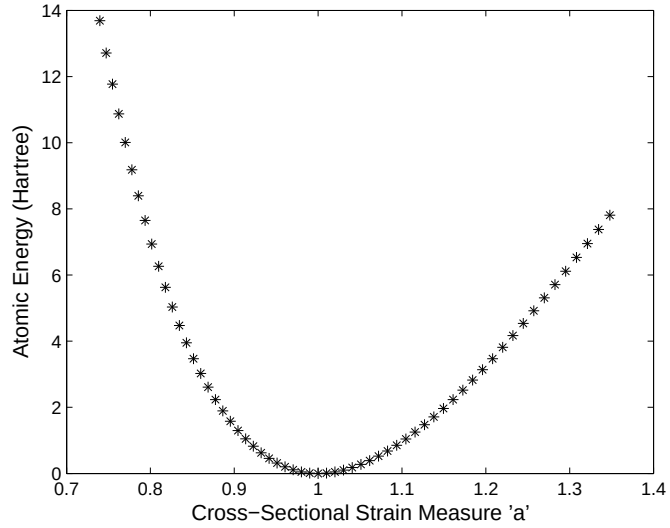

Figure 5.2: Variation in the total inter-atomic energy as the nanotube's cross-section is deformed according to simulation #1

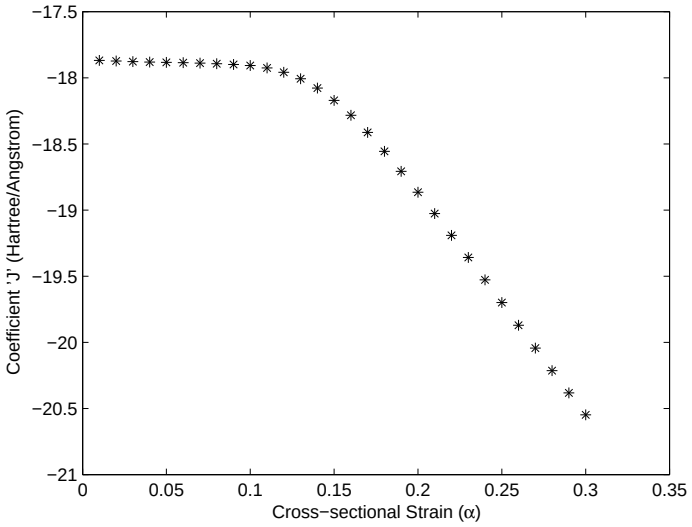

Figure 5.3: Coefficient 'J' as a nanotube's cross-section is deformed according to simulation #2

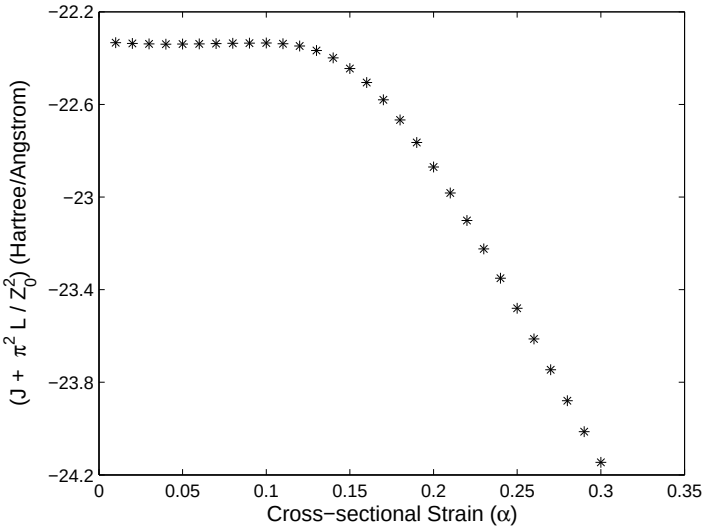

Figure 5.4: Variation in $\left[J + \pi^2 L/Z_0^2\right]$ as a nanotube's cross-section is deformed according to simulation #3

formed according to simulation #2. It may be observed that the quadratic model fits well upto even 12% strain. Here, a nanotube's cross-section is stretched as well as compressed along the two perpendicular directions, thereby cancelling the effect of asymmetry in energy as associated with simulation #1. The same pattern is observed even in Fig.5.4 that corresponds to simulation #3. This shows that the coefficient L also remains constant upto 12% strain. Fig.5.5 corresponds to simulation #4. Here, again the asymmetry could be seen just as in Fig.5.1. It is certainly due to activation of the coefficient I during this simulation. The coefficient K is expected to have symmetric values within the neighbourhood of the reference configuration. It is also expected to remain constant upto a large strain level (just as the coefficients J and L do) since the coefficient K corresponds to the energy associated with any non-uniformity in the strain invariant $a + b$. Thus, it does not matter whether the bonds are being stretched or compressed but what matters here is the level of non-uniformity in this stretch/compression of a bond along the length of a nanotube.

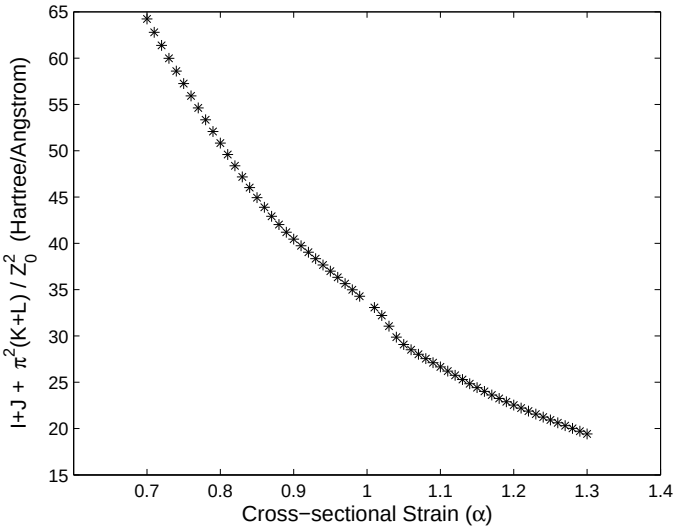

Figure 5.5: Variation in $\left[I + J + \pi^2(K + L)/Z_0^2\right]$ as a nanotube's cross-section is deformed according to simulation #4

Based on the four simulations, the values of the four coefficients (I - L) at the straight state reference configuration (strain $\rightarrow$ 0) are tabulated in Table 5.1. It may be noted that the signs of of all these coefficients respect the strong ellipticity condition as derived in the preceding Chapter but one of the conditions (K > |L|) is violated, signalling instability. In the next section another instability associated due to chirality of this nanotube is shown.

Table 5.1: Values of the coefficients I, J, K and L for a nanotube at the straight state reference configuration

I	52.5 (hartree/angstrom)
J	-17.9 (hartree/angstrom)
K	123.1 (hartree×angstrom)
L	-150.4 (hartree×angstrom)

5.3 Coupling between Axial stretch, Twist and Shrinkage of a Cross-section for a Chiral Nanotube - Explanation of Certain Instabilities

Based on the theory proposed in the preceding Chapter, a chiral carbon nanotube should show coupling between axial stretch and twist (E), axial stretch and cross-sectional shrinkage (G) as well as twist and cross-sectional shrinkage (H). Out of these three, the last coupling mode has not been explored much. The existence of all these three coupling terms will be established now based on the atomistic simulation data where a nanotube is axially stretched (no constraint is imposed on rotation or cross-sectional shrinkage at the two ends). The relaxed equilibrium configuration obtained shows isotropic (a = b, c = 0) and uniform (a′ = b′ = 0) shrinkage of each of the nanotube's cross-sections. The data also shows that during the imposed extension on a unit cell of (9,6) SWCNT, each of the neighboring "cross-sections" rotate by the same magnitude but in alternate directions. This is in contrast to the extension-twist coupling behavior in other chiral molecules, such as collagen [15], where all the cross-sections rotate in the same direction resulting in a finite end to end rotation. Surprisingly, the axial stretch during the imposed extension of a (9,6) SWCNT is also observed to be non-uniform. These peculiar observations are explained now based on the theory proposed in the preceding Chapter. The atomistic simulation data should satisfy the following constraints (if continuum theory has to hold at atomic level):

1. Axial force n_3 should be uniform throughout the length of a nanotube, i.e., $\frac{\partial \Phi}{\partial \nu_3}$ = constant $\Rightarrow$ (a) D($\nu_3 - 1$) + Eκ_3 + G($a - 1$) = constant and (b)

$D\triangle\nu_3 + E\triangle\kappa_3 = 0$ since a is found to be uniform throughout the length of a nanotube. Condition (b) can also be put in the following form:

$$\frac{D}{E} = -\frac{\triangle\kappa_3}{\triangle\nu_3} \tag{5.2}$$

2. Twisting moment m_3 should vanish, i.e., $\frac{\partial\Phi}{\partial\kappa_3} = 0 \Rightarrow (a)\ B\kappa_3 + E(\nu_3 - 1) + H(a - 1) = 0$ and (b) $B\triangle\kappa_3 + E\triangle(\nu_3 - 1) = 0$. The two conditions can also be written as:

$$\frac{\kappa_3}{(\nu_3 - 1)} = -\frac{E}{B} - \frac{H}{B}\frac{(a-1)}{(\nu_3 - 1)} \quad \text{and} \quad \frac{E}{B} = -\frac{\triangle\kappa_3}{\triangle\nu_3} \tag{5.3}$$

3. No radial stress should develop due to "free" shrinkage of the cross-sections, i.e., $\frac{\partial\Phi}{\partial a} = 0 \Rightarrow G(\nu_3 - 1) + H\kappa_3 + (I+J)(a-1) = 0$. The same can be written as:

$$\frac{\kappa_3}{(\nu_3 - 1)} = -\frac{G}{H} - \frac{I+J}{H}\frac{(a-1)}{(\nu_3 - 1)} \tag{5.4}$$

Upon comparing (5.2), (5.3) and (5.4), one can show that:

$$\frac{D}{E} = \frac{E}{B} = \frac{G}{H} \quad \text{and} \quad \frac{H}{B} = \frac{I+J}{H} \tag{5.5}$$

Figures 5.6 and 5.7 have been plotted using the atomistic simulation data corresponding to the average axial stretch of 2.5%. From the top and bottom figures in Fig.5.6, it can be seen that both twist(κ_3) and axial strain ($\nu_3 - 1$) are not uniform but each of them attain two different values alternately (the two levels are almost constant along the length). The same alternations between two different values are seen even for the strain ratios $\frac{\kappa_3}{\nu_3 - 1}$ and $\frac{(a-1)}{\nu_3 - 1}$ in the top and middle of Fig.5.7. Further, the bottom of Fig.5.7 shows that the ratio -$\frac{\triangle\kappa_3}{\triangle\nu_3}$ is almost constant (except for the fluctuations at the center which is observed to be negligible

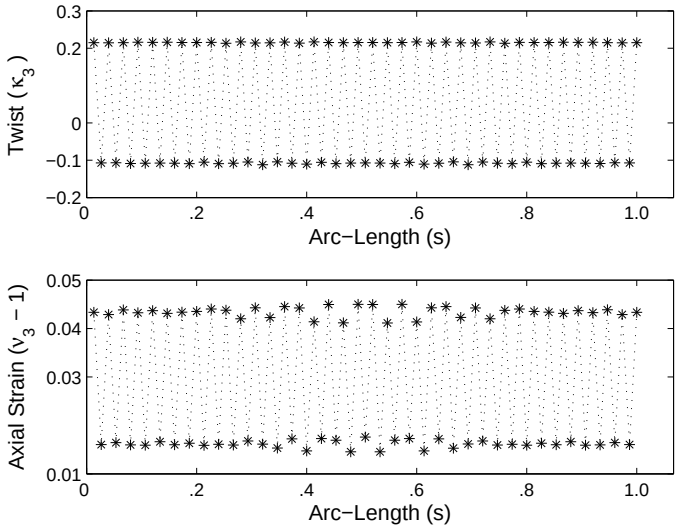

Figure 5.6: Variation in the strains (top: κ_3, bottom: (ν_3−1)) along the length of a representative unit cell of a (9,6) SWCNT

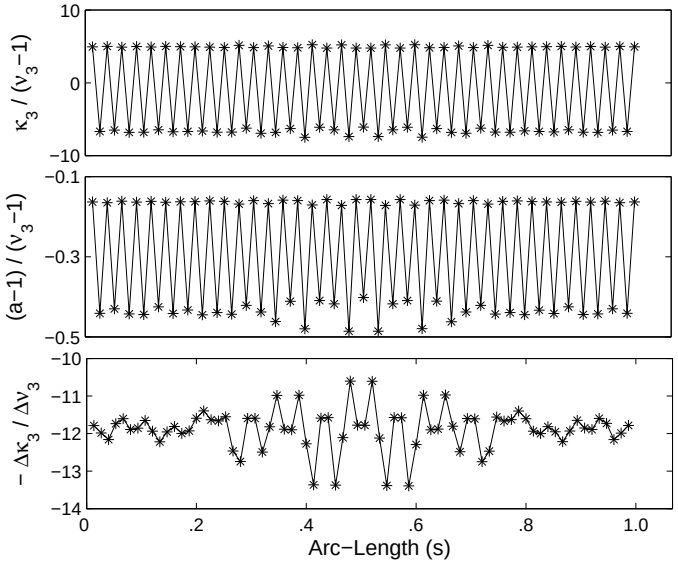

Figure 5.7: Variation in the strain ratios (top: $\frac{\kappa_3}{\nu_3-1}$, middle: $\frac{(a-1)}{\nu_3-1}$, bottom: -$\frac{\Delta\kappa_3}{\Delta\nu_3}$) along the length of a representative unit cell of a (9,6) SWCNT

at other levels of imposed average axial stretch) along the length of a unit cell. This is in agreement with the equations (5.2) and (5.3)(ii). Equations (5.3)(i) and (5.4) further allow each of the two strain ratios to take two different values as each of these equations contains two constants. It should be noted that if the special theory of Cosserat rods (having rigid cross-section) is used (H = 0), then the equation (5.3)(i) would restrict the strain ratio $\frac{\kappa_3}{\nu_3 - 1}$ to take a unique value. This illustrates usefulness of the rod model proposed in the preceding Chapter. Also from equation (5.5), $BD - E^2 = 0$ which violates the convexity condition derived in the preceding Chapter. It is well known that this violation of convexity can allow weak and discontinuous equilibrium solutions. This explains why the neighboring cross-sections rotate in the opposite directions. The same effect could also result from a higher order extension-twist coupling term but it is noted that this was observed in the simulation data even at the lowest strain level.

Fig.5.8 shows the ratio $\frac{E}{B}$ computed in two different ways. As equation (5.3)(i) has to be satisfied all along the length of a nanotube, this provides us with an overdetermined system of equations which is solved via least square procedure to obtain the ratios $\frac{E}{B}$ and $\frac{H}{B}$. Another way to obtain $\frac{E}{B}$ or $\frac{D}{E}$, on the basis of equations (5.2) and (5.3)(ii), is to take the average value of the ratio $-\frac{\triangle \kappa_3}{\triangle \nu_3}$ as plotted at the bottom of Fig.5.7. As can be seen in Fig.5.8, both the procedures seem to give approximately the same value for $\frac{E}{B}$ (for a given average axial stretch) which is another check on the use of the theory as well as data analysis. Figures 5.8 and 5.9 both show reasonably constant values for the two ratios $\frac{E}{B} \approx -12$ and $\frac{H}{B} \approx -42$ in the small deformation regime (i.e., low values of average axial stretch) which further justifies the quadratic model (5.1).

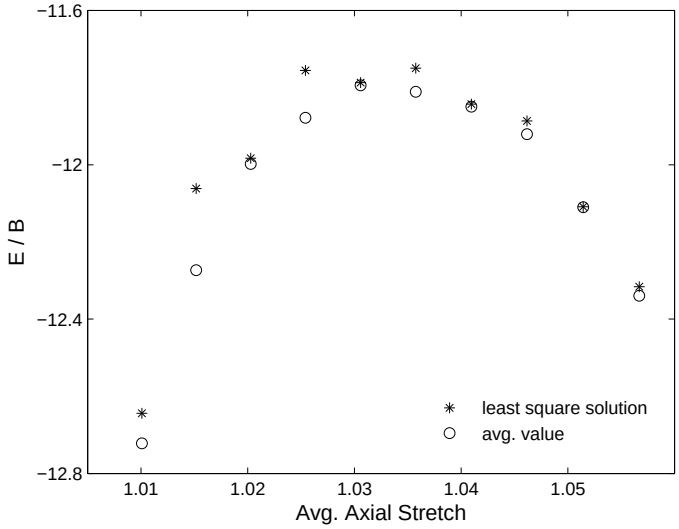

Figure 5.8: Ratio of the coefficients E and B (E/B) as the nanotube is incrementally stretched

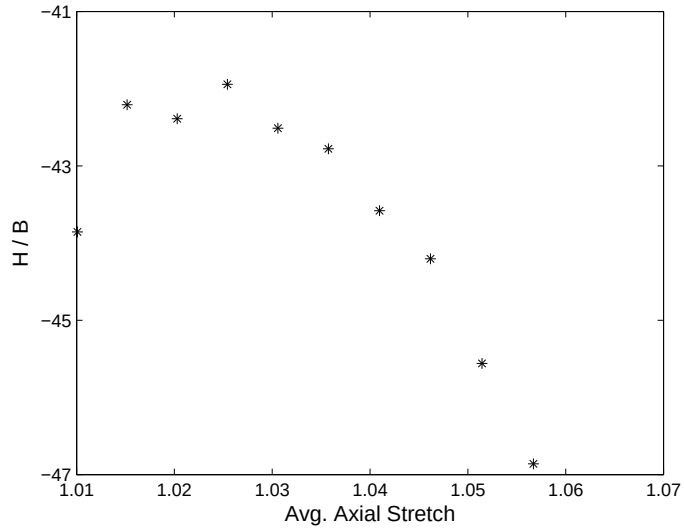

Figure 5.9: Ratio of the coefficients H and B (H/B) as the nanotube is incrementally stretched

Equation (5.4) can also be written in a different form to obtain an expression for the Poisson's ratio (ν) as follows.

$$\nu = -\frac{(a-1)}{(\nu_3 - 1)} = \frac{\mathrm{G}}{\mathrm{I{+}J}} + \frac{\mathrm{H}}{\mathrm{I{+}J}}\frac{\kappa_3}{(\nu_3 - 1)} \tag{5.6}$$

Thus for chiral tubes, the Poisson's ratio is also dependent on the induced twist. At zero twist, the expression (5.6) reduces to that for isotropic tubes and using the values already computed, it turns out to be $\nu \approx \frac{12}{42} = .29$.

5.4 Estimation of the Radial Modulus for a (9,6) SWCNT and its Comparison with the Radial Modulus of an equivalent Continuum Hollow Cylinder

In this Section, we compute the radial modulus for carbon nanotubes, subjected to uniform pressure. In this scenario, deformation of its cross-section would also be uniform as well as isotropic (i.e., $\mathrm{a} = \mathrm{b},\ \mathrm{a}' = \mathrm{b}' = \mathrm{c} = 0$). Thus, the radial modulus can be computed using the energy expression (5.1) as radial modulus = $\frac{\partial^2 \Phi}{\partial \mathrm{a}^2} = \mathrm{I} + \mathrm{J}$. Plugging in the numerical values already computed in the preceding Section, we get:

$$\text{radial modulus} = \mathrm{I} + \mathrm{J} = 34.6 \text{ hartree/angstrom} \approx 1.5 \text{ e-6 joule/meter} \tag{5.7}$$

As the mean radius of a nanotube is typically taken to be 5.16 angstrom while its wall thickness is taken to be 3.37 angstrom [5], it may be appropriate to view it as a thick cylinder. An expression for the radial modulus will now be found assuming the nanotube to be a thick cylinder. From the previous Chapter, the

conjugate stress $\mathrm{q} = \frac{\partial \Phi}{\partial \mathrm{a}}$. As pressure is being applied uniformly, the derivatives of all the quantities with respect to the arc-length would vanish. Hence, using the equilibrium equations derived in the previous Chapter (4.25), an expression for the stress resultant q can be derived as follows:

$$\begin{aligned} \mathrm{q} &= \mathrm{r}_1 + \mathrm{r}_2 \\ &= \int_{\partial\Omega} \mathbf{P}\boldsymbol{\nu} \cdot \mathrm{X}_\alpha \mathbf{e}_\alpha \\ &= -\int_{\partial\Omega} \mathrm{p}\boldsymbol{\nu} \cdot \mathrm{r}\boldsymbol{\nu} \\ &= -2\pi(\mathrm{p}_o \mathrm{r}_o^2 + \mathrm{p}_i \mathrm{r}_i^2) \end{aligned} \tag{5.8}$$

Here p_i and p_o are the internal and external pressures, respectively, acting on a nanotube. Now assuming small strain conditions, the radial modulus can be defined as:

$$\text{radial modulus} \approx \frac{\mathrm{q}}{a-1} = -2\pi \frac{(\mathrm{p}_o \mathrm{r}_o^2 + \mathrm{p}_i \mathrm{r}_i^2)}{a-1} \tag{5.9}$$

Assuming that the nanotube is unrestrained to deform in the axial direction, we can further assume plane-stress condition. Thus, from 3-d continuum mechanics, we can write an expression for the radial stress in an isotropic (assumption of isotropy would need to be verified for a chiral tube) cylinder as:

$$\begin{aligned} \sigma_{rr} &= \frac{E}{1-\nu^2}\left[\epsilon_{rr} + \nu\epsilon_{\theta\theta}\right] \\ &= \frac{E}{1-\nu}\epsilon_{rr}, \ (\epsilon_{rr} = \epsilon_{\theta\theta}, \text{ as per the kinematics used in the preceding Chapter}) \\ &= \frac{E}{1-\nu}(a-1) \end{aligned} \tag{5.10}$$

Also the radial stress in a thick cylinder varies as $\sigma_{rr} = A + B/r^2$ where 'A' and 'B' are the constants that depend on the internal and external pressures. A straighforward algebraic manipulation shows the average radial stress to be:

$$\langle \sigma_{rr} \rangle = -\frac{(\mathrm{p}_o \mathrm{r}_o + \mathrm{p}_i \mathrm{r}_i)}{\mathrm{r}_o + \mathrm{r}_i} \tag{5.11}$$

Using (5.11) in (5.10), we get:

$$\frac{(\mathrm{p}_o \mathrm{r}_o + \mathrm{p}_i \mathrm{r}_i)}{\mathrm{r}_o + \mathrm{r}_i} = -\frac{E}{1-\nu}(a-1) \tag{5.12}$$

Further substituting (5.12) in (5.9), we get:

$$\begin{aligned} \text{radial modulus} &= 2\pi\, \mathrm{r}_o^2 \frac{E}{1-\nu}(1 + \frac{\mathrm{r}_i}{\mathrm{r}_o}) = 6.25 \text{ e-6 (joule/meter, no int. pressure)} \\ &= 2\pi\, \mathrm{r}_i^2 \frac{E}{1-\nu}(1 + \frac{\mathrm{r}_o}{\mathrm{r}_i}) = 3.17 \text{ e-6 (joule/meter, no ext. pressure)} \end{aligned} \tag{5.13}$$

The continuum radial modulus computed in (5.13) compares very well with the radial modulus of the nanotube as shown in (5.7), the latter being based on the atomistic simulation data.

Furthermore, the axial stretch modulus may be defined as the product of Young's modulus of a nanotube (assumed to be 1 terrapascal) and its area of cross-section. The stretch modulus turns out to be 1.09 e-6 joule/meter. This is definitely comparable with the radial modulus shown in (5.7). Thus, rigidity of cross-sections may not be a valid assumption for carbon nanotubes.

5.5 Conclusions

A chiral carbon nanotube was modeled using a new one dimensional rod model that allows in-plane deformation of its cross-section. The parameters of the strain energy for this rod model were estimated using the atomistic simulation data for a (9,6) carbon nanotube. The model can capture accurately one-dimensional deformation of nanotubes and hence is much less expensive to use than a 2-d shell model. It also captures three dimensional deformation

of a naontube somewhat accurately. A new coupling effect between twist and shrinkage of a cross-section is also estabilished for chiral tubes. The model is also able to explain some of the peculiar behaviors such as (i) rotation of the neighboring cross-sections in alternate directions (ii) oscillation of the strains such as twist and axial stretch between two different levels.

An important next step is to re-evaluate the remaining paramters corresponding to the special Cosserat theory of rods as it is found that the radial modulus of a nanotube is comparable to its axial stretch modulus. One of the coefficients (I) is found to be not constant even at very small strain levels. As it signals activation of a higher order term, it may be important to realize all the higher order terms that get activated appreciably at ”moderate” strain levels. The carbon nanotube investigated here is found to be unstable as it does not obey the convexity requirements. It is also probably weakly stable in twist-stretch coupled deformation mode. Certainly, this is dependent on the chirality as other molecules do not exhibit the same. It will be an important step to come up with a general formulation encompassing tubes of all chirality and then investigate how stability/instability of a tube depends on its chirality.

CHAPTER 6

CONCLUSIONS AND FUTURE WORK

We make the following remarks to conclude this dissertation.

- This dissertation is primarily motivated by the need to address theoretical and computational challenges associated with rods in order to increase its range of applicability.
- A generalized computational approach to deduce stability of constrained elastic rods is present in Chapter 2. A new numerical algorithm is proposed that removes the singularity associated with the constraints present and at the same time maintains its efficiency. It would be an important step ahead to address the limitations of the algorithm as mentioned in the concluding remarks of Chapter 2.
- In Chapter 3, a mixed variational principle is proposed for extensible and unshearable rods. This leads to a reduced set of the equilibrium equations which would be beneficial for both theoretical and numerical analysis of such rods.
- A novel extension to the special theory of Cosserat rods is presented in Chapter 4. This allows in-plane deformation of a rod's cross-section. Based on symmetry arguments, the most general expression for its quadratic strain energy is derived. This model is then used to explain some of the peculiar behavior of a (9,6) chiral carbon nanotube in Chapter 5. A new coupling between twist and shrinkage of cross-sections is also established. The model also predicts that the numerical values of its material parameters (especially the one denoting its chirality) are such that the resulting elasticity tensor is only positive semi-definite. This may imply the

nanotube to be only weakly stable in the coupled extension-twist deformation mode. Atomistic simulation data also shows co-existence of two phases: the same was also explained using the new rod model. There is certainly a potential phase transition problem to be investigated here. It is envisioned that this new rod model for carbon nanotubes would be more effective and efficient to study its deformation. The ideas presented could also be extended to other nanotubes composed of silicon [53] or boron nitride [17].

- An important next step is to extend the rod model developed in Chapter 4 to account for out-of-plane warping of its cross-section [55]. Such a model would be important for rods with ″open-face″ cross-sections where the effect of warping may be significant. It would also be interesting to deduce strain energy density of higher order for the rod model proposed in Chapter 4 to study material non-linearity.
- A general formulation which can link tubes of all chirality may be a good idea to pursue. It may further be important to investigate how stability/instability of a nanotube is affected as its chirality is varied.

BIBLIOGRAPHY

[1] Antman, S.S., 1995. Nonlinear Problems of Elasticity. Springer-Verlag, New York.

[2] Bolotin, V.V., 1963. Nonconservative Problems of the Theory of Elastic Stability. Pergamon Press, Macmillan, New York.

[3] Bozec, L., Vander Heijden, G.H.M., Horton, M., 2007. Collagen Fibrils: Nanoscale Ropes. Biophysical Journal 92, 70-75.

[4] Chandraseker, K., and Mukherjee, S., 2006. Coupling of Extension and Twist in Single-Walled Carbon Nanotubes. J. Appl. Mech 73, 315-326.

[5] Chandraseker, K., and Mukherjee, S., Paci, J. T., Schatz, G. C., 2009. An atomistic-continuum Cosserat rod model of carbon nanotubes. Journal of the Mechanics and Physics of Solids 57, 932-958.

[6] Cliffe, K.A., Garratt, T.J., Spence, A., 1993. Eigenvalues of the discretized Navier-Stokes equation with application to the detection of Hopf bifurcations. Advances in Computational Mathematics 1, 337-356.

[7] Coleman, B. D., Dill, E. H., Swigon, D., 1995. On the dynamics of flexure and stretch in theory of elastic rods. Archive for rational Mechanics and Analysis 129, 147-174.

[8] Dichmann, D., Li, Y., Maddocks, J.H., 1996. Hamiltonian formulation and symmetries in Rod Mechanics. Mathematical Approaches to Biomolecular Structure and Dynamics, 71-113.

[9] Doedel, E.J., 2000. AUTO2000: Continuation and Bifurcation Software for Ordinary Differential Equations.

[10] Domokos, G., Szeberenyi, I., 2001. A hybrid parallel approach to one-parameter nonlinear boundary value problems. Computer Assisted Mechanics and Engineering Sciences 11, 1-20.

[11] Domokos, G., Healey, T.J., 2005. Multiple Helical Perversions of Finite, Intrinsically Curved Rods. International Journal of Bifurcation and Chaos 15, 871-890.

[12] Elstner, M., Porezag, D., Jungnickel, G., Elsner, J., Haugk, M., Frauenheim, Th., 1998. Self-consistent-charge density-functional tight-binding method for simulations of complex materials properties. Phys. rev. B 58, 7260-7268.

[13] Falk, W., James, R. D., 2006. Elasticity theory for self-assembled protein lattices with application to the martensitic phase transition in bacteriophage T4 tail sheath. Phys. Rev. E 73, 011917.

[14] Frauenheim, Th., Seifert, G., Elstner, M., Niehaus, T., Kohler, C., Amkreutz, M., Sternberg, M., Hajnal, Z., Di Carlo, A., Sahai, S., 2002. Atomistic simulations of complex materials: Ground-state and excited-state properties. J. Phys.: Condens. Matter 14, 3015-3047.

[15] Gautieri, A., Buehler, M.J., Redaelli, A., 2009. Deformation rate controls elasticity and unfolding pathway of single tropocollagen molecules. Journal of the Mechanical Behavior of Biomedical Materials 2, 130-137.

[16] Gelfand, I. M., and Fomin, S. M., 1991. Calculus of Variations. Dover Publications, New York.

[17] Golberg, D., Bando, Y., Tang, C.C., Zhi, C.Y., 2007. Boron nitride nanotubes. Advanced Materials 19(18), 2413-2432.

[18] Golub, G.H., Van Loan, C.F., 1996. Matrix Computations. The Johns Hopkins University Press, Baltimore.

[19] Goriely, A., Robertson-Tessi, M., Tabor, M., Vandiver, R., 2008. Elastic Growth Models. Book Chapter- Mathematical Modeling of Biosystems. Springer, Berlin Heidelberg.

[20] Goriely, A., Tabor, M., 1997. Nonlinear dynamics of filaments I. Dynamic instabilities. Physica D 10, 20-44.

[21] Goriely, A., Vandiver, R., 2010. On the Mechanical Stability of Growing Arteries. IMA Journal of Applied Mathematics.

[22] Gould, T., and Burton, D. A., 2006. A Cosserat rod model with microstructure. New J. Phys. 137, 1-17.

[23] Goyal, S., Perkins, N. C., Lee, C. L., 2005. Nonlinear dynamics and loop formation in Kirchhoff rods with implications to the mechanics of DNA and cables. Journal of Computational Physics 209, 371-389.

[24] Green, A. E., and Laws, N., 1966. A General Theory of Rods. Proc. R Soc. Lond. A 293, 145-155.

[25] Green, A. E., and Laws, N., 1973. Remarks on the theory of Rods. Journal of Elasticity 3, 179-184.

[26] Healey, T. J., 2008. Lecture Notes on Nonlinear Elasticity: Rod Theory. Theoretical & Applied Mechanics, Cornell University.

[27] Healey, T. J., 2010. A Rigorous Derivation of Hemitropy In Nonlinearly Elastic Rods (to appear).

[28] Healey, T.J., 2002. Material Symmetry and Chirality in Nonlinearly Elastic Rods. Math. Mech. Solids 7, 405-420.

[29] Healey, T.J., Mehta, P.G., 2005. Straightforward Computation of Spatial Equilibria of Geometrically Exact Cosserat Rods. International Journal of Bifurcation and Chaos 15, 949-965.

[30] Hodges, D. H., 1990. A Mixed variational Formulation Based on Exact Intrinsic Equations For Dynamics of Moving Beams. Int. J. Solids. Structures 26, 1253-1273.

[31] Hodges, D. H., 2003. Geometrically Exact, Intrinsic Theory for Dynamics of Curved and Twisted Anisotropic Beams. AIAA Journal 41, 1131-1137.

[32] Hodges, D. H., 2009. Geometrically-Exact, Intrinsic Theory for Dynamics of Curved and Twisted Anisotropic Beams (Corrigendum). AIAA Journal 47, 1308-1309.

[33] Hoffman, K.A., Manning, R.S., Paffenroth, R.C., 2002. Calculation of the stability index in parameter-dependent calculus of variations problems: Buckling of a twisted elastic strut. SIAM Journal on Applied Dynamical Systems 1, 115-145.

[34] Jiang, H., Zhang, P., Liu, B., Huang, Y., Guebelle, P. H., Gao, H., and Hwang, K. C., 2003. The Effect of Nanotube Radius on the Constitutive Model for Carbon Nanotubes. Comput. Mater. Sci. 28, 429-442.

[35] Kumar, A., Healey, T. J., 2010. A Generalized Computational Approach to Stability of Static Equilibria of Nonlinearly Elastic Rods in the Presence of Constraints. Comput. Methods App. Mech. Engg 199, 1805-1815.

[36] Lee, E. H., 1981. Some comments on Elastic-Plastic Analysis. Int J. Solids Struct 17, 859-872.

[37] Lehoucq, R.B., Scott, J.A., 1997. Implicitly Restarted Arnoldi Methods and Eigenvalues of the Discretized Navier Stokes Equations. Technical Report, SAND97-2712J, Sandia National Laboratory.

[38] Macewen, K.W., Healey, T.J., 2003. A Simple Approach to the 1:1 Resonance Bifurcation in Follower-Load Problems. Nonlinear Dynamics 32, 143-159.

[39] Maddocks, J.H., 1984. Stability of nonlinearly elastic rods. Archive for Rational Mechanics and Analysis 85, 311-354.

[40] Maddocks, J.H., 1987. Stability and folds. Archive for Rational mechanics and Analysis 99, 301-328.

[41] Manning, R.S., Maddocks, J.H., Kahn, J.D., 1996. A Continuum Rod Model of Sequence-Dependent DNA Structure. J. Chem Physics 105, 5626-5646.

[42] Manning, R.S., 2009. Conjugate Points Revisited and Neumann-Neumann Problems. Siam Review 51, 193-212.

[43] Manning, R.S., Rogers K.A., Maddocks, J.H., 1998. Isoperimetric conjugate points with application to the stability of DNA minicircles. Proc. R. Soc. Lond. A 454, 3047-3074.

[44] Marco J.F., Siggia, E.D., 1994. Bending and Twisting Elasticity of DNA. Macromolecules 27, 981-988.

[45] McMillen T., Goriely, A., 2002. Tendril Perversion in Intrinsically Curved Rods. J. Nonlin. Sci. 12, 169-205.

[46] Meerbergen, K., Spence, A., Implicitly Restarted Arnoldi With Purification For the Shift-Invert Transformation. Mathematics of Computation 66, 667-689.

[47] Meerbergen, K., Spence A., Roose, D., 1994. Shift-Invert and Cayley Transforms for Detection of Rightmost Eigenvalues of NonSymmetric Matrices. BIT Numerical Mathematics 34, 409-423.

[48] Merkin, D.R., 1997. Introduction to the Theory of Stability. Springer-Verlag, New York.

[49] Pantano, A., Boyce, M. C., Parks, D. M., 2004. Mechanics of Axial Compression of Single and Multi-walled Carbon Nanotubes. J. Eng. Mater. Technol. 126, 279-289.

[50] Papadopoulos, C.M., 1999. Nonlinear buckled states of Hemitropic Rods. Ph.D. Thesis, Cornell University, Ithaca New York.

[51] Rommes, J., 2008. Arnoldi and Jacobi-Davidson methods for generalized eigenvalue problems Ax = I Bx with singular B. Mathematics of Computation 77, 995-1015.

[52] Rubin, M. B., 2000. Cosserat Theories: Shells, Rods and Points. Kluwer Academic Publishers, The Netherlands.

[53] Sha, J., Niu, J., Ma, X., Xu, J., Zhang, X., Yang, Q., Yang, D., 2002. Silicon nanotubes. Advanced Materials 14(17), 1219-1221.

[54] Simo, J.C., Vu-Quoc, L., 1986. A Three-Dimensional Finite-Strain Rod Model. Part II: Computational Aspects. Comput. Methods App. Mech. Engrg 58, 79-116.

[55] Simo, J. C., and Vu-Quoc, L., 1991. A Geometrically-Exact Rod Model Incorporating Shear and Torsion-Warping Deformation. Int. J. Solids Structures 27, 371-393.

[56] Sorensen, D.C., 1992. Implicit Application of Polynomial Filters in a K-Step Arnoldi Method. SIAM. J. Matrix Anal. Appl. 13, 357-385.

[57] Strichartz, R.S., 1995. The Way of Analysis. Jones and Bartlett.

[58] Swigon, D., Coleman B.D., Tobias, I., 1998. The Elastic Rod Model for DNA and its Application to the Tertiary Structure of DNA Minicircles in Mononucleosomes. Biophysical Journal 74, 2515-2530.

[59] Thompson, J.M.T., Vander Heijden, G.H.M., Neukirch, S., 2002. Supercoiling of DNA Plasmids: Mechanics of the generalized Ply. Proc. R. Soc. Lond. A 458, 959-985.

[60] Upamanyu, M., Wang, H. L., Liang, H. Y., and Mahajan, R., 2008. Strain-dependent twist-stretch elasticity in chiral filaments. J. R. Soc. Interface 5, 303-310.

[61] Yakobson, B.I., Brabec, C.J., Bernholc, J., 1996. Nanomechanics of carbon tubes: Instabilities beyond linear response. Phys. Rev. Lett. 76, 2511-2514.